https://doi.org/10.15388/vu.thesis.54
https://orcid.org/0000-0003-4277-3688

VILNIAUS UNIVERSITETAS
FIZINIŲ IR TECHNOLOGIJOS MOKSLŲ CENTRAS

Justinas
GLEMŽA

Šiuolaikinių lazerinių ir šviesos diodų žemadažnio triukšmo spektroskopija

DAKTARO DISERTACIJA

Gamtos mokslai,
Fizika N 002

VILNIUS 2020

Disertacija rengta 2016 – 2020 metais Vilniaus universiteto Taikomosios elektrodinamikos ir telekomunikacijų institute.

Mokslinis vadovas:
prof. dr. Jonas Matukas (Vilniaus universitetas, gamtos mokslai, fizika, N 002).

Gynimo taryba:
Pirmininkas – **prof. habil. dr. Jūras Banys** (Vilniaus universitetas, gamtos mokslai, fizika, N 002).

Nariai:
prof. dr. Kęstutis Arlauskas (Vilniaus universitetas, gamtos mokslai, fizika, N 002);
doc. dr. Edvardas Kazakevičius (Vilniaus universitetas, gamtos mokslai, fizika, N 002);
dr. Šarūnas Meškinis (Kauno technologijos universitetas, gamtos mokslai, fizika, N 002);
prof. habil. dr. Gintaras Valušis (Fizinių ir technologijos mokslų centras, gamtos mokslai, fizika, N 002).

Disertacija ginama viešame Gynimo tarybos posėdyje 2020 m. spalio mėn. 2 d. 14 val. Vilniaus universiteto Fizikos fakulteto 401 auditorijoje.
Adresas: Saulėtekio al. 9, III rūmai, LT-10222, Vilnius, Lietuva.
Tel. +370 5 223 4578.

Disertaciją galima peržiūrėti Vilniaus universiteto bibliotekoje ir VU interneto svetainėje adresu: https://www.vu.lt/naujienos/ivykiu-kalendorius

https://doi.org/10.15388/vu.thesis.54
https://orcid.org/0000-0003-4277-3688

VILNIUS UNIVERSITY
CENTER FOR PHYSICAL SCIENCES AND TECHNOLOGY

Justinas
GLEMŽA

Low-frequency noise spectroscopy of novel laser diodes and light-emitting diodes

DOCTORAL DISSERTATION

Natural Sciences,
Physics N 002

VILNIUS 2020

This dissertation was written between 2016 and 2020 at Vilnius University, Institute of Applied Electrodynamics and Telecommunications.

Academic supervisor:
Prof. Dr. Jonas Matukas (Vilnius University, Natural Sciences, Physics, N 002).

This doctoral dissertation will be defended in a public meeting of the Dissertation Defence Panel:
Chairman – Prof. Habil. Dr. Jūras Banys (Vilnius University, Natural Sciences, Physics, N 002).

Members:
Prof. Dr. Kęstutis Arlauskas (Vilnius University, Natural Sciences, Physics, N 002);
Assoc. Prof. Dr. Edvardas Kazakevičius (Vilnius University, Natural Sciences, Physics, N 002);
Dr. Šarūnas Meškinis (Kaunas University of Technology, Natural Sciences, Physics, N 002);
Prof. Habil. Dr. Gintaras Valušis (Center for Physical Sciences and Technology, Natural Sciences, Physics, N 002).

The dissertation shall be defended at a public meeting of the Dissertation Defence Panel at 14 h on 2 October 2020 in Room 401 of Vilnius University Faculty of Physics.
Address: Saulėtekio av. 9, III bld., LT-10222, Vilnius, Lithuania.
Tel. +370 5 223 4578.

The text of this dissertation can be accessed at the library of Vilnius University, as well as on the website of Vilnius University: www.vu.lt/lt/naujienos/ivykiu-kalendorius

TURINYS

SANTRUMPOS 7
ĮVADAS 8
PUBLIKACIJŲ SĄRAŠAS 16
1. METODAI 19
1.1. Žemadažnio triukšmo matavimas 19
1.2. Koreliacinės analizės metodas 21
1.3. Generacinio-rekombinacinio triukšmo spektroskopija 22
2. REZULTATAI IR JŲ APTARIMAS 24
2.1. GaSb lazerinių diodų žemadažnio triukšmo tyrimai 24
2.1.1. Elektrinio triukšmo charakteristikos priešslenkstinėje veikoje 25
2.1.2. Triukšmai lazerinės generacijos veikoje 26
2.1.3. Generacinis-rekombinacinis triukšmas GaSb lazeriniuose dioduose ir jo kilmė 29
2.1.4. Veidrodžių pasyvavimo įtaka žemadažnio triukšmo charakteristikoms 30
2.2. GaAsBi lazerinių diodų žemadažnio triukšmo tyrimai 32
2.2.1. Elektrinio triukšmo charakteristikos 32
2.2.2. Lazerinių diodų ekvivalentinių grandinių sudarymas 33
2.2.3. Elektrinių fliuktuacijų kilmė GaAsBi lazeriniuose dioduose 36
2.3. InGaN šviesos diodų žemadažnio triukšmo tyrimai 38
2.3.1. Tunelinė srovė ir elektrinis triukšmas artimosios UV srities šviesos dioduose 38
2.3.2. Koreliacijos koeficiento tarp elektrinių ir optinių fliuktuacijų analizė artimosios UV srities šviesos dioduose 41
2.3.3. Triukšmo charakteristikos baltos šviesos diode ilgalaikio sendinimo eksperimento metu 42
2.3.4. Fosforo sluoksnio įtaka optinėms charakteristikoms baltos šviesos diode 46

2.4. Apibendrinimas 49
IŠVADOS 51
SUMMARY 53
LITERATŪROS SĄRAŠAS / REFERENCES 66
PADĖKA 75
CURRICULUM VITAE 76
PUBLIKACIJŲ KOPIJOS / COPIES OF PUBLICATIONS 77
UŽRAŠAMS 130

SANTRUMPOS

EŠP – epitaksinis šoninis priauginimas (*angl*. epitaxial lateral overgrowth);
FP – Fabri-Pero (*angl.* Fabry-Perot, FP);
GLRS – giliųjų lygmenų relaksacinė spektroskopija (*angl*. deep level transient spectroscopy, DLTS);
G-r – generacinis-rekombinacinis (*angl*. generation-recombination, g-r);
IR – infraraudonoji spinduliuotė (*angl*. infrared, IR);
I-U – voltamperinė charakteristika (*angl.* current-voltage characteristic, *I-V*);
KD – kvantinė duobė (*angl*. quantum well, QW);
KOVA – katastrofinis optinis veidrodžių ardymas (*angl*. catastrophic optical mirror damage, COMD);
KT – kambario temperatūra (*angl.* room temperature, RT);
LD – lazerinis diodas (*angl.* laser diode, LD);
MOJGE – metaloorganinio junginio garinė epitaksija (*angl*. metal-organic vapor phase epitaxy, MOVPE);
MPE – molekulinio pluošto epitaksija (*angl*. molecular beam epitaxy, MBE);
MTS – mažatriukšmis stiprintuvas (*angl*. low-noise amplifier, LNA);
PSTM – paspartinto sendinimo tyrimo metodas (*angl*. highly accelerated stress testing, HAST);
SAR – spalvų atgavos rodiklis (*angl*. color rendering index, CRI);
SPR – safyro padėklo reljefas (*angl*. sapphire substrate pattern, SBP);
SST – susietoji spalvinė temperatūra (*angl.* correlated color temperature, CCT);
ŠD – šviesos diodas (*angl.* light-emitting diode, LED);
UV – ultravioletinė spinduliuotė (*angl.* ultraviolet, UV).

ĮVADAS

Šiandieninis gyvenimas yra neįsivaizduojamas be lazerinių (LD) ir šviesos diodų (ŠD). Tai kompaktiški, lengvi ir sąlyginai pigūs tiesiogine kryptimi veikiantys *pn* sandūros įtaisai, kurių pirmieji veikiantys prototipai pademonstruoti praeito šimtmečio septintojo dešimtmečio pradžioje [1, 2]. Lyginant su pirmaisiais prietaisais, dabartiniai LD ar ŠD yra žymiai modernesni, tačiau vis dar yra ieškoma naujų puslaidininkinių junginių, kurių naudojimas padėtų išspręsti įtaiso veikos efektyvumą ribojančias problemas, o esamų junginių gamybos technologijos yra tobulinamos siekiant dar kokybiškesnių puslaidininkinių darinių. Taigi, bandinių charakterizavimo, kokybės ir patikimumo klausimai yra kaip niekad aktualūs.

Plačios taikymo galimybės infraraudonojoje (IR) spektro srityje lėmė spartų lazerinių diodų vystymąsi. Bangos ilgių intervale nuo 1,8 μm iki 4 μm yra gausu molekulių sugerties juostų, pavyzdžiui, NH_3, CO_2, SO_2 ir t.t. [3], todėl tokie LD gali būti naudojami molekulių spektroskopijoje ar dujų aptikimui [4, 5]. 1,9 μm bangos ilgio LD masyvai gali būti panaudoti holmiu legiruotiems kietakūniams lazeriams kaupinti, o medicinoje – kraujagyslių ir audinių priauginimo operacijose [6, 7]. Nemažiau svarbios taikymo galimybės kariuomenėje ir lidaruose [8]. Minėto bangos ilgio spinduliuotė gali būti gauta naudojant LD, pagamintus InP pagrindu su II-ojo tipo kvantinėmis duobėmis (KD) [9], GaSb-pagrindu pagamintus tarpjuostinius daugiapakopius lazerius [10, 11] arba GaSb-pagrindu pagamintus LD su I-ojo tipo kvantinėmis duobėmis. Lazeriniuose dioduose su II-tipo KD krūvininkai – elektronai ir skylės – yra atskirti gretimuose sluoksniuose, o LD su I-ojo tipo KD – tiek elektronai, tiek ir skylės yra sulaikomi tame pačiame sluoksnyje [9]. Būtent pastaroji GaSb LD grupė yra ypač patraukli, kadangi I-tojo tipo KD realizuojami tiesioginiai tarpjuostiniai krūvininkų šuoliai lemia efektyvią spinduliuojamąją rekombinaciją [5, 12]. Lyginant su kitomis IR LD grupėmis, darinių struktūra ir technologinė gamyba yra paprastesnė, o tai lemia mažesnę galutinę įtaiso kainą [4, 13]. Aktyviąją sritį sudaro GaInAsSb kvantinės duobės ir keturnariai AlGaAsSb barjerai, o bangos ilgiui virš 3 μm pasiekti ir, norint, kad KD išliktų I-ojo tipo, yra naudojami penkianariai AlGaInAsSb barjerai bei bangolaidiniai sluoksniai [4, 14].

Tokių reikalingų daugianarių aktyviosios srities junginių auginimas yra technologiškai sudėtingas, kadangi šiluminio atkaitinimo metu vyksta

draudžiamosios energijos juostos padidėjimas, taigi, spinduliuojamas bangos ilgis trumpėja [15]. Pavyzdžiui, nuo pirmojo LD, generuojančio 3,26 μm bangos ilgio spinduliuotę kambario temperatūroje (KT), pademonstravimo praėjo 3 metai, kol pavyko pasiekti 3,36 μm bangos ilgio spinduliuotę. Šiuo metu jau yra sukurti LD su I-ojo tipo KD, veikiantys impulsinėje veikoje, ir kurių bangos ilgis KT net 3,37 μm [4]. GaInAsSb/AlGaAsSb struktūrose spinduliuojamosios rekombinacijos efektyvumą mažina šiluminis skylių nuotėkis iš aktyviosios srities dėl prasto skylių sulaikymo kvantinėse duobėse [16]. IR lazeriniams diodams ypatingai aktuali problema yra tai, kad didėjant spinduliuojamam bangos ilgiui, sparčiai auga nespinduliuojamoji Ožė rekombinacija ir laisvųjų krūvininkų sugertis [5, 8].

Nespinduliuojamosios rekombinacijos sukeliami nuostoliai aktualūs ir optinėse telekomunikacijų linijose naudojamiems LD, spinduliuojantiems intervale nuo 1,3 μm iki 1,5 μm. Šių nuostolių praktiškai galima išvengti LD ar ŠD aktyviajai sričiai naudojant naujovišką ir daug žadantį $GaAs_{1-x}Bi_x$ junginį [17, 18]. Net ir nedidelis bismuto (Bi) kiekis, įterptas į galio arsenidą (GaAs), efektyviai sumažina junginio draudžiamosios energijos juostą (84 – 91) meV/%Bi [19]. Jeigu įterpiamo Bi daugiau nei 10 %, sukininio-orbitinio suskilimo energija (Δ_{so}) tampa didesnė nei medžiagos draudžiamosios energijos juosta. Esant tokioms sąlygoms galima tikėtis, kad Ožė rekombinacija ir sugertis valentinėje juostoje bus nuslopintos [17, 19]. Tai leistų pagaminti dar efektyviau veikiančius LD su daug stabilesne spinduliuotės galia ir bangos ilgiu. Tačiau technologinę plėtrą stabdo šio darinio auginimo sudėtingumas. Norint išvengti Bi paviršinės segregacijos, auginimo temperatūra turi būti sumažinta lyginant su optimalia temperatūra galio arsenidui, o tai lemia nespinduliuojamosios rekombinacijos centrų formavimąsi [17–21]. Dėl šios priežasties metaloorganinio junginio garinės epitaksijos (MOJGE) būdu pavyksta išauginti darinius tik su 4,4 % bismuto, o norint jo įterpti daugiau, reikalingas auginimas molekulinio pluošto epitaksijos (MPE) būdu [17]. Deja, bet paviršinė segregacija nėra vienintelė problema, bloginanti GaAsBi sluoksnių kokybę, – net ir nedidelės augimo sąlygų fliuktuacijos gali lemti didelį paviršiaus šiurkštumą ar Bi lašelių formavimąsi [18, 20, 22]. Todėl pastaraisiais metais yra intensyviai ieškoma būdų, kaip įveikti šiuos technologinius iššūkius.

Neseniai buvo pristatyta dvitemperatūrė auginimo MPE technologija, kur GaAsBi KD auginamos žemesnėje temperatūroje, o GaAs sluoksniai – aukštesnėje. Tai ženkliai sumažina Bi segregaciją [18]. Taip pat taikoma mišri auginimo technologija, kur aktyvioji sritis auginama MPE būdu, o likusi LD struktūra – MOJGE būdu [17, 23]. Jau yra pademonstruoti ŠD su $GaAs_{0,96}Bi_{0,04}$/GaAs aktyviąja sritimi, kurių spinduliuojamas bangos ilgis yra

net 1,23 μm kambario temperatūroje [18], bei LD su x = 5,8 % Bi KD, generuojantys 1,14 μm bangos ilgio spinduliuotę KT. Deja, šių lazerinių diodų slenkstinė srovė yra dar daug kartų didesnė nei šiandien plačiai naudojamų InGaAsP/InP telekomunikacinių LD [24]. Norint šias vertes sumažinti bei pasiekti ilgesnį spinduliuojamą bangos ilgį, yra būtinas geras fizikinių procesų, vykstančių šiuose GaAsBi LD, supratimas.

Priešingoje optinio spektro pusėje regimosios šviesos atžvilgiu, t. y. artimojoje ultravioletinėje (UV) srityje, kaip aktyvusis optoelektroninių įtaisų sluoksnis plačiai naudojamas InGaN junginys. Nors praėjo jau nemažai laiko nuo pirmųjų InGaN/GaN ŠD pristatymo [25], jų gamybos technologija intensyviai tobulinama. Pavyzdžiui, safyro padėklas vis dar plačiai naudojamas ŠD auginimui, nors didelis jo gardelės nesutapimas su GaN (net 16 %) lemia defektų – sraigtinių dislokacijų – formavimąsi [26, 27]. Siekiant sumažinti dislokacijų tankį bei pagerinti kvantinį ŠD efektyvumą, yra pasiūlyti įvairūs technologiniai sprendimai: GaN, AlN buferinių sluoksnių auginimas [28], safyro padėklo reljefo (SPR) formavimas [27, 29], epitaksinis šoninis priauginimas (EŠP) [26] ir kt. Laikoma, kad indžio sudėties fliuktuacijos junginyje yra atsakingos už efektyvią spinduliuojamąją rekombinaciją InGaN įtaisuose [30]. Kadangi UV šviesos dioduose lyginant su mėlynos šviesos ŠD, indžio dalis kvantinėse duobėse yra mažesnė, tai šių sudėties fliuktuacijų įtaka spinduliuojamosios rekombinacijos efektyvumui yra silpnesnė, o tai lemia išaugusią krūvininkų sąveiką su dislokacijomis [31, 32]. Didelio našumo UV ŠD galėtų būti naudojami fluorescencinėse lempose sužadinti raudonam, žaliam ir mėlynam fosforams ir taip išvengti pavojingo sveikatai gyvsidabrio naudojimo apšvietimo sistemose. Tokie šviesos šaltiniai pasižymėtų aukštu spalvų atgavos rodikliu (SAR), t. y. apšvietus tokiu įtaisu objektų spalvos būtų daug mažiau iškraipytos, lyginant su šiuo metu plačiai naudojamais fosforo konversijos baltos šviesos ŠD [33]. Pastaruosiuose fosforo sluoksnis verčia dalį puslaidininkinio lusto mėlynos spinduliuotės į geltoną, o visa ištrūkusi iš tokio įtaiso šviesa akies suvokiama kaip balta [34]. Tokių ŠD taikymas apšvietimo tikslams iškėlė ilgaamžiškumo bei patikimumo tyrimų svarbą ir būtinybę.

Kuriant naujoviško technologinio dizaino įtaisus ir naudojant naujas puslaidininkines medžiagas, tuo pat metu išauga poreikis jautriam ir neardančiam bandinių charakterizavimo metodui. Žemadažnio triukšmo spektroskopija tam puikiai tinka. Pagrindiniai eksperimentinio triukšmų tyrimo privalumai yra šie: matavimai atliekami artimomis pusiausvyrai sąlygomis, patys matavimai yra spartūs ir ypatingai jautrūs puslaidininkinių darinių defektams, įvairiems netobulumams ir jų pokyčiams struktūroje [35–

37]. Elektrinis triukšmas (ypač 1/*f* fliuktuacijos) yra puikus elektroninių prietaisų patikimumo ir kokybės indikatorius, kadangi įtaisui gendant jo fliuktuacijų lygis auga, o mažiau patikimi bandiniai paprastai pasižymi didesniu triukšmu [38]. Žemadažnio triukšmo spektroskopija yra tinkamas įrankis ir tokių optoelektroninių įtaisų, kaip lazeriniai ar šviesos diodai, diagnostikai [37, 39]. Ji teikia žinių apie vykstančius fizikinius procesus bandiniuose, jų kilmę, vietą ir galimas priežastis.

Charakterizuojant ŠD ar LD, nemažiau svarbu yra tirti ne tik elektrinį, bet ir optinį triukšmą, t. y. spinduliuotės galios fliuktuacijas [40, 41]. Aukštas elektrinio triukšmo lygis nebūtinai reiškia didelį aktyviosios (šviesą skleidžiančios) srities defektingumą [42]. Matuojant abu triukšmo signalus vienu metu, galima įvertinti abipusės koreliacijos koeficientą tarp elektrinių ir optinių fliuktuacijų. Žemadažnis optinis triukšmas laikomas moduliaciniu, kadangi LD ar ŠD tekančios srovės fliuktuacijos moduliuoja išspinduliuotų fotonų srautą, t. y. spinduliuotės galią [43]. Taikant koreliacinės analizės metodą galima nustatyti, kuri elektrinio triukšmo dalis yra susijusi su aktyviąja LD ar ŠD sritimi, ir taip įvertinti vieno ar kito triukšmo šaltinio vietą bandinyje bei atskirų triukšmo spektrinių sandų įtaką abipusės koreliacijos koeficientui [43, 44]. Fizikinę prasmę turi ir koreliacijos koeficiento ženklas, kuris gali būti tiek teigiamas, tiek neigiamas. Koeficientas yra laikomas teigiamu, kai krūvininkų skaičiaus nedidelis pokytis aktyviojoje srityje, tarkime, padidėjimas, lemia ir atitinkamą spinduliuotės intensyvumo padidėjimą [45].

Deja, tam tikrais atvejais optinio triukšmo ir abipusės koreliacijos koeficiento matavimas yra komplikuotas. Pavyzdžiui, daugiamodžių Fabri-Pero (FP) LD atveju lazerinės generacijos metu vyksta intensyvūs išilginių modų šuoliai, o jų metu triukšmas drastiškai išauga. Nepaisant to, modų šuolių sukelti elektrinio ir optinio triukšmo sandai stipriai teigiamai ar neigiamai koreliuoja [46, 47], o tai apsunkina tokių LD charakterizavimą. Išeitis – atlikti triukšmų tyrimus tik priešslenkstinėje veikoje, kadangi nustatyti fizikiniai procesai ir aptiktos problemos struktūroje (defektai, nuotėkio srovės ir t. t.) daro didesnę ar mažesnę įtaką LD veikai ir lazerinės generacijos metu [48, 49]. Toks charakterizavimo būdas leidžia išvengti bandinio gadinimo matavimo metu, kadangi didelės galios LD slenkstinė srovės vertė paprastai taip pat yra didelė (amperų eilės) [50].

Neardančio elektroninių įtaisų tyrimo metodo pasirinkimas yra svarbus ir atliekant ilgalaikį sendinimo eksperimentą. Triukšminės diagnostikos pagalba siekiama pastebėti vykstančius pokyčius bandiniuose anksčiau, negu jie taps akivaizdūs kitose elektrinėse charakteristikose [37], pavyzdžiui voltamperinėse (*I*-*U*). Tiriamasis LD ar ŠD eksperimento metu veikia

įprastomis sąlygomis. Tai yra pagrindinis skirtumas nuo, pavyzdžiui, paspartinto sendinimo tyrimo metodų (PSTM), kuomet įtaisas veikia gerokai aukštesnėje nei kambario temperatūroje ar tekant didesnei srovei negu yra leistina gamintojo [51, 52]. Taigi, šiuo atveju vykstantys fizikiniai procesai nebūtinai pasireikš prietaisui veikiant įprastomis sąlygomis [42].

Charakterizuojant panašios kokybės bandinius, matavimai, atlikti esant tiesioginiam priešįtampiui, gali nesuteikti pakankamai informacijos, reikalingos jų patikimumo ar kokybiškumo įvertinimui. Todėl tyrimo metodiką yra bandoma patobulinti atliekant LD triukšmų matavimus jais tekant atgalinei srovei bei ieškant sąsajos su tiesioginio priešįtampio tyrimo rezultatais [53]. Nekokybiškas LD veidrodinių sienelių pasyvavimo procesas didelio ir mažo atspindžio dangomis gali pabloginti veidrodinių paviršių kokybę ir lemti naujų defektų paviršiuje formavimąsi. Jie gali kurti nuotėkio srovės kanalus ir taip didinti atgalinę srovę [54], tekančią per LD, o tai – paspartinti katastrofinį optinį veidrodžių ardymą (KOVA) [55–57]. Todėl atsiveria galimybė įvertinti veidrodžių sienelių pasyvavimo proceso kokybiškumą tiriant elektrinio triukšmo charakteristikas atgaline kryptimi [58].

Atliekant LD ar ŠD fliuktuacijų tyrimus, yra susiduriama su beveik visais žemadažnio triukšmo tipais. Bet koks elementas, turintis ne nulinę varžą, kuria šiluminį (dar vadinamą Džonsono ar Naikvisto) triukšmą. Jį sukelia atsitiktinis krūvininkų (Brauno) judėjimas, o jo kuriamų įtampos fliuktuacijų spektrinis tankis išreiškiamas Naikvisto formule $S_U = 4kTR$, kuri galioja iki $\sim 6 \cdot 10^{12}$ Hz, čia k – Bolcmano konstanta, T – temperatūra, R – bandinio varža [36–38]. Atsitiktiniai ir nepriklausantys vienas nuo kito krūvininkų pralėkimo pro potencialo barjerą vyksmai lemia šratinį triukšmą, stebimą dioduose. Jo srovės fliuktuacijų spektrinis tankis proporcingas elektrono krūvio ir tekančios srovės stiprio sandaugai [36, 38]. Dažnai eksperimentiniuose LD ar ŠD žemadažniuose spektruose tiriamame dažnių intervale šios fliuktuacijos yra užgožtos kitų triukšmų. Tiek šiluminio, tiek ir šratinio triukšmo spektriniai tankiai yra „balti“, t. y. plačiame intervale nepriklausantys nuo dažnio. Dėl šios savybės šiluminis triukšmas gali būti naudojamas aparatūros kalibravimui [36]. LD ar ŠD tyrimuose šratinis triukšmas dažniau stebimas optinių fliuktuacijų spektruose dėl atsitiktinio fotonų išspinduliavimo [42, 45, 59].

Bandinių triukšminė diagnostika, jų kokybės bei patikimumo įvertinimas yra neatsiejami nuo generacinio-rekombinacinio (g-r) ir $1/f$ triukšmų tyrimo. Tai bandinio laidžio (ar varžos) fliuktuacijos, t. y. laisvųjų krūvininkų skaičius bandinyje fliuktuoja dėl atsitiktiniu būdu vykstančių generacijos ir rekombinacijos vyksmų. Šios krūvininkų skaičiaus fliuktuacijos sukelia

tekančios bandiniu nuolatinės srovės (ar įtampos) fliuktuacijas. Įvairūs defektai elgiasi kaip krūvininkų pagavimo centrai (arba g-r centrai) ir yra charakterizuojami energine padėtimi, tankiu, krūvininkų pagavimo ir išlaisvinimo procesų nulemta relaksacijos trukme ir būdingu Lorenco pavidalo spektriniu tankiu [36, 38]. G-r triukšmo intensyvumas yra proporcingas aktyvių pagavimo centrų skaičiui [35, 60]. Jei šių nepriklausomų g-r procesų relaksacijos trukmės yra skirtingos ir pasiskirsčiusios plačiame laiko intervale, tai daugybės tokių vyksmų su Lorenco spektrais superpozicija duos $1/f$ pavidalo spektrinį tankį. Tai relaksacinis $1/f$ triukšmo modelis [37, 61].

$1/f$ triukšmas kietuosiuose kūnuose tiriamas jau daugiau nei 60 metų [61]. Praktiškai visą tyrimų laiką jo kilmės klausimas buvo diskusijų objektas. Yra dvi vyraujančios teorijos: aiškinimas krūvininkų judrio fliuktuacijomis dėl sklaidos gardelės virpesiais ir jau minėtas relaksacinis modelis [36, 61–63]. Būtent pastarasis modelis yra universalesnis, gerai aprašo eksperimento metu stebimą $1/f^{\alpha}$ triukšmą, kur α gali kisti nuo 0,8 iki 1,3, bei paaiškina spektrinio tankio proporcingumą $1/f^{\alpha}$ plačiame dažnių intervale [49, 61, 64, 65]. Šiuo metu yra parodyta, kad pagrindinė $1/f$ fliuktuacijų priežastis yra krūvininkų pagavimo ir išlaisvinimo procesai, o ne judrio fliuktuacijos. Kai kuriuose puslaidininkiuose (pavyzdžiui, Ge, Si, GaAs) galima gauti $1/f$ triukšmo intensyvumo proporcingumą judrio kvadratui tam tikrame laisvųjų krūvininkų tankių intervale, tačiau tai yra tik atvaizdavimo pasekmė [61, 66, 67].

Be šių žemadažnių fliuktuacijų, veikiant LD ar ŠD, gali būti stebimi ir specifiniai triukšmai, būdingi tik jiems ir ribojantys praktinį šių įtaisų taikymą. Pavyzdžiui, optinėje linijoje perduodant informaciją LD modų šuolių triukšmas didina klaidų tikimybę [68], signalo-triukšmo santykį blogina ir aukštuose dažniuose stebimos triukšmų smailės ties LD relaksacinių virpesių dažniais [69], realiose sistemose spinduliuotės koherentiškumą gali sumažinti optinio grįžtamojo ryšio triukšmas [70, 71], o spinduliuotės dažnio fliuktuacijos nulemti optinio spektro praplatėjimą [72, 73].

Taigi, šios įvardintos aptartų šiuolaikinių LD ir ŠD problemos rodo didelę atliekamų tyrimų praktinę reikšmę ir aktualumą bei tinkamo ir patikimo charakterizavimo metodo – žemadažnio triukšmo spektroskopijos – reikalingumą.

Darbo tikslas

Ištirti šiuolaikinių lazerinių ir šviesos diodų su GaInAsSb, GaAsBi ir InGaN kvantinėmis duobėmis žemadažnio triukšmo charakteristikas, nustatyti įtaisų žemadažnio triukšmo šaltinius bei jų kilmę.

Darbo uždaviniai

1. Atlikti elektrinių ir optinių triukšmų charakteristikų tyrimus priešslenkstinėje bei LD atveju – ir lazerinės generacijos veikose atsižvelgiant į tiriamų bandinių savybes. Siekiant įvertinti bandinių paviršiaus kokybiškumą, atlikti triukšmų matavimus ir esant pridėtam atvirkštiniam priešįtampiui.
2. Atlikti abipusės koreliacijos koeficiento tarp elektrinių ir optinių fliuktuacijų analizę bei įvertinti fliuktuacijų kilmės vietą bandinyje.
3. Taikant generacinio-rekombinacinio triukšmo spektroskopiją nustatyti pagavimo lygmenų bandiniuose aktyvacijos energijas.
4. Susieti bandinių triukšmo savybes su jų atitinkamomis voltamperinėmis ir spinduliuotės galios charakteristikomis. Siekiant detaliai išaiškinti triukšmo šaltinių kilmę, pateikti LD ekvivalentines triukšmų grandines ir palyginti eksperimentinius įtampos fliuktuacijų spektrinius tankius su apskaičiuotais pagal šias ekvivalentines grandines.
5. Atlikti ilgalaikį InGaN pagrindu pagaminto ŠD sendinimo eksperimentą ir įvertinti vykstančius fizikinius procesus tiriant žemadažnes fliuktuacijas. Nustatyti, ar fosforo sluoksnis elgiasi kaip galimas triukšmų šaltinis.

Mokslinis naujumas ir praktinė reikšmė

Medžiagos, kurių pagrindu pagaminti tiriamieji lazeriniai ar šviesos diodai, yra pakankamai naujos ir perspektyvios. Todėl gauti rezultatai gali būti įdomūs tiek besidomintiems šiuolaikinių LD ar ŠD elektrinėmis ir optinėmis savybėmis bei patikimumu, tiek ir norintiems daugiau sužinoti apie žemadažnių triukšmų fiziką ir jų savybes. Lazerinių diodų, pagamintų GaSb pagrindu, triukšmų tyrimų pasauliniu mastu yra labai mažai, yra aprašyti vien tik elektrinių fliuktuacijų matavimai [74–76]. Mūsų atlikti optinių fliuktuacijų ir abipusės koreliacijos tyrimai leidžia detaliau paaiškinti fizikinius reiškinius, vykstančius šiuose LD. Disertacijos rengimo metu lazerinių diodų su GaAsBi kvantinėmis duobėmis žemadažnio triukšmo rezultatai mokslinėje literatūroje dar nebuvo aprašyti. Pirmą kartą disertacijoje pateikta išsami GaAsBi LD elektrinių fliuktuacijų analizė.

Kadangi daugelis sendinimo eksperimentų atliekama taikant PSTM, ilgalaikių (bent 28000 val.) ŠD charakteristikų tyrimų jam veikiant įprastomis veikos sąlygomis ir atliekant triukšmų matavimus nėra. Pirmą kartą koreliacinės analizės metodas pritaikytas tokios trukmės sendinimo eksperimentui ir pademonstruotas jo jautrumas fizikinių procesų pokyčiams įtaise. Nustatyta, kad baltos šviesos ŠD naudojamas fosforo sluoksnis ilgalaikio sendinimo metu (28000 val.) nesielgia kaip papildomas triukšmo šaltinis, bet prisideda prie ŠD chromatinių savybių kitimo.

Šiame darbe taip pat parodyta, kad LD ar ŠD elektrinio triukšmo spektrinio tankio priklausomybės nuo srovės pobūdis, t. y. turinti maksimumų ar „V“ formos priklausomybė, yra charakteringa ir teikia pradinę informaciją apie tekančios srovės kelius (vyraujantį srovės sandą) bandiniuose. Pateikta unikali metodika, padedanti įvertinti žemadažnių fliuktuacijų kilmę susiejant minėtas triukšmų priklausomybes su bandinių *I-U* charakteristikomis ir jų ekvivalentinėmis grandinėmis.

Bandinių charakterizavimo metu yra įprasta, kad tokių puslaidininkinių įtaisų, kurie veikia esant pridėtam atvirkštiniam priešįtampiui, pavyzdžiui, fotodiodų, triukšmų charakteristikos ir yra tiriamos atgaline kryptimi. Parodyta, kad LD atveju tokie saugūs tyrimai nepramušant pačios *pn* sandūros tekant atgalinei srovei gali būti taikomi paviršinei nuotėkio srovei aptikti ar paviršiaus kokybiškumui įvertinti.

Šiame darbe aptarti rezultatai ne tik teikia informacijos apie fizikinius procesus, vykstančius įtaisuose, bet ir leidžia skirtingus bandinius tarpusavyje palyginti ir taip įvertinti jų kokybę. Tyrimo rezultatai gali būti panaudoti įtaisų patikimumo ir galimos veikimo trukmės prognozavimui.

Kadangi žemadažnių triukšmų matavimai atliekami prietaisui – lazeriniam ar šviesos diodui – veikiant, tai to paties eksperimento metu gaunama informacija apie reiškinius, vykstančius skirtingose įtaiso dalyse: pačiame puslaidininkiniame darinyje, kontaktuose ar paviršiuje, todėl galima įvertinti veidrodžių dangų, fosforo sluoksnio ar korpuso įtaką elektrinėms ir optinėms prietaiso savybėms. Vienalaikis elektrinių ir optinių charakteristikų tyrimas yra ne tik tikslus, bet ir taupantis laiką.

Taigi, remiantis disertacijoje aprašytais rezultatais, galima teigti, kad lazerinių ir šviesos diodų gamybos technologija gali būti tobulinama atsižvelgiant į nustatytų žemadažnio triukšmo šaltinių kilmę ir susiejant ją su bandinių sandara.

PUBLIKACIJŲ SĄRAŠAS

Disertacijos tema

[P1] **J. Glemža**, S. Pralgauskaitė, V. Palenskis, J. Matukas, Low-frequency noise investigation of 2–3 μm GaSb-based laser diodes, Solid State Electron. **133**, 70–77 (2017); doi: 10.1016/j.sse.2017.05.002.

[P2] **J. Glemža**, V. Palenskis, S. Pralgauskaitė, J. Vyšniauskas, J. Matukas, Properties of the surface generation-recombination noise in 1.94 μm GaSb-based laser diodes, Infrared Phys. Technol. **91**, 101–106 (2018); doi: 10.1016/j.infrared.2018.04.002.

[P3] **J. Glemža**, V. Palenskis, A. Geižutis, B. Čechavičius, R. Butkutė, S. Pralgauskaitė, J. Matukas, Low-frequency noise investigation of 1.09 μm GaAsBi laser diodes, Materials **12**, 673 (2019); doi: 10.3390/ma12040673.

[P4] **J. Glemža**, J. Matukas, S. Pralgauskaitė, V. Palenskis, Low-frequency noise characteristics of high-power white LED during long-term aging experiment, Lith. J. Phys. **58**, 194–203 (2018); doi: 10.3952/physics.v58i2.3749.

[P5] **J. Glemža**, S. Pralgauskaitė, V. Palenskis, J. Matukas, Low-frequency noise of near UV LEDs, Lith. J. Phys. **59**, 146–155 (2019); doi: 10.3952/physics.v59i3.4081.

Kitos publikacijos

[P6] V. Palenskis, J. Vyšniauskas, **J. Glemža**, J. Matukas, Charge carrier mobility fluctuations due to capture-emission process, Lith. J. Phys. **58**, 261–266 (2018); doi: 10.3952/physics.v58i3.3814.

[P7] **J. Glemža**, J. Matukas, S. Pralgauskaitė, V. Palenskis, Mid-infrared laser diodes investigation via low-frequency noise spectroscopy and electrical derivative characteristics. *Proc. International Conference on Noise and Fluctuations (ICNF)* (IEEE, 2017) pp. 1–4; doi: 10.1109/ICNF.2017.7986012.

[P8] V. Palenskis, **J. Glemža**, J. Vyšniauskas, J. Matukas, Carrier density and mobility fluctuations due to carrier retrapping process in homogeneous semiconductors. *Proc. International Conference on Noise and Fluctuations (ICNF)* (IEEE, 2017) pp. 1–4; doi: 10.1109/ICNF.2017.7986019.

[P9] **J. Glemža**, J. Matukas, S. Pralgauskaitė, Low frequency noise spectroscopy and threshold characteristics of laser diodes. *Proc. 21st International Conference on Microwave, Radar and Wireless Communications (MIKON)* (IEEE, 2016) pp. 1–4; doi: 10.1109/MIKON.2016.7491951.

[P10] S. Pralgauskaitė, V. Palenskis, J. Matukas, **J. Glemža**, G. Muliuk, B. Šaulys, A. Trinkūnas, Reliability investigation of light-emitting diodes via low frequency noise characteristics. Microelectron. Reliab. **55**, 52–61 (2015); doi: 10.1016/j.microrel.2014.09.027.

Pranešimai konferencijose

[K1] **J. Glemža**, V. Palenskis, A. Geižutis, B. Čechavičius, R. Butkutė, S. Pralgauskaitė, J. Matukas, GaAsBi lazerinių diodų žemadažnio triukšmo charakteristikos esant tiesioginiam ir atvirkštiniam priešįtampiui, *43-oji Lietuvos nacionalinė fizikos konferencija (LNFK43): Programa ir pranešimų tezės, Kaunas, 2019 m. spalio 3-5 d.* (Kaunas, 2019) p. 264.

[K2] **J. Glemža**, V. Palenskis, S. Pralgauskaitė, J. Matukas, The relation between electrical fluctuations and current-voltage characteristics of the mid-IR laser diodes in the subthreshold region, *8th International Conference on Unsolved Problems on Noise (UPON): Book of Abstracts, Gdansk, 2018 July 9-13.* (Gdansk, 2018) pp. 128–129.

[K3] **J. Glemža**, V. Palenskis, S. Pralgauskaitė, J. Matukas, Investigation of charge carrier transport in MID-IR laser diodes through the low-frequency noise spectroscopy, *Advanced Properties and Processes in Optoelectronic Materials and Systems (Apropos 16): Book of Abstracts, Vilnius, 2018 October 10-12.* (Vilnius, 2018) p. 70.

[K4] **J. Glemža**, J. Matukas, S. Pralgauskaitė, V. Palenskis, Mid-infrared laser diodes investigation via low-frequency noise spectroscopy and electrical derivative characteristics, *24th International Conference*

on Noise and Fluctuations (ICNF): programme and abstracts, Vilnius, 2017 June 20-23. (Vilnius, 2017) p. 13.

[K5] V. Palenskis, **J. Glemža**, J. Vyšniauskas, J. Matukas, Carrier density and mobility fluctuations due to carrier retrapping process in homogeneous semiconductors, *24th International Conference on Noise and Fluctuations (ICNF): programme and abstracts, Vilnius, 2017 June 20-23*. (Vilnius, 2017) p. 20.

[K6] **J. Glemža**, J. Matukas, S. Pralgauskaitė, V. Palenskis, GaSb pagrindu pagamintų lazerinių diodų triukšmų ir elektrinių charakteristikų tyrimas atliekant sendinimo eksperimentą, *42-oji Lietuvos nacionalinė fizikos konferencija (LNFK42): Programa ir pranešimų tezės, Vilnius, 2017 m. spalio 4-6 d.* (Vilnius, 2017) p. 299.

[K7] **J. Glemža**, J. Matukas, S. Pralgauskaitė, Low-frequency noise spectroscopy and threshold characteristics of laser diodes, *MIKON 2016 - 21st International Conference on Microwave, Radar and Wireless Communications, May 9-11, Krakow, Poland*.

[K8] **J. Glemža**, J. Matukas, S. Pralgauskaitė, Low-frequency noise spectroscopy and threshold characteristics of laser diodes. *Open Readings 2016: 59th Scientific Conference for Students of Physics and Natural Sciences, March 15-18, 2016, Vilnius: programme and abstracts* (Vilnius University, Vilnius, 2016) p. 234.

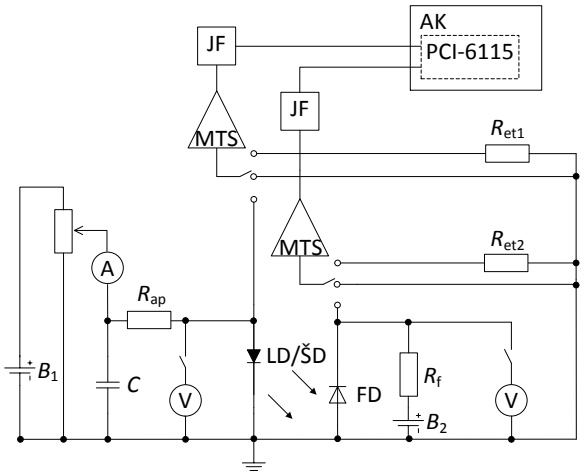
[K9] **J. Glemža**, J. Matukas, S. Pralgauskaitė, B. Šaulys, V. Palenskis, Koreliacijos tarp elektrinių ir optinių fliuktuacijų analizė didelės galios šviesos diodų kokybės ir patikimumo įvertinimu. *41-oji Lietuvos nacionalinė fizikos konferencija: programa ir pranešimų tezės, Vilnius, 2015 m. birželio 17-19 d.* (Vilnius, 2015) p. 235.

1. METODAI

Šiame skyriuje pateikiami pagrindiniai eksperimentiniai ir teoriniai metodai naudoti darbe tiriant žemadažnio triukšmo charakteristikas.

1.1. Žemadažnio triukšmo matavimas

Eksperimentinė žemadažnio triukšmo matavimo schema yra pateikta 1.1 pav. Elektrinis triukšmas (paties lazerinio ar šviesos diodo įtampos fliuktuacijos) gali būti tiriamas dažnių intervale nuo 10 Hz iki 500 kHz. Matavimų metu yra išlaikomas pastovios srovės režimas. Tai pasiekiama parenkant atitinkamą LD ar ŠD maitinimo įtampą ir apkrovos varžą R_{ap}, kuri bent 10 kartų didesnė nei bandinio diferencialinė varža. Matuojamos fliuktuacijos stiprinamos mažatriukšmiu stiprintuvu (MTS), kurio ekvivalentinė triukšmų varža lygi 13 Ω esant 1 kHz dažniui. Naudojamas MTS nulemia triukšmų matavimo sistemos jautrį. Tuomet sustiprintas analoginis signalas verčiamas į skaitmeninį. Tam naudojamas analogas-skaičius keitiklis (National Instruments PCI-6115). Įtampos fliuktuacijų spektrinis tankis gaunamas atliekant sparčiąją Furjė transformaciją bei gautąjį spektrinį tankį vidurkinant (apie 300 realizacijų).



1.1 pav. Triukšmų matavimo schema: AK – asmeninis kompiuteris; B_1, B_2 – maitinimo šaltiniai; C – kondensatorius, galimiems kontaktų ar maitinimo šaltinio triukšmams pašalinti; FD – fotodiodas; JF – juostiniai filtrai; LD – lazerinis diodas arba ŠD – šviesos diodas; MTS – mažatriukšmis stiprintuvas; R_{ap}, R_f – lazerinio diodo ir fotodiodo apkrovos varžos; R_{et1}, R_{et2} – etaloninės varžos.

Tiriant šviesą skleidžiančių įtaisų triukšmus, nemažiau naudingos informacijos gaunama ir iš optinių – spinduliuotės galios fliuktuacijų. Jos matuojamos dažnių intervale nuo 10 Hz iki 20 kHz. Kaip ir elektrinės fliuktuacijos, stiprinamos MTS, verčiamos į skaitmeninį signalą ir atliekama Furjė transformacija. Vienalaikis optinio triukšmo matavimas su elektriniu triukšmu leidžia iškart apskaičiuoti abipusės koreliacijos koeficientą tarp elektrinių ir optinių fliuktuacijų. Spinduliuotei registruoti buvo naudojami skirtingi fotodiodai ir fotodetektoriai:

a) GaSb pagrindu pagamintiems LD – švino selenido fotodetektorius, registruojantis (1,5 – 4,8) μm bangos ilgio spinduliuotę;

b) GaAsBi LD – germanio fotodiodas, registruojantis (0,4 – 1,9) μm bangos ilgio spinduliuotę;

c) InGaN UV ŠD – silicio fotodiodas, jautrus (0,2 – 1,1) μm spinduliuotei; baltos šviesos ŠD – silicio fotodiodų matrica, sudaryta iš trijų skirtingam matomos šviesos spektrui jautrių dalių: raudonos, mėlynos ir žalios šviesos spinduliuotei. Šios matricos panaudojimo tikslas tiriant baltos šviesos ŠD – atskirti paties puslaidininkinio ŠD lusto spinduliuotę ir perspinduliuotą fosforo sluoksnio bei taip įvertinti jį kaip galimą triukšmo šaltinį. Plačiau apie šį eksperimentą 2.3 skyriuje.

Absoliučioji išmatuotojo elektrinio (ar optinio) triukšmo spektrinio tankio vertė apskaičiuojama palyginimo būdu su žinomos vertės etaloninės varžos (1.1 pav. $R_{\text{et}\,1}$ ir $R_{\text{et}\,2}$) kuriamu šiluminiu triukšmu:

$$S_U = \frac{\left\langle u^2_{\text{el (opt)}}(t)\right\rangle - \left\langle u^2_{\text{sist}}(t)\right\rangle}{\left\langle u^2_{\text{et}}(t)\right\rangle - \left\langle u^2_{\text{sist}}(t)\right\rangle} 4kT_0R_{\text{et}}; \qquad (1)$$

čia $\left\langle u^2_{\text{el (opt)}}(t)\right\rangle$, $\left\langle u^2_{\text{sist}}(t)\right\rangle$ ir $\left\langle u^2_{\text{et}}(t)\right\rangle$ – atitinkamai, tiriamo bandinio (elektrinio ar optinio triukšmo signalo), matavimo sistemos ir etaloninės varžos įtampos fliuktuacijų dispersijos siaurame dažnių intervale, T_0 – absoliučioji temperatūra. Formulė (1) išsamiau paaiškinta [77].

Abipusės koreliacijos koeficientas k dažnių intervale nuo 10 Hz iki 20 kHz tarp elektrinių ir optinių fliuktuacijų apskaičiuojamas pagal šią išraišką:

$$k = \frac{\left\langle u_{\text{el}}(t)\cdot u_{\text{opt}}(t)\right\rangle}{(\sigma^2_{\text{el}}\cdot\sigma^2_{\text{opt}})^{1/2}}; \qquad (2)$$

čia $\langle ... \rangle$ žymi vidurkinimą pagal laiką ir realizacijų skaičių; $\sigma^2_{\text{el}} = \left\langle u^2_{\text{el}}(t)\right\rangle$ ir

$\sigma^2_{\text{opt}} = \left\langle u^2_{\text{opt}}(t) \right\rangle$ – elektrinių ir optinių fliuktuacijų dispersijos tiriamame dažnių intervale. Koreliacijos koeficientas buvo apskaičiuotas ir kiekvienai dažnių oktavai. Tuo atveju, kai elektrinio ir optinio triukšmo signalai yra priešingų fazių, koreliacijos koeficientas yra neigiamas.

Triukšmų analizę praplečia šių papildomų elektrinių ir optinių charakteristikų: voltamperinių, spinduliuotės išeigos (galios) charakteristikų ir optinių spektrų tyrimas. LD ar ŠD spinduliuotės galia yra proporcinga fotodiodo apkrovos varžos R_{f} (1.1 pav.) registruojamai įtampai, toliau vadinamai fotoįtampa. Konkreti eksperimentinė matavimo aparatūra pateikta [48, 58, 59, 77, 78]. Matavimų metu visi tirtieji bandiniai buvo įtvirtinti ypatingai gero šiluminio laidumo metaliniuose (vario ar aukso) laikikliuose, o temperatūrai stabilizuoti ir kontroliuoti buvo naudojamas Peltjė elementas. Siekiant išvengti išorinio elektromagnetinio lauko poveikio triukšmų matavimai atlikti ekranuotoje laboratorijoje, o patys laikikliai su bandiniais ir fotodiodais buvo papildomai ekranuoti permalojaus dėžėje.

1.2. Koreliacinės analizės metodas

Bendru atveju ne visos žemadažnės lazerinio ar šviesos diodo elektrinės fliuktuacijos koreliuoja su optinėmis fliuktuacijomis: kontaktai arba elektriniai triukšmai pasyviojoje prietaiso dalyje nesukelia išspinduliuotos šviesos intensyvumo fliuktuacijų. Taigi, koreliacinės analizės metodas padeda įvertinti, kuri elektrinio triukšmo dalis yra susijusi su aktyviąja įtaiso dalimi, bei kokį įnašą į abipusės koreliacijos koeficientą turi atskiri elektrinių fliuktuacijų spektrinio tankio sandai.

Patogumo dėlei išmatuotieji elektrinių ir optinių fliuktuacijų spektriniai tankiai yra išreiškiami kaip suma statistiškai nepriklausomų $1/f$, $1/f^{\alpha}$, Lorenco tipo (patiems intensyviausiems g-r vyksmams) ir šratinio triukšmo sandų. Eksperimento metu matuojami triukšmai yra suminiai, t. y. tuo pačiu laiku turėti atskirai kiekvieną triukšmo sandą yra neįmanoma. Dėl to skaičiuojant suminę elektrinių ar optinių fliuktuacijų dispersiją konkrečioje dažnių oktavoje, reikia įskaityti ir matavimo sistemos savuosius triukšmus:

$$\begin{aligned}\sigma^2_{\text{el (opt) okt}} = \sigma^2_{\text{el (opt) } 1/f \text{ okt}} + \sigma^2_{\text{el (opt) } 1/f^{\alpha} \text{ okt}} + \sigma^2_{\text{el (opt) g-r okt}} \\ + \sigma^2_{\text{el (opt) šr okt}} + \sigma^2_{\text{el (opt) sist okt}};\end{aligned} \tag{3}$$

čia $\sigma^2_{\text{el (opt) } 1/f \text{ okt}}$, $\sigma^2_{\text{el (opt) } 1/f^{\alpha} \text{ okt}}$, $\sigma^2_{\text{el (opt) g-r okt}}$ ir $\sigma^2_{\text{el (opt) šr okt}}$ žymi elektrinių (optinių) $1/f$, $1/f^{\alpha}$, g-r ir šratinio triukšmo sandų dispersijas; $\sigma^2_{\text{el (opt) sist okt}}$ – elektrinio (optinio) triukšmo matavimo sistemų savųjų triukšmų dispersijas.

Kiekvienas dispersijos sandas $\sigma^2_{j\,\mathrm{okt}}$ randamas integruojant atitinkamą triukšmo spektrinį sandą $S_j(f)$ dažnių oktavos rėžiuose $f_2 = 2f_1$:

$$\sigma^2_{j\,\mathrm{okt}} = \int_{f_1}^{f_2} S_j(f)\mathrm{d}f. \tag{4}$$

Taip pat kiekvienas elektrinio triukšmo spektrinis sandas $S_{\mathrm{el}\,j}(f)$ gali būti išreikštas kaip koreliuojančios $S_{\mathrm{el}\,j\,\mathrm{kor}}(f)$ ir nekoreliuojančios $S_{\mathrm{el}\,j\,\mathrm{nekor}}(f)$ dalių suma:

$$S_{\mathrm{el}\,j}(f) = S_{\mathrm{el}\,j\,\mathrm{kor}}(f) + S_{\mathrm{el}\,j\,\mathrm{nekor}}(f) = d_j S_{\mathrm{el}\,j}(f) + (1-d_j)S_{\mathrm{el}\,j}(f); \tag{5}$$

čia dydis d_j rodo, kuri elektrinio triukšmo spektrinio sando $S_{\mathrm{el}\,j}(f)$ dalis yra susijusi su išspinduliuotos šviesos intensyvumo fliuktuacijomis. Taigi, koreliuojantys triukšmai yra tik iš aktyviosios diodo srities ir to paties spektro: $u_{\mathrm{el}\,1/f\,\mathrm{akt}}(t)$ ir $u_{\mathrm{opt}\,1/f}(t)$, $u_{\mathrm{el}\,1/f^{\alpha}\,\mathrm{akt}}(t)$ ir $u_{\mathrm{opt}\;1/f^{\alpha}}(t)$, $u_{\mathrm{el\,g\text{-}r\,akt}}(t)$ ir $u_{\mathrm{opt\,g\text{-}r}}(t)$. Nors eksperimentiniame optinių fliuktuacijų spektre buvo stebimas šratinio triukšmo sandas, tiriamų bandinių atveju šratinio triukšmo indėlis į koreliacijos koeficientą yra nykstamai mažas (elektriniame triukšme šio sando lygis daug žemesnis (3 – 5 eilėmis) už likusių spektrinių sandų lygį).

Dabar abipusės koreliacijos koeficientas gali būti užrašytas taip:

$$k_{\mathrm{okt}} = \frac{\sum_{j=1}^{3}(d_j\sigma^2_{j\,\mathrm{el\,okt}}\cdot\sigma^2_{j\;\mathrm{opt\,okt}})^{1/2}}{(\sigma^2_{\mathrm{el\,sum\,okt}}\cdot\sigma^2_{\mathrm{opt\,sum\,okt}})^{1/2}}; \tag{6}$$

čia indeksas $j = 1$ žymi $1/f$ tipo fliuktuacijas, $j = 2$ – $1/f^{\alpha}$ ir $j = 3$ – g-r tipo fliuktuacijas. Dydžiai d_j randami lyginant eksperimento metu gautą koreliacijos koeficientą su apibrėžtu lygtimi (6) [43, 44].

1.3. Generacinio-rekombinacinio triukšmo spektroskopija

Aiškaus generacinio-rekombinacinio triukšmo sando egzistavimas išmatuotame spektriniame tankyje leidžia tolesnei analizei pritaikyti g-r triukšmo spektroskopiją ir taip nustatyti bei identifikuoti už šį sandą atsakingą pagavimo lygmenį puslaidininkyje ar puslaidininkiniame įtaise [60, 79–81]. Šiam tikslui pasiekti atliekami spektrinių tankių matavimai skirtingose temperatūrose. Kintant temperatūrai Fermio lygmens padėtis pagavimo lygmens atžvilgiu puslaidininkyje kinta [80]. Kai Fermio energijos lygmuo sutampa su pagavimo, egzistuoja maksimali tikimybė krūvininkams

būti pagautiems ar išlaisvintiems iš šio pagavimo centro, t. y. šis pagavimo lygmuo yra pusiau užpildytas, o normuotas spektrinis tankis (S_U/U^2, S_I/I^2 ar S_R/R^2) priklausomybėje nuo dažnio įgyja didžiausią vertę [48].

Atlikus spektrinių tankių $S(f)$ matavimus, juos patogu atvaizduoti kaip spektrinio tankio ir dažnio sandaugos $S(f)f$ priklausomybes nuo dažnio esant skirtingoms temperatūroms. Ties kiekviena temperatūros verte nustatomas dažnis f_0, ties kuriuo $S(f)f$ vertė yra maksimali. Dažnį f_0 atitinkanti laiko konstanta:

$$\tau = 1/(2\pi f_0). \tag{7}$$

Ši trukmė vadinama efektyviąja krūvininkų relaksacijos trukme ir išreiškiama:

$$1/\tau = 1/\tau_e + 1/\tau_c. \tag{8}$$

čia τ_e – vidutinė krūvininko išlaisvinimo trukmė, o τ_c – vidutinė krūvininko pagavimo trukmė [79].

Vykstant krūvininkų pagavimui ir išlaisvinimui dėka šiluminės aktyvacijos, trukmė τ yra proporcinga $\exp[\Delta E/(kT)]$ (čia ΔE – aktyvacijos energija, k – Bolcmano konstanta). Atvaizdavus $\ln(\tau)$ priklausomybę nuo atvirkštinės temperatūros $1/(kT)$, iš kreivės polinkio galima nustatyti pagavimo lygmens aktyvacijos energiją ΔE [79, 81] bei įvertinti krūvininko pagavimo skerspjūvį $\sigma = 1/(\tau_c v_t n)$, čia v_t – šiluminis krūvininkų greitis temperatūroje T, n – laisvųjų krūvininkų tankis [60].

2. REZULTATAI IR JŲ APTARIMAS

Šiame skyriuje aptariami rezultatai, pateikti su disertacijos tema susijusiose publikacijose, bei pateikiamas jų apibendrinimas. Rezultatų aptarimas suskirstytas pagal bandinių medžiagas, kurių pagrindu pagaminti šviesos ar lazeriniai diodai.

2.1. GaSb lazerinių diodų žemadažnio triukšmo tyrimai

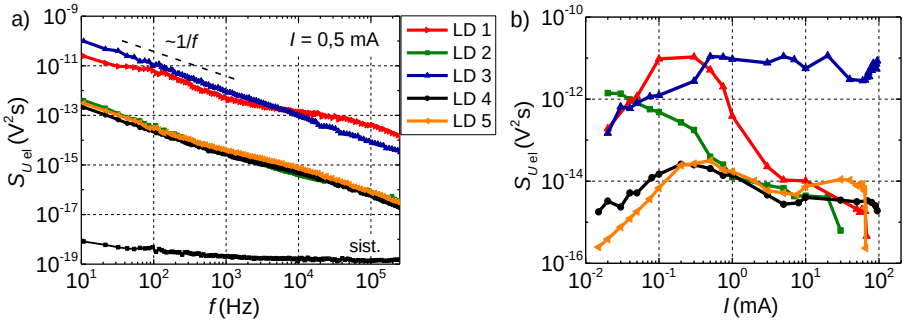
Pirmoji tirtų bandinių grupė yra GaSb pagrindu pagaminti LD. Visi šie bandiniai buvo užauginti ant n^+ GaSb pagrindo MPE būdu. Visų LD apvalkaliniai sluoksniai yra AlGaAsSb, o kvantinės duobės – I-ojo tipo. Siekiant, kad LD spinduliuotų vieną skersinę optinę modą, buvo suformuotas siauras (3 – 5) μm keterinis bangolaidis, kurio ilgis 1 mm. Bandiniai buvo suskirstyti į grupes pagal jų savybes ir pasirinktų LD rezultatai palyginti (2.1 lentelė). Pagrindiniai GaSb LD rezultatai publikuoti [P1] ir [P2] straipsniuose. Tyrimai buvo atlikti priešslenkstinėje, lazerinės generacijos veikoje ir esant atvirkštiniam piešįtampiui.

2.1 lentelė. Tirti bandiniai ir jų savybės

Bandiniai	**LD 1**	**LD 2**	**LD 3**
KD skaičius	2	2	3
KD/barjeras	GaInAsSb/AlGaAsSb		GaInAsSb/ AlGaInAsSb
Slenkstinė srovė (mA)	68	36	96
Centrinis bangos ilgis (μm)	2,44 (400 mA)	2,1 (300 mA)	2,93 (200 mA)
Veidrodžių dangos	Yra	Yra	Nėra
Bandiniai	**LD 4**	**LD 5**	**Didelės galios LD 6**
KD skaičius	2	2	2
KD/barjeras	GaInAsSb/AlGaAsSb		GaInSb/ AlGaAsSb
Slenkstinė srovė (mA)	100	67	550
Centrinis bangos ilgis (μm)	2,43 (300 mA)	2,43 (250 mA)	1,95 (1,3 A)
Veidrodžių dangos	Yra	Nėra	Nėra

2.1.1. Elektrinio triukšmo charakteristikos priešslenkstinėje veikoje

Didžiosios dalies tirtų bandinių elektrinio triukšmo spektriniai tankiai priešslenkstinėje veikoje yra $1/f^{\alpha}$ pavidalo, tačiau kai kurių LD elektrinės fliuktuacijos turi papildomų g-r triukšmo spektrinių sandų (2.1 pav. a). Jie stebimi tik tekant tam tikro stiprio srovei, pavyzdžiui, LD 1 atveju, kai I = 0,5 mA, o LD 4 ir LD 5, kai I = 0,02 mA. G-r triukšmo spektroskopijos pagalba buvo nustatytos pagavimo lygmenų, atsakingų už šiuos spektrinius sandus, aktyvacijos energijos. Jos yra pasiskirsčiusios intervale nuo 0,1 eV iki apytiksliai pusės barjero draudžiamosios energijos vertės (0,4 eV), o tai leidžia teigti, kad šio g-r triukšmo šaltinis yra barjeriniuose sluoksniuose.

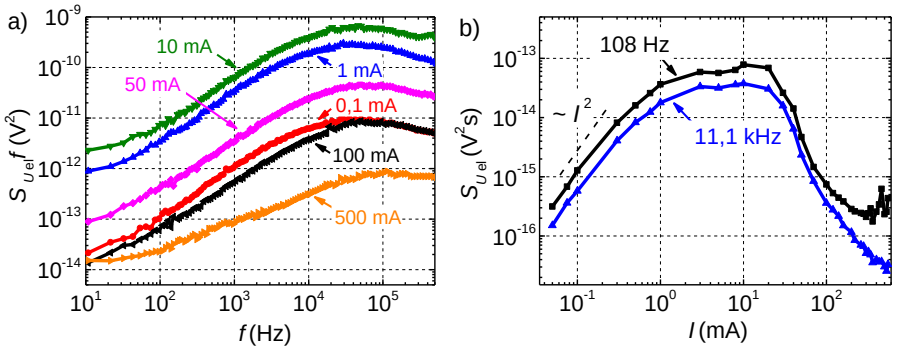


2.1 pav. a) Bandinių LD 1 – LD 5 elektrinio triukšmo spektriniai tankiai $S_{U\,\mathrm{el}}$, kuomet bandiniais teka 0,5 mA stiprio tiesioginė srovė („sist.“ žymi matavimo sistemos savųjų triukšmų lygį); b) elektrinio triukšmo spektrinių tankių $S_{U\,\mathrm{el}}$ priklausomybės nuo LD tiesioginės srovės I priešslenkstinėje veikoje esant 108 Hz dažniui.

Tiriant žemadažnes fliuktuacijas, yra svarbu nagrinėti elektrinio triukšmo priklausomybę nuo LD tekančios srovės. Spektrinio tankio S_U proporcingumas srovės stipriui teikia informacijos apie tekančios srovės pobūdį bei tuo pačiu – triukšmo kilmę [49]. Paprastai srovės fliuktuacijų spektrinis tankis S_I *pn* sandūros įtaisuose yra proporcingas tiesioginei srovei I [82, 83], tuomet įtampos fliuktuacijų spektrinis tankis $S_U \sim S_I \cdot R_{\mathrm{dif}}^2 \sim 1/I$, kadangi diodo diferencialinė varža $R_{\mathrm{dif}} \sim 1/I$. Kaip matyti iš 2.1 pav. b), elektrinio triukšmo priklausomybėse nuo srovės egzistuoja didesnis ar mažesnis maksimumas, kur S_U didėja proporcingai I^2 apytiksliai iki 0,3 mA. Tai rodo augantį pagavimo lygmenų užimtumą [84]. Bandinio LD 3 priklausomybė išsiskiria – lyginant su kitais bandiniais nėra aiškaus spektrinio tankio maksimumo, o triukšmo lygis išlieka aukštas iki pat lazerinės generacijos pradžios. Šiuo atveju didesnį defektingumą lemia LD

bangolaidinis sluoksnis, kadangi tik LD 3 grupės bandiniai turi penkianarį AlGaInAsSb darinį. Šiam teiginiui pagrįsti buvo atlikti abipusės koreliacijos koeficiento tarp elektrinių ir optinių fliuktuacijų matavimai lazerinės generacijos veikoje.

Dar didesniais triukšmo charakteristikų skirtumais pasižymi didelės galios LD 6 bandinių grupė. Jų elektrinių fliuktuacijų spektriniai tankiai yra Lorenco pavidalo visame tirtame srovių intervale. Tokį spektro pavidalą lemia g-r triukšmas [37, 80]. Patogumo dėlei 2.2 pav. a) pateikti normuoti spektriniai tankiai $S_{U\,\mathrm{el}}f$, iš kurių maksimumų galima lengvai nustatyti dažnį f_0 ir įvertinti relaksacijos trukmę remiantis (7): $\tau \approx 3.7$ µs. Dažnis f_0 praktiškai nekinta keičiant LD tekančią srovę. Elektrinių fliuktuacijų priklausomybė nuo srovės stiprio dar labiau skiriasi nuo minėtosios tipinės *pn* sandūrai, kuomet $S_U \sim 1/I$, – šiuo atveju priklausomybėje stebimas vienas aiškus triukšmų maksimumas (2.2 pav. b). Tam tikrais atvejais technologinės variacijos LD gamybos metu, pavyzdžiui, temperatūros pokytis ar atkaitinimo procesai, gali lemti stebimą didelį g-r triukšmą. Šių fliuktuacijų savybės ir kilmė plačiau bus aptarta 2.1.3 skirsnyje.

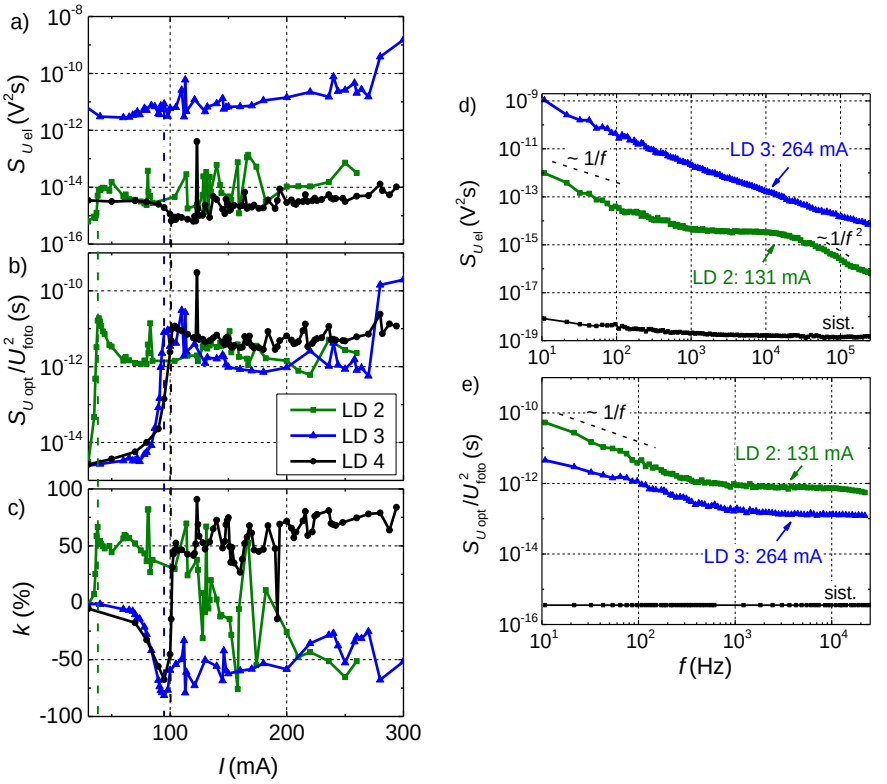


2.2 pav. a) Normuoti LD 6 elektrinio triukšmo spektriniai tankiai $S_{U\,\mathrm{el}}f$ tekant skirtingo stiprio srovėms tiesiogine kryptimi; b) LD 6 elektrinio triukšmo spektrinių tankių $S_{U\,\mathrm{el}}$ priklausomybės nuo LD tiesioginės srovės I esant 180 Hz ir 11,1 kHz dažniui.

2.1.2. Triukšmai lazerinės generacijos veikoje

Lazerinės generacijos metu elektrinio ir optinio triukšmo priklausomybėse nuo srovės stiprio yra gausu smailių (2.3 pav. a, b), kuomet triukšmo lygis staigiai išauga (net iki dviejų eilių). Šias smailes lemia modų šuolių reiškinys. Jo metu vyksta šuoliškas spinduliuojamos modos bangos ilgio kitimas, kai LD stiprinimo spektro didžiausia vertė pasislenka ties kitos

išilginės modos bangos ilgiu [46]. Tam tikru metu gali būti spinduliuojamos ir pora panašaus intensyvumo išilginių modų (vyksta modų konkurencija).



2.3 pav. a) Elektrinio $S_{U\,\mathrm{el}}$ ir b) normuoto optinio triukšmo $S_{U\,\mathrm{opt}}/U^2_{\mathrm{foto}}$ priklausomybės nuo srovės stiprio I esant 108 Hz dažniui lazerinės generacijos veikoje; c) abipusės koreliacijos koeficiento k priklausomybė nuo srovės stiprio I visame tirtame dažnių intervale nuo 10 Hz iki 20 kHz (čia punktyrinės linijos žymi slenkstinės srovės vertes); LD 2 ir LD 3 d) elektrinio $S_{U\,\mathrm{el}}$ ir e) normuoto optinio triukšmo $S_{U\,\mathrm{opt}}/U^2_{\mathrm{foto}}$ spektriniai tankiai vykstant modų šuoliams.

Nemaži skirtumai egzistuoja tarp tirtų bandinių abipusės koreliacijos koeficiento tarp elektrinių ir optinių fliuktuacijų priklausomybių nuo srovės stiprio (2.3 pav. c). Nepaisant modų šuolių smailių (stabilioje lazerinės generacijos veikoje) galima pastebėti, kad LD 1, LD 4 ir LD 5 grupės bandinių koreliacijos koeficientas yra teigiamas, LD 3 – neigiamas, o LD 2 atveju – pereinantis iš teigiamo į neigiamą. Teigiamas koreliacijos koeficientas rodo, kad daugelis defektų, atsakingų už koreliuotas elektrines ir optines fliuktuacijas, yra aktyviojoje LD srityje. Šie defektai atsitiktinai moduliuoja laisvųjų krūvininkų skaičių aktyviojoje srityje, o tai lemia tos

pačios fazės išspinduliuotų fotonų skaičiaus fliuktuacijas. Pažymėjus elektrines fliuktuacijas $\Delta u_{el}(t)$ ir joms įgijus teigiamą ar neigiamą ženklą, optinės fliuktuacijos $\Delta u_{opt}(t)$ taip pat įgis tokį pat ženklą. Neigiamas koreliacijos koeficientas rodo nuotėkio srovės iš aktyviosios srities egzistavimą, kuomet didžioji dalis defektų yra sąlytyje su aktyviąja sritimi. Jie formuoja defektų kanalus ir taip perskirsto tekančią srovę tarp KD ir gretimų sluoksnių. Augant nuotėkio srovei, mažėja krūvininkų skaičius aktyviojoje srityje bei išspinduliuotų fotonų skaičius. Tai atitinka situaciją, kai formulėje (2) dydis $\Delta u_{el}(t)$ yra teigiamas, o $\Delta u_{opt}(t)$ tampa neigiamas, taigi, elektrinės ir optinės fliuktuacijos yra priešingų fazių [58]. Neigiamu abipusės koreliacijos koeficientu tarp elektrinių ir optinių fliuktuacijų yra linkę pasižymėti mažiau patikimi bandiniai, kaip rodo atlikti telekomunikacinių InGaAsP LD tyrimai [68].

Modų šuolių metu elektrinių ir optinių fliuktuacijų spektriniai tankiai pakinta – iš $1/f^{\alpha}$ tipo (stabilioje veikoje) į Lorenco. Tai reiškia, kad modų šuolių metu už išaugusią triukšmo amplitudę yra atsakingi krūvininkų pagavimo ar išlaisvinimo reiškiniai iš defektų suformuotų g-r centrų. Konkretaus modų šuolio metu atsitiktinai išauga kurio nors g-r centro įtaka elektrinėms fliuktuacijoms. LD 2 bandiniui tokių spektrų pavyzdys pateiktas 2.3 pav. d) ir e). Kaip ir InGaAsP FP LD atveju [46, 47], šie Lorenco pavidalo elektriniai ir optiniai triukšmų sandai stipriai teigiamai ar neigiamai koreliuoja, o tai rodo, kad už šias fliuktuacijas atsakingi g-r centrai yra aktyviojoje LD srityje ar sąlytyje su ja. Atitinkamų g-r procesų relaksacijos trukmės atskirų modų šuolių metu yra skirtingos. Taigi, šias fliuktuacijas lemia g-r centrai su besiskiriančiais krūvininkų pagavimo centrų skerspjūviais.

Kaip ir priešslenkstinėje veikoje, taip ir lazerinės generacijos veikoje LD 3 bandinio, spinduliuojančio didžiausią bangos ilgį, elektrinio triukšmo lygis yra aukščiausias (2.3 pav. a). Šio LD spinduliuotės galia – mažiausia. Kaip parodyta [85], GaSb lazerinių diodų su AlGaInAsSb barjerais spinduliuotės galia ir darinio kokybė yra ypatingai jautrūs auginimo sąlygoms: temperatūrai bei įtempimams, atsiradusiems dėl nevisiško gretimų sluoksnių gardelių sutapimo [86]. Taigi, technologiškai išauginti tokius darinius su penkianariais junginiais yra sudėtinga, o triukšmo charakteristikos tai pagrindžia. Vienintelio LD 3 elektrinės fliuktuacijos net ir modų šuolio metu išlieka $1/f^{\alpha}$ (2.3 pav. d), o neigiamas koreliacijos koeficientas patvirtina didelį penkianarių barjerinių sluoksnių defektingumą.

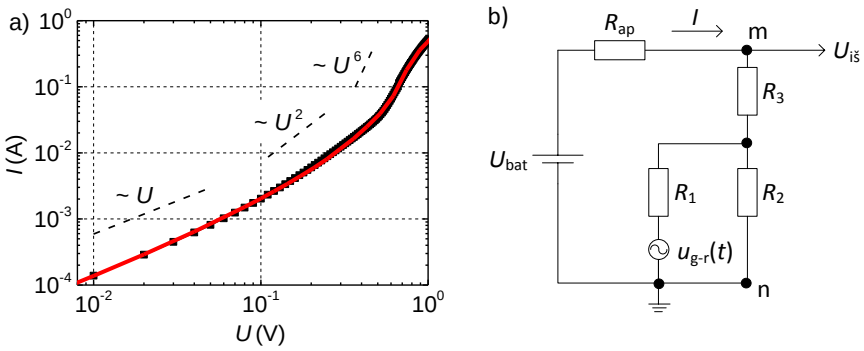
2.1.3. Generacinis-rekombinacinis triukšmas GaSb lazeriniuose dioduose ir jo kilmė

Yra žinoma, kad egzistuoja stiprus ryšys tarp LD ar ŠD triukšmo ir voltamperinių charakteristikų [83, 87, 88]. Taigi, norint kiek galima daugiau sužinoti apie g-r triukšmą ir jo kilmę LD 6 grupės bandiniuose, pirmiausia reikia detaliai panagrinėti šių LD *I-U* charakteristikas. Remiantis 2.4 pav. a) ir kaip parodyta [P2], ją patogu aprašyti tokiu daugianariu:

$$I = \mathrm{a}U + \mathrm{b}U^2 + \mathrm{c}U^n; \tag{9}$$

čia a, b, c – koeficientai, o laipsnio rodiklis n parenkamas siekiant geriausio sutapimo su eksperimentine *I-U* kreive.

Atsižvelgiant į tai, 2.4 pav. b) yra pateikta ekvivalentinė LD 6 elektrinė grandinė. Nuotėkio kanalo varža R_1 įvertinama iš tiesinės (ominės) *I-U* charakteristikos dalies, ji nuo pridėtos įtampos nepriklauso ir lygi 75 Ω. Varža R_2 atžvilgiu R_1 elgiasi kaip šuntuojanti diferencialinė LD varža ir randama taip $R_2 = (\mathrm{d}U/\mathrm{d}I) - R_3$, čia R_3 – kontaktų ir stipriai legiruotų n^+ ir p^+ sričių varža (nuoseklioji varža), ji daug kartų mažesnė už R_1.

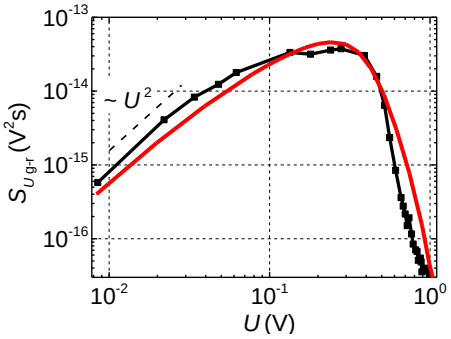


2.4 pav. a) Tipinė LD 6 bandinių grupės voltamperinė charakteristika: juodi simboliai žymi eksperimentinius duomenis, raudona kreivė – *I-U* charakteristika aprašyta (9); b) ekvivalentinė LD grandinė su g-r įtampos triukšmo šaltiniu, čia $R_{ap} >> R_{mn}$.

Tiesiniuose įtaisuose g-r triukšmas paprastai didėja proporcingai srovės (ar įtampos) kvadratui [89]. Jei g-r triukšmo šaltinis yra R_1 varžos nuotėkio kanalas, tai įtampos fliuktuacijų spektrinis tankis gali būti apskaičiuojamas taip:

$$S_{U\,\mathrm{g-r}} = \mathrm{A}U^2 \frac{\tau}{1+(2\pi f\tau)^2} \cdot \left(\frac{R_2}{R_1+R_2}\right)^2; \tag{10}$$

čia dydis A žymi triukšmo šaltinio intensyvumą. Eksperimentinių rezultatų ir apskaičiuotų pagal (10) palyginimas pateiktas 2.5 pav. Matyti, kad kol LD veikia tiesinėje *I-U* srityje, elektrinis triukšmas $S_{U\,\mathrm{g\text{-}r}}$ auga proporcingai U^2. Kai $U > 0{,}3$ V, $S_{U\,\mathrm{g\text{-}r}}$ mažėja, nes diferencialinė LD varža R_2 šuntuoja varžą R_1. Geras sutapimas tarp eksperimentinių ir apskaičiuotų spektrinių tankių verčių patvirtina iškeltą idėją, kad R_1 – tai nuotėkio kanalo varža tarp n^+ GaSb ir p^+ GaSb kontaktų.



2.5 pav. Įtampos fliuktuacijų spektrinio tankio $S_{U\,\mathrm{g\text{-}r}}$ priklausomybė nuo tiesioginės įtampos *U* esant 11,1 kHz dažniui: juodi simboliai žymi eksperimentinius duomenis, raudona kreivė apskaičiuota pagal (10).

Atlikus spektrinių tankių matavimus temperatūrų intervale nuo 230 K iki 295 K, nustatyta g-r vyksmo aktyvacijos energija $\Delta E = 0{,}37$ eV. Ta pati procedūra buvo atlikta ir esant pridėtam atvirkštiniam priešįtampiui. Pastebėta, kad *I-U* charakteristika taip pat pasižymi tiesine dalimi, spektriniai tankiai yra Lorenco pavidalo su ta pačia relaksacijos trukme τ, o įvertinta aktyvacijos energija sutampa su nustatytąja matuojant tiesiogine kryptimi. Tai, kad kanalo varža R_1 nepriklauso nuo tekančios srovės krypties ir yra to paties dydžio, leidžia teigti, kad šis nuotėkio kanalas yra paviršiuje. Jį lemia didelis defektų su 0,37 eV aktyvacijos energija tankis bandinio paviršiuje.

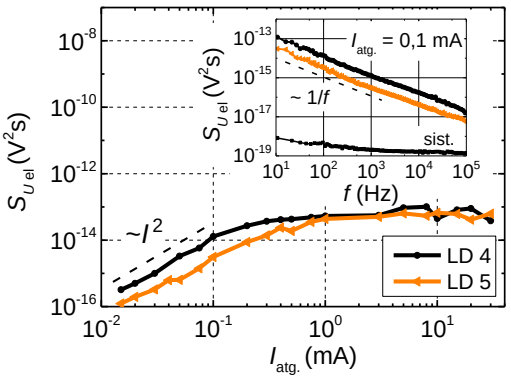
2.1.4. Veidrodžių pasyvavimo įtaka žemadažnio triukšmo charakteristikoms

Kaip buvo minėta įvade, lazerinių diodų triukšmai esant pridėtam atvirkštiniam priešįtampiui paprastai tiriami siekiant įvertinti ir atrasti galimus skirtumus tarp labai panašios kokybės bandinių. Skeliant kristalą veidrodžių formavimo metu yra pažeidžiamas kristalo periodiškumas, o tai lemia didelį paviršinių būsenų tankį [90, 91]. Prie tokio paviršiaus lengvai

jungiasi aplinkos atomai ir formuojasi defektai. Tinkamas pasyvavimo procesas sumažina paviršinių būsenų tankį bei rekombinacijos centrų skaičių paviršiuje, taigi ir žemadažnio triukšmo lygį [55].

Tirtieji LD 4 ir LD 5 grupės bandiniai yra tos pačios gamybos partijos, t. y. jų epitaksinė struktūra yra vienoda ir išauginta tomis pačiomis sąlygomis. Vienintelis skirtumas, kad bandinių LD 4 veidrodinės sienelės yra padengtos specialiomis dangomis, o LD 5 – ne. Stipriai atspindinčiai (95 %) sienelei padengti naudotas Si/SiO_2, o neatspindinčiai (iki 5 %) – Ta_2O_5. Akivaizdžių skirtumų tarp abiejų bandinių grupių elektrinio triukšmo charakteristikose tiesiogine kryptimi nepastebėta (2.1 pav.).

Atgaline kryptimi matavimai atlikti saugiai nepramušant *pn* sandūros. Visame tirtame srovių intervale elektrinės fliuktuacijos yra $1/f^{\alpha}$ (2.6 pav.). Mažų atgalinių srovių intervale elektrinis triukšmas auga proporcingai I^2, kas rodo, kad pagrindinis triukšmo šaltinis yra nuotėkio varžos fliuktuacijos [49]. Toliau didinant srovę, S_U sotinasi dėl diferencialinės varžos šuntavimo.



2.6 pav. LD 4 ir LD 5 elektrinio triukšmo $S_{U\,el}$ priklausomybės nuo atgalinės srovės $I_{atg.}$ esant 108 Hz dažniui. Įterptinis paveikslas vaizduoja elektrinio triukšmo spektrus tekant $I_{atg.}$ = 0,1 mA atgalinei srovei.

Deja, bet bandinių su dangomis (LD 4) elektrinio triukšmo lygis yra šiek tiek didesnis negu LD be dangų (iki ~ 0,2 mA), – tai rodo, kad veidrodžių pasyvavimo procesas yra neoptimalus ir jam turi būti skiriamas didesnis dėmesys.

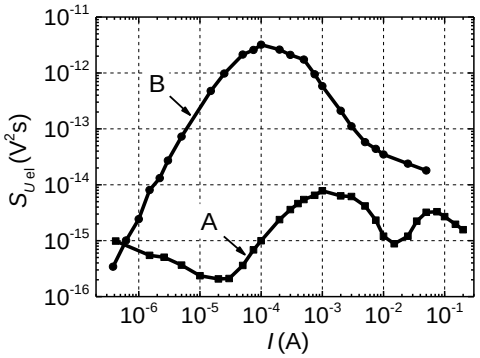
2.2. GaAsBi lazerinių diodų žemadažnio triukšmo tyrimai

Antroji bandinių grupė – tai bismidiniai lazeriniai diodai. Visi tirti lazeriniai diodai buvo užauginti ant *n*-tipo GaAs pagrindo MPE būdu. Aktyviąją sritį sudaro penkios 8 nm storio $GaAs_{1-x}Bi_x$ I-ojo tipo KD (x = 8 %), apsuptos GaAs barjerų. Apvalkaliniai AlGaAs sluoksniai buvo užauginti 600 °C, KD – 360 °C, o barjerai – 450 °C temperatūroje. FP rezonatorių ilgis (2 – 3) mm, o LD veidrodžiai suformuoti skėlimo būdu ir papildomomis dangomis nedengti. Spinduliuojamas bangos ilgis lygus 1,09 μm.

Svarbiausi GaAsBi LD rezultatai publikuoti [P3] straipsnyje. Buvo atlikti matavimai priešslenkstinėje veikoje (iki 100 mA) tiesiogine kryptimi, kuomet temperatūros stabilizavimas leido patikimai išvengti LD savikaitimo. Dėl šios priežasties bei siekiant išvengti aktyviosios srities sugadinimo, lazerinė generacija galima tik impulsinėje veikoje.

2.2.1. Elektrinio triukšmo charakteristikos

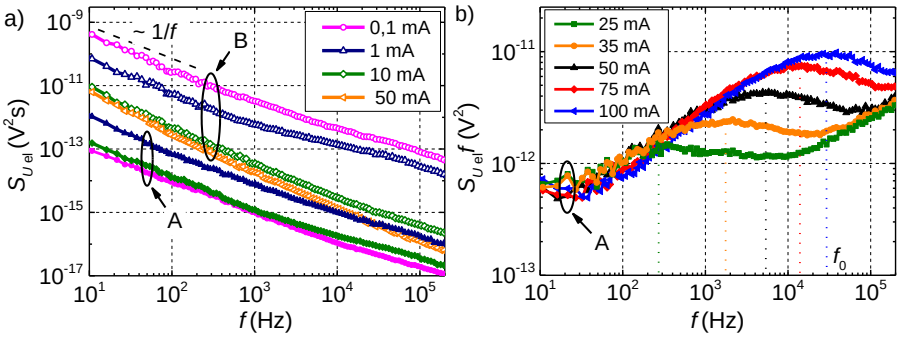
Atsižvelgiant į skirtingas elektrinio triukšmo priklausomybes nuo tiesioginės srovės stiprio, tirti GaAsBi lazeriniai diodai gali būti suskirstyti į dvi gupes (2.7 pav.). A grupės LD turi porą triukšmų maksimumų minėtoje priklausomybėje, o B – tik vieną. Nepaisant to, kad A grupės bandinių elektrinių fliuktuacijų lygis nežymiai skiriasi tarpusavyje, bet tirtame srovių intervale stebimų maksimumų skaičius $S_{U\,\mathrm{el}}(I)$ priklausomybėse yra pastovus.



2.7 pav. A ir B grupės bandinių tipinės elektrinio triukšmo spektrinių tankių $S_{U\,\mathrm{el}}$ priklausomybės nuo tiesioginės srovės I esant 1 kHz dažniui.

Šių grupių lazerinių diodų triukšmų spektriniai tankiai taip pat skiriasi. B grupės LD pasižymi $1/f^{\alpha}$ elektrinėmis fliuktuacijomis visame tirtame

tiesioginės srovės intervale (2.8 pav. a). A grupės bandinių elektrinis triukšmas taip pat yra $1/f^{\alpha}$, tačiau tik iki antrojo triukšmų maksimumo (2.8 pav. a), kuris skirtingiems LD stebimas intervale nuo 15 mA iki 25 mA (2.7 pav.). Jam pasirodžius, elektrinių fliuktuacijų spektrinis tankis pakinta ir tampa būdingu g-r triukšmui – Lorenco pavidalo (2.8 pav. b).



2.8 pav. a) A grupės (iki antrojo triukšmų maksimumo, $I < 15$ mA) ir B grupės bandinių elektrinio triukšmo spektriniai tankiai tekant skirtingo stiprio tiesioginei srovei; b) A grupės LD normuoto elektrinio triukšmo spektriniai tankiai $S_{U\,el}f$, kai $I > 15$ mA (antrojo triukšmų maksimumo srovių intervale).

2.2.2. Lazerinių diodų ekvivalentinių grandinių sudarymas

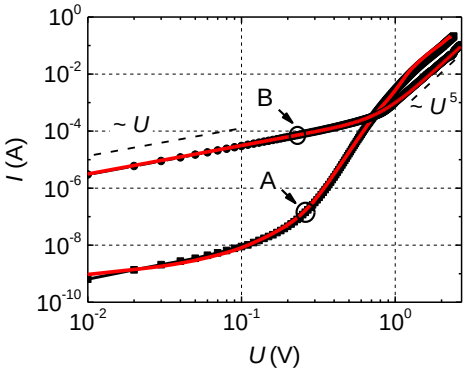
Dideli skirtumai yra pastebimi A ir B grupių voltamperinėse charakteristikose (2.9 pav.). B grupės LD *I-U* charakteristika visai nepanaši į eksponentinę, kuri yra būdinga *pn* sandūrai, ir, panašiai kaip ir GaSb LD atveju (2.1.3 skirsnis), gali būti aprašyta daugianariu:

$$I = \mathrm{a}U + \mathrm{b}U^{n}; \tag{11}$$

čia a, b – koeficientai, o $n > 1$. A grupės *I-U* charakteristika aprašoma įprastai – eksponentine priklausomybe:

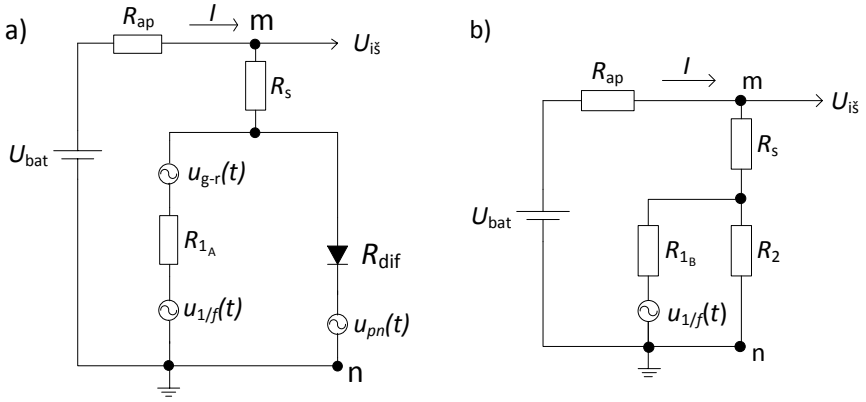
$$I = I_0 \exp[q(U - IR_{\mathrm{S}}) / (\eta kT)] + \mathrm{a}_1 U; \tag{12}$$

I_0 – diodo soties srovė, q – elektrono krūvis, R_{S} – LD nuoseklioji varža, η – *I-U* charakteristikos neidealumo koeficientas, a_1 – koeficientas, čia $\exp[q(U - IR_{\mathrm{S}})/(\eta kT)] >> I_0$.



2.9 pav. Tipinės A ir B grupių LD voltamperinės charakteristikos tiesiogine kryptimi: juodi simboliai žymi eksperimentinius duomenis, raudonos kreivės apskaičiuotos pagal (11) ir (12).

Atsižvelgiant į 2.7 ir 2.9 pav. bei (11) ir (12) išraiškas, pasiūlytos A ir B grupių LD ekvivalentinės grandinės su įtampos triukšmų šaltiniais (2.10 pav.). Čia R_1 žymi nuotėkio kanalo varžą, kuri A ir B grupių bandiniams skirtingai priklauso nuo įtampos. 2.10 pav. a) diodo simbolis žymi idealios *pn* sandūros diferencialinę varžą $R_{\text{dif}} = \mathrm{d}U_{pn}/\mathrm{d}I$. B grupės lazerinių diodų diferencialinė varža pažymėta R_2 (2.10 pav. b), kadangi jų *I-U* charakteristikos aprašomos ne eksponentinėmis priklausomybėmis. Apskaičiuotosios šių varžų priklausomybės nuo tiesioginės įtampos pavaizduotos 2.11 pav. a). Toks atvaizdavimas yra ypatingai svarbus siekiant paaiškinti elektrinio triukšmo kilmę bandiniuose.



2.10 pav. a) A ir b) B grupių LD ekvivalentinės elektrinės grandinės su įtampos triukšmų šaltiniais, $R_{\text{ap}} >> R_{\text{mn}}$.

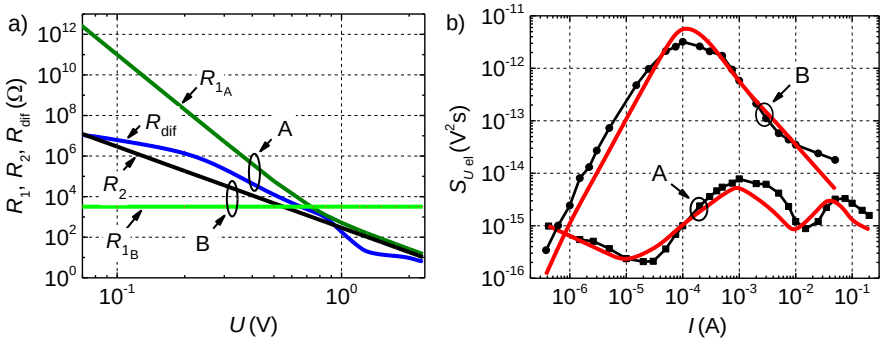
Kaip jau buvo minėta, $1/f$ fliuktuacijoms *pn* sandūroje yra būdinga, kad $S_U \sim 1/I$. Atitinkamas triukšmo šaltinis 2.10 pav. a) pažymėtas $u_{pn}(t)$. Jo kuriamos fliuktuacijos

$$S_{U\,pn} = \frac{\mathrm{C}}{f} \cdot \frac{1}{I^{\gamma}}; \tag{13}$$

yra stebimos A grupės bandiniuose iki I = 0,01 mA (2.7 pav.), čia C – žymi triukšmo intensyvumą, o laipsnio rodiklis γ artimas 1. Toliau didinant tekančią srovę per LD, elektrinio triukšmo S_U proporcingumas srovės stipriui kinta. Kadangi A grupės bandinių pirmajam triukšmo maksimumui yra būdingos $1/f^{\alpha}$ fliuktuacijos, o antrajam – g-r tipo fliuktuacijos, tai ekvivalentinė A grupės LD grandinė turi būti papildyta lygiagrečiai *pn* sandūrai egzistuojančiais įtampos triukšmų šaltiniais, atitinkamai $u_{1/f}(t)$ ir $u_{\text{g-r}}(t)$. Taigi, kai $I > 0{,}01$ mA, suminis elektrinių įtampos fliuktuacijų spektrinis tankis yra lygus šių nepriklausomų $1/f^{\alpha}$ ir g-r triukšmo šaltinių sumai:

$$S_{U\,\mathrm{A}} = S_{U\,1/f} + S_{U\,\text{g-r}}. \tag{14}$$

B grupės atveju stebimos tik $1/f^{\alpha}$ elektrinės fliuktuacijos, jas 2.10 pav. b) žymi triukšmo šaltinis $u_{1/f}(t)$. Tiek A, tiek B LD įtampos fliuktuacijų spektriniai tankiai buvo apskaičiuoti ir palyginti su eksperimentiniais (2.11 pav. b). Skaičiuojant triukšmo šaltinių vertes, svarbu įskaityti šuntuojančių varžų įtaką (pavyzdys – (10) išraiška). Triukšmų spektriniams tankiams apskaičiuoti naudotos pilnos išraiškos yra pateiktos [P3].



2.11 pav. a) Apskaičiuotos varžų R_1, R_2 ir R_{dif} priklausomybės nuo tiesioginės įtampos U; b) A ir B grupių LD eksperimentinių (juodi simboliai) ir apskaičiuotų (raudonos kreivės) įtampos fliuktuacijų spektrinių tankių $S_{U\,\text{el}}$ priklausomybių nuo tiesioginės srovės I esant 1 kHz palyginimas.

2.2.3. Elektrinių fliuktuacijų kilmė GaAsBi lazeriniuose dioduose

B grupės bandinių atveju tiesinėje voltamperinės charakteristikos srityje, kuomet nuotėkio kanalo varža R_{1B} šuntuoja varžą R_2, (iki apytiksliai 0,1 mA, atitinkanti įtampa 0,5 V) (2.11 pav. a), R_{1B} kuriamos elektrinės fliuktuacijos didėja proporcingai I^2 (2.11 pav. b). Triukšmo lygio mažėjimas stebimas, kuomet varža R_2 pradeda šuntuoti varžą R_{1B}. Nuotėkio kanalo varža R_{1B} nepriklauso nuo įtampos, o ši B grupės LD nuotėkio srovė net iki keturių eilių didesnė nei A grupės bandinių (srityje, kur $I \sim a_1 U$ (12)). Taigi, kaip ir GaSb LD atveju (2.1.3 skirsnis), galima teigti, kad GaAsBi B grupės bandiniuose už elektrines fliuktuacijas yra atsakingas paviršinis nuotėkio kanalas. Tačiau lyginant su GaSb LD, šių nuotėkio kanalų varžų kuriamų fliuktuacijų spektriniai tankiai skiriasi. GaAsBi nuotėkio kanalą lemia defektai paviršiuje, kurių relaksacijos trukmės yra pasiskirsčiusios plačiame laiko intervale, kas ir formuoja $1/f$ fliuktuacijų spektrą. GaSb atveju, paviršinių g-r procesų trukmės yra panašios, todėl triukšmų spektras yra Lorenco pavidalo.

A grupės bandinių nuotėkio kanalo varžos R_{1A} atveju yra kiek kitaip. Šios grupės LD varžos R_{1A} kuriamų fliuktuacijų lygis daug žemesnis už B grupės, varžos R_{1A} vertė nėra konstanta ir ji priklauso nuo įtampos (2.11 pav. a). Taip pat, $S_{U\,\mathrm{el}}(I)$ priklausomybėje pasirodžius antrajam triukšmų maksimumui, $1/f$ fliuktuacijas keičia g-r fliuktuacijos. G-r triukšmo spektroskopijos pagalba temperatūrų intervale nuo 180 K iki 295 K buvo nustatyta stebimo g-r proceso aktyvacijos energija. Skirtingiems A grupės bandiniams ji yra pasiskirsčiusi intervale nuo 0,16 eV iki 0,18 eV. Panašios aktyvacijos energijos buvo nustatytos giliųjų lygmenų relaksacinės spektroskopijos (GLRS) metodu ir MPE būdu užaugintuose *n*-tipo GaAsBi sluoksniuose ant GaAs pagrindo [22]. Šiame darbe taip pat parodyta, kad kompleksiniai defektai, savo sandaroje turintys Bi atomą, yra atsakingi už šį aptiktą pagavimo lygmenį. Nedidelis Bi atomų įterpimas į GaAs gardelę gali netgi sumažinti kai kurių giliųjų pagavimo lygmenų tankį, kurie aptinkami tiriant GaAs, tačiau didinant įterpiamo Bi kiekį tuo pat metu formuojasi defektai, kuriuose dalyvauja pats bismutas [22]. Atsižvelgiant į įvertintą aktyvacijos energiją, galima teigti, kad, esant įtampai $U > 0{,}9$ V, A grupės bandiniuose išauga g-r centro (su būdingomis Lorenco tipo fliuktuacijomis) įtaka, kurį kuria defektai savo sandaroje turintys Bi. Taigi, antrasis triukšmų maksimumas yra susijęs su LD aktyviąja KD sritimi. Toks žematemperatūrinis bismidinių LD auginimas didina defektų tankį ir AlGaAs apvalkaliniuose sluoksniuose [17]. Todėl $S_{U\,\mathrm{el}}(I)$ priklausomybėje

pirmąjį triukšmų maksimumą su $1/f^{\alpha}$ fliuktuacijomis lemia įvairūs defektai bei krūvininkų pagavimo centrai tiek atvyviojoje LD srityje, tiek ir pasyviojoje.

2.3. InGaN šviesos diodų žemadažnio triukšmo tyrimai

Trečioji tirtų bandinių grupė – tai didelės galios (1 W) InGaN šviesos diodai. Buvo tirti artimosios UV srities šviesos diodai su daugelio InGaN KD dariniu, kurių spinduliuojamas bangos ilgis yra nuo 380 nm iki 410 nm (2.2 lentelė). Taip pat atliktas baltos šviesos diodo ilgalaikio sendinimo eksperimentas (28000 val.). Šį dalinės fosforo konversijos ŠD sudaro puslaidininkinis lustas su daugeliu InGaN KD, spinduliuojantis mėlyną šviesą (λ_c = 452 nm), ir fosforo sluoksnis (YAG:Ce^{3+}), dalį mėlynos šviesos verčiantis į geltoną.

Pagrindiniai rezultatai publikuoti [P4] ir [P5] straipsniuose. Tyrimai atlikti tekant tiesioginei srovei ir neviršijant maksimalios leistinos srovės vertės. Sendinimo eksperimentas atliktas kambario temperatūroje tekant maksimaliai srovei (350 mA) periodiškai pertraukiant ŠD veiką ir atliekant matavimus: triukšmų, *I-U*, spinduliuotės galios charakteristikų ir optinių spektrų. Siekiant atskirti fizikinius procesus, vykstančius pačiame ŠD luste bei fosforo sluoksnyje, optinės charakteristikos buvo registruojamos fotodiodų matrica, kurios mėlynai šviesai jautri sritis fiksavo InGaN lusto spinduliuotę, o raudonai šviesai jautri sritis – fosforo sluoksnio.

2.2 lentelė. InGaN bandinių grupės ir jų savybės

Grupė	**A**	**B**	**C**	**D**	**E**
Centrinis bangos ilgis (nm)	Artimoji UV sritis				Baltos šviesos
	380	390	400	410	

2.3.1. Tunelinė srovė ir elektrinis triukšmas artimosios UV srities šviesos dioduose

Pirmiausia, atlikus voltamperinių charakteristikų tyrimą, pastebėta, kad kai kurių ŠD *I-U* neidealumo koeficientas kambario temperatūroje tam tikrame įtampų intervale yra labai didelis ($\eta \approx 4$). Tai rodo galimą tunelinės srovės sandą. Todėl siekiant nustatyti laidumo mechanizmą bandiniuose, buvo remtasi metodika, aprašyta [92] ir [93].

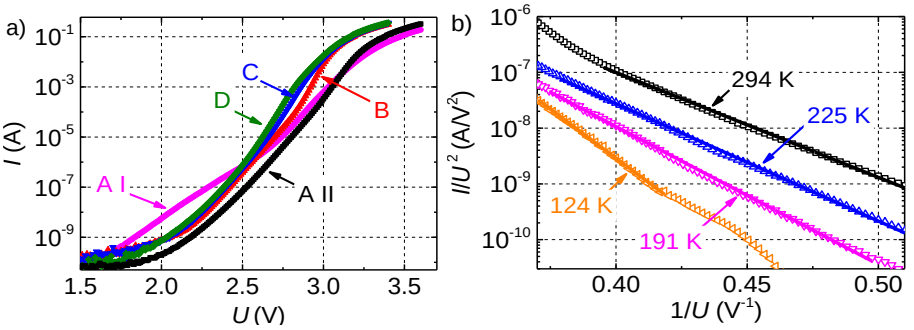
Vykstant tuneliavimui, tekančios srovės proporcingumas elektrinio lauko stipriui *E* išreiškiamas taip:

$$I \sim P \cdot E^2 \exp(-1/E); \tag{15}$$

čia *P* nuo temperatūros nepriklausantis daugiklis [92, 94]. Jei tunelinės srovės sandas yra vyraujantis, tai $\log(I/U^2)$ nuo $1/U$ priklausomybė turėtų

būti tiesinė, o charakteringoji energija E_T *I-U* išraiškoje $I = I_0\exp(qU/E_T)$ turėtų nepriklausyti nuo temperatūros [92, 95].

Dalies A grupės ŠD *I-U* charakteristikos išsiskiria lyginant su likusių grupių bandiniais (2.12 pav. a). Šių ŠD $\log(I/U^2)$ nuo $1/U$ priklausomybės yra tiesinės (2.12 pav. b), o įvertinta charakteringoji energija E_T mažų įtampų srityje lygi 100 meV. Likusių A grupės bandinių bei kitų grupių ŠD E_T kambario temperatūroje yra apie 60 meV ir pasižymi stipresne priklausomybe nuo temperatūros. Taigi, dalies A grupės bandinių laidumas mažų įtampų srityje yra nulemtas tunelinės srovės (šie ŠD toliau žymimi AI, o neturintys tunelinės srovės sando – AII). Didesnių įtampų srityje laidumas tampa mišrus, nulemtas difuzinės ir rekombinacinės srovės sandų. Likusių B – D grupių bandiniuose tunelinės srovės sandai yra nepastebimi.



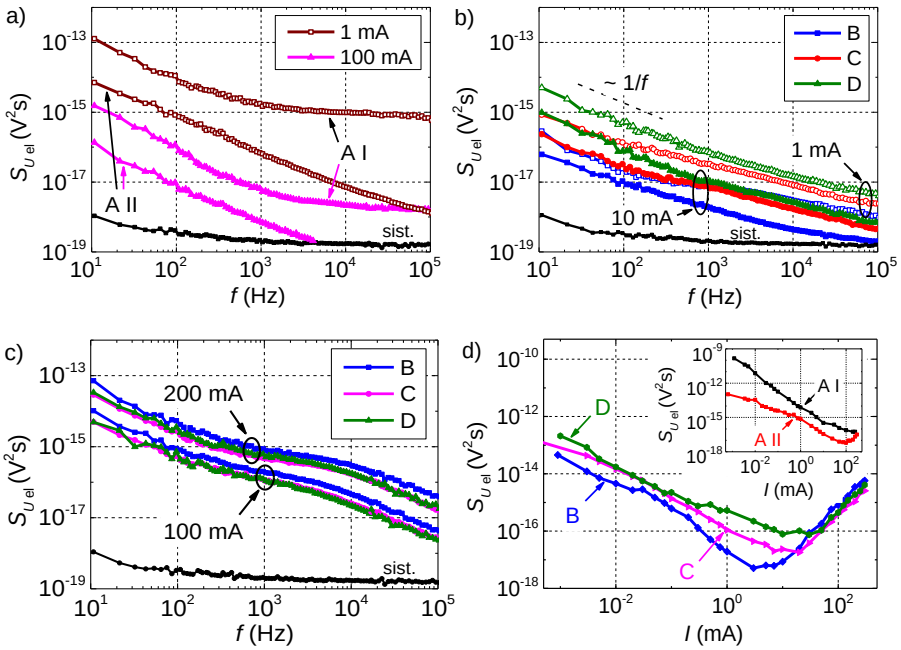
2.12 pav. a) Tipinės skirtingo bangos ilgio artimosios UV srities A – D grupių ŠD *I-U* charakteristikos tiesiogine kryptimi; b) AI bandinio $\log(I/U^2)$ nuo $1/U$ priklausomybės temperatūrų intervale nuo 124 K iki 294 K mažų įtampų srityje (nuo 1,95 V iki 2,7 V).

Galima įtarti, kad AI ŠD yra prastesnės kokybės dėl didesnio defektingumo lyginant su likusiais bandiniais. Tai leistų paaiškinti tuneliavimo procesą dalyvaujant defektams, t. y. per giliuosius pagavimo lygmenis [95]. Šį teiginį praplečia žemadažnio triukšmo tyrimas.

Vieninteliai AI grupės ŠD pasižymi Lorenco pavidalo ($\tau < 1{,}6$ μs) elektrinio triukšmo spektrais visame tirtame srovių intervale (2.13 pav. a) su nedideliais $1/f^{\alpha}$ fliuktuacijų sandais žemuose dažniuose (iki ~ 1 kHz). Šios g-r fliuktuacijos stebimos ir mažų įtampų srityje, kur laidumas yra nulemtas tuneliavimo proceso. Tai pagrindžia anksčiau iškeltą idėją, kad tuneliavimo procesas vyksta dalyvaujant defektams. Didelį AI grupės ŠD defektingumą rodo ne tik aukštesnis elektrinio triukšmo lygis, bet ir tai, kad fotoįtampa U_{foto} (kuri proporcinga spinduliuotės galiai) yra proporcinga tiesioginei srovei taip: $U_{foto} \sim I^r$, kur $r > 2$ plačiame srovių intervale net iki 20 mA.

Laipsnio rodiklis $r > 1$ rodo didelę nespinduliuojamosios rekombinacijos centrų įtaką ŠD spinduliavimo efektyvumui [93, 96].

AII ir B – D grupių bandinių elektrinis triukšmas yra $1/f^{\alpha}$ (2.13 pav. b). Tekančiai srovei per ŠD didėjant ir diferencialinei varžai R_{dif} pasiekus nuosekliosios ŠD varžos R_{S} vertę, įtampos fliuktuacijų spektriniuose tankiuose pastebimi ir Lorenco tipo triukšmų sandai (2.13 pav. c). Tikslią tiesioginės srovės vertę, kai $R_{\mathrm{dif}} \approx R_{\mathrm{S}}$ galima nustatyti iš triukšmų spektrinių tankių priklausomybių nuo srovės stiprio (2.13 pav. d). Visų šviesos diodų šios priklausomybės yra „V“ formos, išskyrus AI grupės bandinių dėl didesnio defektingumo. Elektrinio triukšmo S_U proporcingumas $S_U \sim 1/I$ (aprašytas 2.1.1 skirsnyje) galioja, kol $R_{\mathrm{dif}} \sim 1/I$, o srovei didėjant ir pasiekus sąlygą $R_{\mathrm{dif}} \approx R_{\mathrm{S}}$ (R_{S} = const), elektrinio triukšmo priklausomybė tampa $S_U \sim I^2$ [49]. Kaip matyti iš 2.13 pav. d), sąlygą $R_{\mathrm{dif}} \approx R_{\mathrm{S}}$ atitinkanti srovės stiprio vertė skirtingų bangos ilgių diodams yra kitokia.



2.13 pav. a) A grupės ŠD, b) B – D grupių ŠD iki ir c) pasiekus nuosekliosios varžos apribotą laidumo sritį elektrinio triukšmo spektriniai tankiai $S_{U\,\mathrm{el}}$, tekant skirtingo stiprio tiesioginei srovei; d) B – D grupių ŠD įtampos fliuktuacijų spektrinių tankių $S_{U\,\mathrm{el}}$ priklausomybės nuo tiesioginės srovės I esant 108 Hz dažniui (A grupės ŠD rezultatai pavaizduoti įterptiniame paveiksle).

Pritaikius g-r triukšmo spektroskopiją temperatūrų intervale nuo 110 K iki 293 K, buvo įvertintos atsakingų g-r procesų aktyvacijos energijos srityje, kai tekanti srovė apribota nuosekliosios varžos R_S. Skirtingiems B – D grupių bandiniams ši aktyvacijos energija kinta nuo 0,03 eV iki 0,045 eV.

Kai kuriuose B grupės ŠD tiesioginės srovės intervale nuo 0,5 mA iki 10 mA aptinkamas dar vienas papildomas g-r triukšmo šaltinis su $\tau = 0{,}2$ ms relaksacijos trukme ir 0,19 eV aktyvacijos energija. Norint įvertinti šių g-r triukšmo šaltinių vietą, yra reikalinga atlikti abipusės koreliacijos koeficiento tarp elektrinių ir optinių fliuktuacijų analizę.

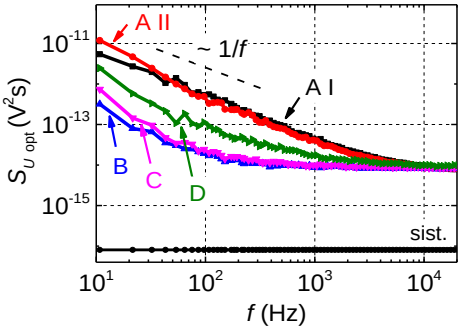
2.3.2. Koreliacijos koeficiento tarp elektrinių ir optinių fliuktuacijų analizė artimosios UV srities šviesos dioduose

Visų tirtųjų bandinių optinio triukšmo spektriniai tankiai yra $1/f^{\alpha}$, pereinantys į šratinį triukšmą (2.14 pav.). A grupės bandinių $1/f^{\alpha}$ triukšmo sandai yra didžiausi. Kaip matyti iš 2.15 pav., maksimali abipusės koreliacijos koeficiento vertė visame tirtame dažnių intervale nuo 10 Hz iki 20 kHz skirtingų grupių bandiniams yra pasiekiama tekant skirtingo stiprio srovėms. Kol tekanti srovė yra nedidelė, koreliuojantys optiniai $1/f^{\alpha}$ ar g-r triukšmo sandai taip pat yra nedidelio intensyvumo, iš kitos pusės – tekant didelio stiprio srovei, optinių fliuktuacijų spektre išauga šratinio triukšmo sandas, o elektriniame triukšme pradeda vyrauti ŠD pasyviosios ar kontaktų srities fliuktuacijos, kurios tarpusavyje nekoreliuoja. Didžiausias abipusės koreliacijos koeficientas stebimas AI grupės bandiniuose – net iki 70 %. Tai rodo didelį ŠD aktyviosios srities defektingumą. Šių AI grupės ŠD elektrinio triukšmo spektrinių tankių Lorenco pavidalas nepakito visame tirtame srovių intervale. Atsižvelgiant į tai bei į didelį abipusės koreliacijos koeficientą, galima teigti, kad už elektrines g-r fliuktuacijas atsakingas pagavimo lygmuo ir dalyvaujantis tuneliavimo procese, yra aktyviojoje ŠD KD srityje.

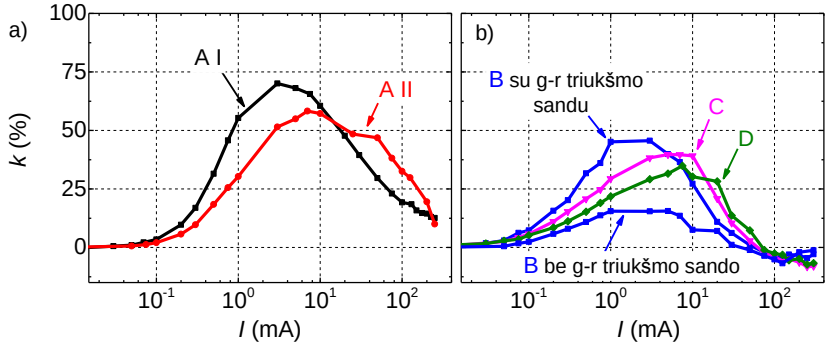
B – D grupių bandinių abipusės koreliacijos koeficientas sumažėja iki nulio (tampa net šiek tiek neigiamas) (2.15 pav. b) srityje, kai $R_{dif} \approx R_S$. Taigi, už šias g-r fliuktuacijas atsakingi pagavimo lygmenys su (0,03 – 0,045) eV aktyvacijos energija yra nesusiję su ŠD aktyviąja sritimi. Kadangi laidumo srovę riboja nuoseklioji varža R_S, triukšmo šaltinis gali būti stipriai legiruotuose n^+ ir p^+ sluoksniuose ar priekontaktinėse srityse.

B grupės bandinių, kurie pasižymi papildomomis g-r fliuktuacijomis elektrinio triukšmo spektruose srovių intervale nuo 0,5 mA iki 10 mA, koreliacijos koeficientas yra didesnis (daugiau nei du kartus) lyginant su B

grupės diodais neturinčiais šio g-r triukšmo sando (2.15 pav. b). Tai rodo, kad šis aptiktas g-r centras yra aktyviojoje ŠD srityje.



2.14 pav. Optinio triukšmo spektriniai tankiai $S_{U\,opt}$ tekant 100 mA stiprio tiesioginei srovei; „sist.“ žymi matavimo sistemos savųjų triukšmų lygį.



2.15 pav. a) A grupės ŠD ir b) B – D grupių ŠD abipusės koreliacijos koeficiento *k* tarp elektrinių ir optinių fliuktuacijų priklausomybės nuo tiesioginės srovės stiprio *I* visame tirtame dažnių intervale nuo 10 Hz iki 20 kHz.

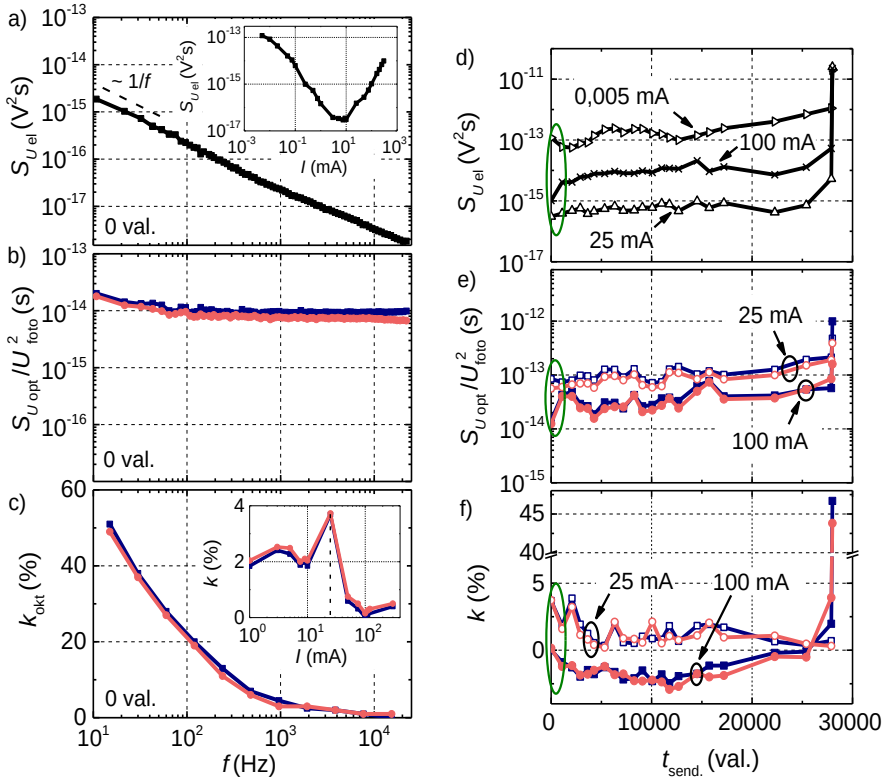
Taigi, tokia abipusės koreliacijos koeficiento tarp elektrinių ir optinių fliuktuacijų analizė leidžia lengvai identifikuoti triukšmo šaltinių vietą – aktyviojoje ar pasyviojoje bandinio srityje.

2.3.3. Triukšmo charakteristikos baltos šviesos diode ilgalaikio sendinimo eksperimento metu

Nesendinto (0 val.) baltos šviesos diodo žemadažnių triukšmų charakteristikos yra gana panašios į artimosios UV srities bandinių charakteristikas. Elektrinės fliuktuacijos yra $1/f^{\alpha}$ tipo, o jų spektrinio tankio priklausomybei nuo srovės yra būdinga jau aptarta „V“ formos

charakteristika (2.16 pav. a). Optinio triukšmo spektrinis tankis sudarytas iš mažo intensyvumo $1/f^{\alpha}$ fliuktuacijų, matomų iki 100 Hz, ir šratinio triukšmo sandų (2.16 pav. b). Lyginant su UV srities diodais, pastebimi skirtumai tarp koreliacijos koeficiento verčių. Nors elektrinis ir optinis $1/f^{\alpha}$ triukšmo sandai žemuose dažniuose stipriai koreliuoja (iki 50 %, 2.16 pav. c), tačiau optinis šratinis triukšmas su elektrinėmis $1/f^{\alpha}$ fliuktuacijomis nekoreliuoja. Todėl abipusės koreliacijos koeficientas visame tirtame dažnių intervale nuo 10 Hz iki 20 kHz yra labai mažas (maksimali vertė ~ 4 % tekant 25 mA srovei).

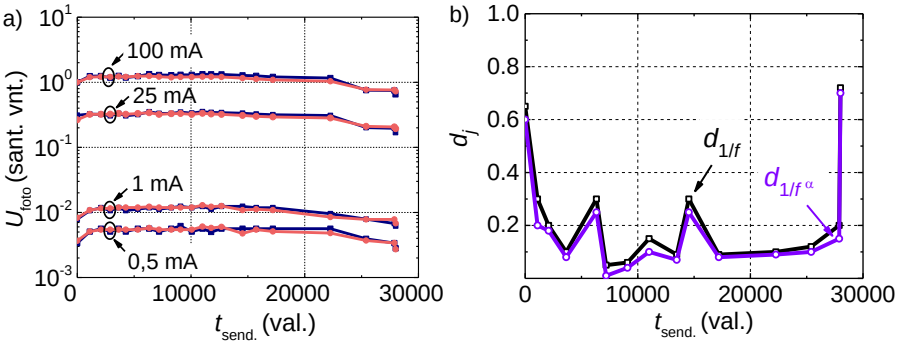
Atlikus sendinimo eksperimentą galima išskirti du pagrindinius etapus, atsižvelgiant į staigius elektrinių ir optinių charakteristikų pokyčius, – pradinį po 1100 val. ir galutinį po 28000 val. Pradinio etapo metu spinduliuotės galia išauga apie 20 % (2.17 pav. a). Tai reiškia, kad potencialinio barjero pokytis lėmė padidėjusį krūvininkų srautą į kvantines duobes, o tai – intensyvesnę spinduliuojamąją rekombinaciją [45]. Taip vyksta dėl medžiagos ar defektų migracijos ir grupavimosi reiškinių. Triukšmo lygio pokyčiai konkretizuoja šiuos vykstančius procesus. Tekant didelei tiesioginei srovei per ŠD (pavyzdžiui, 2.16 pav. d, kai I = 100 mA), elektrinių fliuktuacijų lygis po 1100 val. išaugo, o iš *I-U* charakteristikos analizės matyti, kad nuoseklioji bandinio varža R_S taip pat padidėjo. Šį R_S padidėjimą paprastai lemia elektromigracijos sukeltas kiaurymių formavimasis kontaktų srityje, o didelė tekanti srovė ir temperatūra spartina šį procesą [54]. Tačiau tekant mažoms srovėms per ŠD (pavyzdžiui, 2.16 pav. d, kai I = 0,005 mA) elektrinis triukšmas po 1100 val. sumažėjo. Taigi, dalis defektų, atsakingų už nuotėkio varžos fliuktuacijas, išnyko ar migravo. Pradinio sendinimo etapo pabaigoje abipusės koreliacijos koeficientas tapo neigiamu tekant didelei tiesioginei srovei (2.16 pav. f). Taigi, potencialinio barjero pokytis nors ir lėmė išaugusį spinduliuotės intensyvumą, tačiau tuo pat metu proporcingai padidėjo krūvininkų dalis, nepatenkanti į aktyviąją sritį ir nedalyvaujanti spinduliuojamojoje rekombinacijoje (vyksta srovės persiskirstymas tarp aktyviosios ir gretimų sričių). Palyginus nustatytus dėsningumus su eksperimentų, atliktų taikant PSTM, rezultatais, matyti, kad kai kurių InGaN ŠD charakteristikų pagerėjimas, pavyzdžiui, spinduliuotės galios padidėjimas pačioje sendinimo proceso pradžioje taip pat buvo stebimas [51, 97]. Tačiau tuo atveju, kai senėjimą skatinantis veiksnys – temperatūra – eksperimento metu daugiau nei 4 kartus viršijo KT, jokio charakteristikų pagerėjimo neaptikta, o spinduliuotės galia iškart pradėjo mažėti [51]. Tai rodo, kad stipriai spartinant sendinimo eksperimentą, nors ir laimima laiko, bet prarandama naudinga informacija apie vykstančius procesus bandiniuose arba ji yra užgožiama kitų paspartinto sendinimo sukeltų reiškinių.



2.16 pav. a) Elektrinio $S_{U\,\mathrm{el}}$ ir b) normuoto optinio triukšmo $S_{U\,\mathrm{opt}}/U^2_{\mathrm{foto}}$ spektriniai tankiai tekant 100 mA tiesioginei srovei bei c) abipusės koreliacijos koeficiento k_{okt} tarp elektrinių ir optinių fliuktuacijų priklausomybė nuo centrinio oktavos dažnio tekant 25 mA tiesioginei srovei prieš atliekant sendinimo eksperimentą (0 val.). d) Elektrinio $S_{U\,\mathrm{el}}$ ir e) normuoto optinio triukšmo $S_{U\,\mathrm{opt}}/U^2_{\mathrm{foto}}$ priklausomybės nuo sendinimo trukmės $t_{\mathrm{send.}}$ esant 22 Hz dažniui bei f) abipusės koreliacijos koeficiento k visame tirtame dažnių intervale nuo 10 Hz iki 20 kHz priklausomybės nuo sendinimo trukmės tekant skirtingo stiprio srovėms. Įterptiniuose paveiksluose: a) elektrinio triukšmo spektrinio tankio $S_{U\,\mathrm{el}}$ priklausomybė nuo srovės stiprio I esant 22 Hz dažniui ir c) abipusės koreliacijos koeficiento k visame tirtame dažnių intervale nuo 10 Hz iki 20 kHz priklausomybė nuo srovės stiprio I. Čia mėlynos ir raudonos spalvos kreivės žymi matavimų metu naudotą fotodiodų matricos sritį, atitinkamai jautrią mėlynai ir raudonai šviesai. Žalios spalvos apskritimai d), e) ir f) paveiksluose žymi pradinį sendinimo etapą (po 1100 val.).

Sendinimo proceso eigoje tarp pradinio ir galutinio etapo jokių staigių pokyčių ŠD charakteristikose nestebima. Elektrinis triukšmo lygis nežymiai auga srovių intervale, kur vyrauja nuotėkio varžos kuriamos fliuktuacijos (2.16 pav. d, kai I = 0,005 mA).

Galutinis etapas pasižymi staigiu elektrinio ir optinio triukšmo padidėjimu (2.16 pav. d, e) bei spinduliuotės galios sumažėjimu (iki 65 % pradinės galios) (2.17 pav. a). Paprastai yra laikoma, kad žmogaus akis pastebi spinduliuotės sumažėjimą 30 %, o toks ŠD yra nebetinkamas naudoti ir laikomas sugedusiu remiantis IES (*angl.* Illuminating Engineering Society) standartu [98, 99]. Didelė teigiama abipusė koreliacija tarp elektrinių ir optinių fliuktuacijų po 28000 val. darbo (2.16 pav. f, kai $I = 100$ mA) rodo, kad aktyviojoje srityje ženkliai išaugo nespinduliuojamosios rekombinacijos centrų skaičius. Tekant didelei srovei koreliacijos koeficientas artėti link nulio pradeda daug anksčiau (jau nuo 15000 val.) nei registruojami fotoįtampos verčių pokyčiai tampa pastebimi (2.16 pav. f ir 2.17 pav. a). Tiek elektrinių, tiek optinių fliuktuacijų spektrinių tankių pobūdis visą sendinimo laikotarpį išlieka toks pats, tik optiniame spektre po 28000 val. šratinis triukšmas tampa visiškai užgožtas išaugusio $1/f^{\alpha}$ triukšmo sando.



2.17 pav. a) Fotoįtampos U_{foto} (proporcingos spinduliuotės galiai) priklausomybė nuo sendinimo trukmės $t_{send.}$ tekant skirtingo stiprio srovėms (čia U_{foto} normuota į pradinę 0 val. vertę); b) dydžių d_j priklausomybė nuo sendinimo trukmės $t_{send.}$ tekant 25 mA stiprio tiesioginei srovei.

Norint dar tiksliau įvertinti triukšmo šaltinių dinamiką aktyviojoje ŠD srityje sendinimo metu, yra tikslinga rasti atskirų žemadažnių elektrinių fliuktuacijų sandų įnašą į koreliacijos koeficientą. Buvo pritaikyta metodika, aprašyta 1.2 skyriuje. Dydžių d_j priklausomybės nuo sendinimo trukmės pateiktos 2.17 pav. b), kai tekanti srovė lygi 25 mA, t. y. kuomet abipusės koreliacijos koeficientas įgyja maksimalią vertę sendinimo eksperimento pradžioje (2.16 c įterptinis pav.). Šiuo konkrečiu atveju spektriniuose tankiuose $S_{U\,el}(f)$ nebuvo stebimi g-r triukšmo sandai, todėl $S_{U\,el}(f)$ aprašyti pakako $1/f$ ir $1/f^{\alpha}$ sandų, o dydis $d_3 = 0$. Realiuose eksperimentuose

dažniausiai visada stebimos $1/f^{\alpha}$ fliuktuacijos. Tačiau jas aprašant teoriškai, pavyzdžiui, Hugės lygtimi, ir norint išlaikyti matematinį dimensijų teisingumą, laipsnio rodiklis α privalo būti lygus 1 [61, 67]. Sendinimo pradžioje (0 val.) dydžiai $d_{1/f} = 0{,}65$ ir $d_{1/f^{\alpha}} = 0{,}6$ yra gana panašūs, taigi, daugiau nei pusė visų elektrinių žemadažnių fliuktuacijų kuria atitinkamas žemadažnes optines fliuktuacijas. Po 1100 val. šie dydžiai stipriai sumažėja, o pasiekus galutinį etapą vėl padidėja ir net viršija pradines vertes: $d_{1/f} = 0{,}72$ ir $d_{1/f^{\alpha}} = 0{,}7$. Tai patvirtina išaugusį aktyviosios srities defektingumą.

2.3.4. Fosforo sluoksnio įtaka optinėms charakteristikoms baltos šviesos diode

Fosforo sluoksnio savybių kitimas daro didelę įtaką ŠD optinėms savybėms: spinduliuotės galiai ir susietajai spalvinei temperatūrai (SST). Tam tikruose taikymuose, pavyzdžiui, medicinoje šis chromatinis šviesos šaltinio stabilumas yra esminis. Nemažiau svarbu sužinoti, ar fosforo sluoksnis elgiasi kaip galimas triukšmo šaltinis. Diodo srovės fliuktuacijos moduliuoja fotonų, išspinduliuotų iš ŠD lusto aktyviosios srities, srautą. Tuomet šių mėlynos šviesos fotonų srautas toliau moduliuoja fosforo sluoksnio išspinduliuojamus geltonos šviesos fotonus. Taigi, atskyrus šias spinduliuotės dalis, yra galima įvertinti fosforo sluoksnio daromą įtaką triukšmų charakteristikoms.

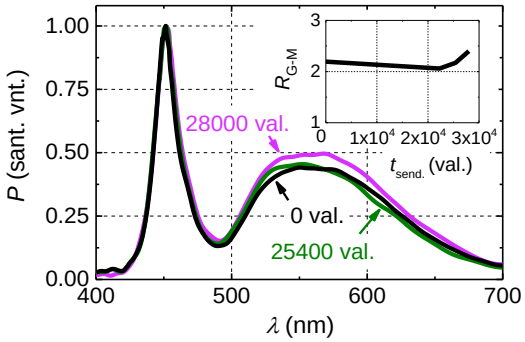
Baltos šviesos ŠD optinį spektrą sudaro InGaN lusto mėlynos šviesos spinduliuotė ($\lambda_c = 452$ nm) ir plati fosforo sluoksnio konversijos geltonoji spinduliuotė (2.18 pav.). Sendinimo proceso eigoje šių spektro dalių intensyvumų santykis, kuris randamas taip:

$$R_{\text{G-M}} = \left(\int_{480}^{780} P(\lambda) d\lambda \right) \Big/ \left(\int_{380}^{480} P(\lambda) d\lambda \right), \qquad (16)$$

kinta, čia $P(\lambda)$ – optinės galios tankis (W/nm) (2.18 įterptinis pav.). Tai rodo, kad susietoji spalvinė temperatūra taip pat kinta.

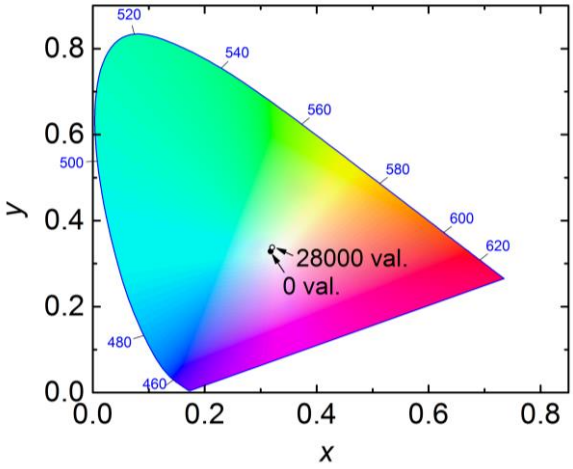
Yra įprasta spalvų sudėtį nusakyti CIE (*pranc.* Commission Internationale de l'Éclairage) 1931 spalvų diagramos koordinatėmis x, y ir $z = 1 - x - y$, vadinamomis spalvio koordinatėmis. Kadangi ŠD spalvio koordinatės nėra tiksliai ant Planko lanko (t. y. ant kreivės diagramoje, kurios taškus atitinka juodojo kūno spinduliuotės spalviai esant įvairioms temperatūroms), tai ŠD spinduliuotė nusakoma susietąja spalvine temperatūra iš izotemperatūrinių linijų, kertančių Planko lanką [99, 100]. Nustačius tiriamojo diodo spalvio koordinates ir remiantis [100] pateikta polinomine lygtimi, buvo apskaičiuotos SST vertės. Ši temperatūra nuo

6225 K (0 val.) padidėjo iki 6306 K praėjus 22600 val., o sendinimo pabaigoje (po 28000 val.) sumažėjo iki 6040 K, – optinis spektras tapo „šiltesnis“ (2.19 pav.). Fosforo konversijos efektyvumo padidėjimas paprastai yra galimas tik pačioje sendinimo proceso pradžioje [101]. Šiuo atveju SST kitimą ir svyravimą lemia šie pagrindiniai veiksniai, kurių procesų spartos yra besiskiriančios, – paties ŠD lusto optinės galios kitimas, fosforo liuminescencijos efektyvumo mažėjimas ir jį gaubiančio sandariklio (arba paties ŠD išorinio lęšiuko) geltonėjimas sendinimo proceso eigoje [34]. Palyginus rezultatus su eksperimentais, atliktais PSTM sąlygomis, matyti, kad jų metu paprastai stebimas tik SST mažėjimas (optinis spektras tampa „šiltesnis“) ar tik didėjimas (optinis spektras tampa „šaltesnis“) visame tirtame laiko intervale [52, 99, 102]. Šiuo atveju, tai, kad baltos šviesos ŠD sendinimas buvo atliekamas įprastomis bandinio veikos sąlygomis, leido aptikti dvepoją SST kitimą eksperimento eigoje.



2.18 pav. E grupės ŠD optiniai spektrai tekant 100 mA stiprio srovei, esant skirtingoms sendinimo trukmėms (visų spektrų optinės galios tankiai P yra normuoti į mėlynos spinduliuotės smailės maksimumą; λ – bangos ilgis). Įterptinis paveikslas rodo santykio $R_{G\text{-}M}$ (16) kitimą sendinimo eksperimento metu.

Remiantis 2.16 pav. e) ir f), pastebima, kad ir optinio triukšmo, ir abipusės koreliacijos koeficiento tarp elektrinių ir optinių fliuktuacijų priklausomybės sendinimo eigoje matuotos tiek su mėlynai šviesai, tiek su raudonai šviesai jautria fotodiodo sritimi neblogai atkartoja viena kitą. Kadangi fosforo sluoksnis tik perspinduliuoja dalį mėlynos InGaN lusto šviesos, tai fosforo efektyvumo kitimas keičia optinių fliuktuacijų, matuotų su raudonai šviesai jautria fotodiodo sritimi, lygį, tačiau šie pokyčiai yra nedideli. Todėl galima teigti, kad tirtame sendinimo eksperimento intervale fosforo sluoksnis nesielgia kaip papildomas triukšmo šaltinis.



2.19 pav. CIE 1931 spalvų diagramos spalvio koordinačių kitimas prieš (SST 6225 K) ir po sendinimo eksperimento (SST 6040 K) tekant 100 mA tiesioginei srovei.

Fosforo spinduliavimo efektyvumo mažėjimas yra susijęs su augančia šio sluoksnio temperatūra. Tai spartina ir paties diodo lusto kaitimas [34]. Sendinimo proceso metu net ir nedidelės kiaurymės ar oro tarpelio atsiradimas tarp ŠD lusto ir šilumai laidaus padėklo lemia spartų įtaiso gedimą [102], – nuosekli ŠD varža didėja, vyksta priemaišų ir kontaktų jonų difuzija, sparčiai formuojasi defektai, apimdami ir aktyviąją sritį, ką ir įrodo didelės nustatytų dydžių $d_{1/f}$ ir $d_{1/f}{}^{\alpha}$ vertės sendinimo eksperimento pabaigoje. Visa tai lemia pastebimą spinduliuotės galios sumažėjimą po 28000 val. ŠD darbo.

2.4. Apibendrinimas

Dažnai yra manoma, kad norint įvertinti skirtingų bandinių defektingumą užtenka palyginti jų elektrinių fliuktuacijų lygį. Atlikti tyrimai rodo, kad elektrinio triukšmo spektrinio tankio priklausomybės nuo tiesioginės srovės $S_{U\,\mathrm{el}}(I)$ pobūdis, t. y. ar ši priklausomybė turi maksimumų, ar yra „V“ formos, yra daug informatyvesnė charakteristika, teikianti pradines žinias apie srovės tekėjimo kelius bandinyje. Apibendrinant pateiktus rezultatus ir remiantis 2.3 lentele, galima teigti, kad, jei šioje priklausomybėje stebimas aiškus triukšmų maksimumas ar pora jų, tai tiriamame srovių intervale vyrauja nuotėkio varžos kuriamos fliuktuacijos, o voltamperinėje charakteristikoje žymi tiesinė dalis. Tam tikrais atvejais, kaip kad LD su penkianariu AlGaInAsSb bangolaidiniu sluoksniu ir esant dideliam defektų tankiui jame, ši priklausomybė gali būti visai nepanaši nė į vieną iš aptartų. Elektrinio triukšmo lygio palyginimas yra tikslingesnis tuo atveju, kai lyginami bandiniai pasižymi tokiu pat triukšmo spektrinio tankio priklausomybės nuo srovės pobūdžiu.

Taip pat iš aptartų rezultatų galima pastebėti, kad paviršiaus ir veidrodžių dangų kokybė turi labai didelę įtaką IR srities lazerinių diodų (tiek pagamintų GaSb pagrindu, tiek ir bismidinių) elektrinėms ir optinėms savybėms, pirmiausia dėl defektų suformuotų didelių paviršinių nuotėkio srovių. Lazerinės generacijos metu jos lemia didesnę slenkstinę srovę bei mažesnę spinduliuotės galią. Ši problema nėra tokia aktuali ŠD su InGaN kvantinėmis duobėmis, tačiau kitas reiškinys – tuneliavimas per defektų kuriamus lygmenis – taip pat blogina įtaiso veiką ir riboja spinduliuojamosios rekombinacijos efektyvumą.

Staigūs pokyčiai elektrinėse ir optinėse triukšmų charakteristikose, o ypač abipusės koreliacijos pokytis iš teigiamos į neigiamą, praėjus pradiniam sendinimo etapui, nėra būdingi vien tik trumpabangiams InGaN šviesos diodams. Teigiamos abipusės koreliacijos koeficiento pokytis į neigiamą po pirmųjų 690 darbo valandų buvo stebėtas ir lazeriniuose dioduose su GaInAsSb KD [103]. Tačiau kiekvienu atveju būtina išsiaiškinti konkrečius fizikinius veiksnius, lemiančius elektrinių ir optinių fliuktuacijų tarpusavio fazės pokytį.

Ilgalaikio sendinimo eksperimentas rodo, kad abipusės koreliacijos koeficiento tarp elektrinių ir optinių fliuktuacijų tyrimas yra jautriausia charakteristika, rodanti pokyčius, vykstančius ŠD. Pavyzdžiui, po pradinio sendinimo etapo nuotėkio varžos kuriamo elektrinio triukšmo lygis nežymiai

auga, o tekant didelėms srovėms fliuktuacijų lygis praktiškai nesikeičia per visą eksperimento trukmę iki pat galutinio etapo. Žymus triukšmo pokytis pastebimas tik po 28000 darbo valandų. Tačiau koreliacijos koeficientas tekant didelei srovei daug anksčiau – jau po 15000 val. – ima kisti – artėja link 0 (auga teigiamai koreliuojančių triukšmų dalis), kas rodo prasidedantį aktyviosios srities gedimą.

2.3 lentelė. Tirtų bandinių rezultatų apibendrinimas pagal elektrinio triukšmo priklausomybės nuo srovės pobūdį (nepaisant triukšmų smailių dėl modų šuolių)

<table>
<tr><th colspan="5"></th><th>$S_{U\,\mathrm{el}}(I)$ priklausomybės pobūdis</th></tr>
<tr><td rowspan="11">Bandinių grupė</td><td rowspan="8">LD</td><td rowspan="5">GaSb pagrindu pagaminti</td><td colspan="2">LD 1</td><td rowspan="4">Turinti triukšmų maksimumą</td></tr>
<tr><td colspan="2">LD 2</td></tr>
<tr><td colspan="2">LD 4</td></tr>
<tr><td colspan="2">LD 5</td></tr>
<tr><td colspan="2">LD 3</td><td>Silpnai priklausanti nuo srovės, bet elektrinio triukšmo lygis aukščiausias. Pastaba: didelis defektingumas, nulemtas penkianario bangolaidinio sluoksnio</td></tr>
<tr><td colspan="2">LD 6</td><td rowspan="2">Vienas aiškus triukšmų maksimumas visame tirtame srovių intervale</td></tr>
<tr><td rowspan="2">GaAsBi</td><td colspan="2">B</td></tr>
<tr><td colspan="2">A</td><td>Du triukšmų maksimumai</td></tr>
<tr><td rowspan="6">ŠD</td><td rowspan="6">InGaN</td><td rowspan="4">Artimosios UV srities</td><td rowspan="2">A</td><td>Dalies bandinių mažėjanti didėjant tekančiai srovei, bet elektrinio triukšmo lygis aukščiausias. Pastaba: bandinių, turinčių tunelinės srovės sandą ir didesnį aktyviosios srities defektingumą</td></tr>
<tr><td rowspan="5">„V“ formos</td></tr>
<tr><td>B</td></tr>
<tr><td>C</td></tr>
<tr><td>D</td></tr>
<tr><td colspan="2">Baltos šviesos</td></tr>
</table>

Taigi, iš pateiktų rezultatų aptarimo matyti, kad žemadažnio triukšmo charakteristikų tyrimas, papildytas pagrindinių elektrinių ir optinių charakteristikų (tokių, kaip *I-U* ir spinduliuotės galios) analize, leidžia tinkamai įvardinti vykstančius fizikinius procesus bei jų kilmę bandiniuose.

IŠVADOS

1. Nustatyta, kad GaInSb ir GaAsBi lazerinių diodų, kurie elektrinio triukšmo nuo srovės priklausomybėse turi vieną būdingą triukšmų maksimumą bei tiesinę voltamperinės charakteristikos dalį, fliuktuacijas lemia defektų suformuotas nuotėkio kanalas bandinių paviršiuje. Priklausomai nuo krūvininkų relaksacijos trukmių pasiskirstymo, gali būti stebimas tiek $1/f^{\alpha}$, tiek ir Lorenco pavidalo fliuktuacijų spektrinis tankis.
2. GaAsBi LD, kurių voltamperinės charakteristikos neturi tiesinės dalies, elektrinio triukšmo nuo srovės priklausomybės pasižymi dviem triukšmų maksimumais. Generacinio-rekombinacinio triukšmo spektroskopijos pagalba identifikuota, kad šių LD elektrinių fliuktuacijų nuo srovės priklausomybėje stebimas antrasis triukšmų maksimumas su jam būdingais Lorenco pavidalo spektriniais tankiais yra nulemtas kvantinių duobių srityje esančių defektų, savo sandaroje turinčių Bi atomų. Pirmąjį triukšmų maksimumą šioje priklausomybėje su jam būdingais $1/f^{\alpha}$ spektriniais tankiais kuria defektai, esantys tiek aktyviojoje, tiek ir pasyviojoje bandinių srityse.
3. Nustatyta, kad aptiktas GaInSb LD paviršinis nuotėkio kanalas pasižymi to paties tipo elektrinėmis (Lorenco pavidalo) fliuktuacijomis su ta pačia relaksacijos trukme ir vienoda g-r proceso aktyvacijos energija tiek esant tiesioginiam, tiek atvirkštiniam priešįtampiui.
4. Elektrinio triukšmo charakteristikų matavimai atgaline kryptimi parodė, kad tirtų GaInAsSb LD veidrodžių pasyvavimo procesas yra neoptimalus.
5. Nustatyta, kad artimosios UV srities 380 nm bangos ilgio InGaN šviesos diodai, turintys vyraujantį tunelinės srovės sandą mažų įtampų srityje, pasižymi Lorenco pavidalo triukšmų spektriniais tankiais. Abipusės koreliacijos koeficiento tarp elektrinių ir optinių triukšmų analizė parodė, kad už šias fliuktuacijas atsakingas ir dalyvaujantis tuneliavimo procese pagavimo lygmuo yra aktyviojoje ŠD srityje. Bandiniai, neturintys tunelinės srovės sando, yra charakterizuojami $1/f^{\alpha}$ elektrinėmis fliuktuacijomis su g-r triukšmo sandais, stebimais ŠD nuosekliosios varžos apribotoje laidumo srityje.

6. InGaN (tiek baltos šviesos, tiek UV) ŠD elektrinio triukšmo nuo srovės priklausomybės pasižymi būdinga „V“ forma, priešingai nei IR srities GaAsBi bei GaSb-pagrindu pagamintų LD elektrinių fliuktuacijų priklausomybės nuo srovės, turinčios didesnių ar mažesnių triukšmų maksimumų.
7. InGaN baltos šviesos diodo ilgalaikio sendinimo eksperimentas parodė, kad, atsižvelgiant į staigius triukšmų charakteristikų pokyčius, yra išskiriami du pagrindiniai etapai. Pradinis etapas (po pirmųjų 1100 val.) pasižymi išaugusia spinduliuotės galia, nuotėkio varžos kuriamo elektrinio triukšmo sumažėjimu ir jo padidėjimu tekant didelei srovei. Tai lemia defektų migracijos ir išnykimo reiškiniai. Galutinis etapas (po 28000 val.) yra charakterizuojamas staigiu žemadažnio triukšmo padidėjimu ir spinduliuotės galios sumažėjimu. Išaugusi koreliuotoji elektrinio triukšmo su optinėmis fliuktuacijomis dalis rodo ženklų nespinduliuojamosios rekombinacijos centrų formavimąsi aktyviojoje ŠD srityje.
8. Nustatyta, kad fosforo sluoksnis ilgalaikio sendinimo metu (28000 val.) nesielgia kaip papildomas triukšmo šaltinis, bet keičia ŠD chromatines savybes.

SUMMARY

Introduction

It is hard to imagine life without laser diodes (LDs) and light emitting diodes (LEDs). These are compact, lightweight, and potential low-cost *pn* junction devices whose first prototypes were demonstrated in the early 1960s [1, 2]. Despite the fact that modern LDs or LEDs have significantly improved, their technology of manufacturing is still being elaborated and new semiconductor compounds are being tested for even more efficient device operation.

The wide range of applications in the infrared (IR) spectrum has led to the rapid development of LDs. A lot of molecules of pollution and combustion gases have strong absorption lines in the region of (1.8 – 4) μm [3]. Laser emission in this wavelength region can be obtained by using GaSb-based LDs with type-I quantum wells (QWs). Such LDs can be used in molecular spectroscopy [4, 5], in pumping solid-state lasers, medicine or military [6–8].Compared to other IR LDs, these GaSb type-I LDs are much more attractive due to their simpler structure [4, 13] and direct interband optical transitions [5, 12]. The active region consists of GaInAsSb QWs and quaternary or quinternary barriers [4, 14]. However, the epitaxial growth of such multinary alloys is complex due to the increase in the bandgap energy during thermal annealing, moreover, narrow-gap semiconductors suffer from non-radiative Auger recombination and free carrier absorption much more than shorter wavelength LDs [5, 8].

These non-radiative recombination losses can be practically avoided by the novel $GaAs_{1-x}Bi_x$ compound used as an active (light emitting) layer in the LD or LED [17, 18]. The incorporation of even a small amount of bismuth (Bi) atoms into GaAs effectively reduces the bandgap energy by (84 – 91) meV/%Bi [19]. For a relatively high Bi composition ($x > 10$ %), the spin-orbit splitting energy (Δ_{so}) becomes larger than the bandgap of the alloy allowing to suppress the Auger recombination and inter-valence band absorption [17, 19]. However, there are some technological difficulties related to the growth of this material system: Bi surface segregation [17–21], surface roughness, or Bi droplets formation [18, 20, 22]. So far, the threshold current of GaAsBi LDs is many times higher compared to telecommunication InGaAsP/InP LDs widely used nowadays [24].

On the other side of the visible light spectrum, i. e., in the near ultraviolet (UV) region, the InGaN material system is of high importance. Due to still

used sapphire substrates, such LEDs suffer from a high density of defects, especially threading dislocations [26, 27]. Non-uniformities in the indium concentration in InGaN/GaN QWs are thought to be responsible for the efficient radiative recombination [30]. However, near UV LEDs contain less indium compared to blue LEDs, and this results in a lower radiative efficiency and in an increased carrier interaction with dislocations [31, 32]. Efficient UV LEDs are expected to be used in fluorescent lamps with a very high color rendering index (CRI). So far, phosphor-converted white LEDs are common [33]. There InGaN chip generates blue light and phosphor, usually yttrium-aluminium-garnet (YAG:Ce^{3+}), produce a broad yellow emission [34]. The application of such LEDs for lighting increased the importance of reliability and lifetime studies of these devices.

When innovative technological ideas and novel semiconductor materials are applied to the device manufacturing, there is a need for a sensitive and non-destructive sample characterization method. Low-frequency noise spectroscopy is a suitable candidate for LDs or LEDs diagnostics [37, 39]. The measurements are performed at a near equilibrium state, are fast and particularly sensitive to defects and various imperfections of the devices [35–37]. It is accepted, that $1/f$ electrical fluctuations are an excellent indicator of the quality of electronic devices [37, 38].

What is more, it is essential to study not only electrical but also optical noise, i. e., radiated power fluctuations [40, 41]. A high level of electrical noise does not necessarily mean high defectiveness of the active area [42]. Measuring both noise signals simultaneously, the cross-correlation coefficient between electrical and optical fluctuations can be estimated. Using the correlation analysis method, it is possible to determine which part of the electrical noise is related to the active LD or LED region, and thus to estimate the location of the noise source and the influence of individual noise spectral components on the cross-correlation coefficient [43, 44].

However, in some cases, the measurement of optical noise and the cross-correlation coefficient is complicated. For example, for multimode Fabry-Perot (FP) LDs the noise analysis at lasing operation is difficult due to intense mode hopping. During mode-hopping the level of noise amplitude increases drastically [46, 47]. Thus, in this case, investigation can be performed only far below the threshold current, because the identified physical processes affect the overall LD reliability [48, 49]. Besides, the internal structure of the sample is protected from the damage caused by high flowing current. The choice of non-destructive testing method is also significant in a long-term ageing experiment. The aim of such study is to detect changes in samples operation before they become apparent in other

characteristics, e.g. current-voltage (*I*-*V*) [37]. The main difference from highly accelerated stress testing (HAST) is that the LD or LED under investigation operates at normal conditions during the entire experiment [51, 52].

Moreover, when samples are of similar quality, measurements made under direct bias may not provide sufficient information to assess their quality or reliability. Poor facet passivation can lead to the formation of new defects or surface leakage channels [54]. In those cases, LD noise measurements are also performed at reverse bias [53]. So, there is an opportunity to evaluate the quality of the LD facets passivation process [58].

Almost all types of low-frequency noise are presented during the LD or LED experimental characterization. Any element with non-zero resistance creates thermal (also called Johnson or Nyquist) noise. It is caused by the random movement of charge carriers (Brownian motion) [36–38]. Random and independent events of charge carriers crossing a potential barrier result in shot noise observed in semiconductor diodes [36, 38]. Both thermal and shot noise are characterized by a "white" spectra, i. e., in a wide range independent of frequency. Because of this, thermal noise is often used to calibrate measuring equipment [36].

For the evaluation of the device quality and reliability generation-recombination (g-r) and 1/*f* (flicker) noise are essential. They are described as fluctuations in the conduction (or resistance) of semiconductor, i. e., the number of free carriers in the sample fluctuates due to random generation-recombination events. Various defects act as charge capture or release centers (g-r centers or traps) and are characterized by trapping level in the bandgap, density, relaxation time, and Lorentzian spectrum [36, 38]. The g-r noise intensity is proportional to a number of active g-r centers [35, 60]. If the relaxation times of these independent g-r events are different and widely distributed, then superposition of Lorentzian type spectra of such many capture-emission processes will give 1/*f*-type noise spectral density [37, 61]. In addition, there is another common theory of the origin of 1/*f*: it is caused by mobility fluctuations due to the electron-lattice interaction [36, 61–63]. However, it has been proved recently that the main source of 1/*f* fluctuations is the charge carrier capture-emission processes [61, 66, 67]. This model, based on superposition of g-r events, well describes the experimentally observed low-frequency spectral density dependence on a frequency in a wide range as $1/f^{\alpha}$ (where α can vary from 0.8 to 1.3) [61, 64, 65].

Also, specific and unique fluctuations for LD or LED can arise during device operation, e. g., LD mode hopping noise [68], optical feedback noise

[70, 71] or frequency noise [72, 73]. These fluctuations usually limit the practical application of these devices and overall system performance.

Thus, these identified problems of modern LDs or LEDs demonstrate the need of a sensitive and appropriate characterization method, such as low-frequency noise spectroscopy, to investigate those devices.

The aim

To investigate low-frequency noise characteristics of novel laser and light-emitting diodes with GaInAsSb, GaAsBi and InGaN quantum wells, to determine low-frequency noise sources of devices and to evaluate their origin.

The main tasks

1. To investigate electrical and optical noise characteristics in the subthreshold and in the case of LD – at lasing operations, taking into account the properties of the studied samples. In order to assess the surface quality of the samples, to perform measurements of noise characteristics at reverse bias.

2. To present the analysis of the cross-correlation coefficient between electrical and optical fluctuations and to evaluate the origin of fluctuations in the sample.

3. To apply generation-recombination noise spectroscopy and to evaluate the activation energies of trap levels.

4. To relate the noise characteristics of the samples with their respective *I-V* and optical power characteristics. In order to elucidate the origin of noise sources in detail, to represent equivalent noise circuits of LDs and compare the experimental and calculated spectral densities of voltage fluctuations according to these equivalent circuits.

5. To perform a long-term ageing experiment of InGaN-based LED and to evaluate the ongoing physical processes by studying low-frequency fluctuations. To determine if the phosphor layer acts as a potential noise source.

Scientific novelty

Materials of the investigated laser or light emitting diodes are sufficiently new and very attractive. Therefore, the obtained results can be of interest to readers in the areas of electrical and optical properties and reliability of modern LDs or LEDs, and also for those who are focused on physics of low-

frequency noise and their properties. There are only several noise studies of GaSb-based LDs where only measurements of electrical fluctuations have been described [74–76]. Our investigation of optical fluctuations and cross-correlation coefficient allow us to explain the physical phenomena occurring in these LDs in a more detail way. At the time of thesis preparation, no research based on GaAsBi LDs low-frequency noise has been published. Hence, we are the first to present a detailed analysis of GaAsBi LDs electrical fluctuations.

As many ageing experiments are based on HAST, there are no published long-term (at least 28000 h) investigations of LED through the noise characteristics under normal operation conditions. For the first time, the method of correlation analysis was applied to the LED ageing experiment of such a long duration. In addition, the method‘s sensitivity to alterations in a device performance was demonstrated.

It has been evaluated that the phosphor layer in a white LED does not act as an additional noise source during long-term ageing (28000 h), but changes the chromatic properties of LED.

Our work also validates that the form of the dependence of the spectral density of LD or LED electrical noise on current, i. e., having maxima or “V”-shape dependence, is characteristic and provides initial information on the current paths (dominant current component) in the samples. A unique methodology estimating the origin of low-frequency fluctuations regarding the above-mentioned noise dependences, the *I-V* characteristics of the samples and their equivalent circuits is presented.

Usually, for devices that operate at reverse bias, such as photodiodes, noise characteristics are investigated at reverse current too. It has been demonstrated that in the case of LDs, such measurements, performed safely at reverse bias, can be used to identify surface leakage current or to assess surface quality of samples.

The obtained results not only provide information about the physical processes taking place in the devices, but also allow us to compare different samples with each other and to evaluate their quality. The results of the research can be used to predict the reliability of devices and their possible lifetime.

Experimental measurement of low-frequency noise provides information about phenomena occurring in different parts of the sample at the same time, e. g., in the semiconductor itself, contacts or surface. This allows to evaluate the influence of mirror coatings, phosphor layer or packaging on the performance of the device. Simultaneous measurement of electrical and optical characteristics is accurate and also time-saving.

Thus, based on the results described in the thesis, the technology of LDs and LEDs manufacturing can be improved considering the origin of the identified low-frequency noise sources and the structure of the samples.

Results

Low-frequency noise characteristics of GaSb-based laser diodes

Investigation of noise characteristics of GaSb-based type-I LDs, radiating in (1.9 – 2.9) μm region, was performed at forward (below the threshold and at lasing) and reverse biases for selected samples. The main results were published in publications [P1] and [P2].

In the subthreshold region most of LDs exhibit $1/f^{\alpha}$-type electrical fluctuations with some appearance of small Lorentzian-type components [6]. However, high power LDs distinguish here – they are characterized by a strong g-r noise with Lorentzian-type spectra at forward and reverse biases with the same relaxation times, and also the same activation energy (0.37 eV). An equivalent electrical noise circuit of these LDs and calculation of the voltage spectral density of the electrical g-r noise has been proposed. According to this, our analysis reveals that the ohmic part of the *I-V* characteristic is related to the resistance of the surface leakage channel between n^{+}GaSb and p^{+}GaSb contacts as the value of this resistance is independent of the applied voltage and its polarity.

At lasing operation mode hopping effect is dominant and it causes intensive highly positively or negatively correlated Lorentzian-type electrical and optical fluctuations. Despite the mode hopping peaks, i. e., at stable LD operation, cross-correlation coefficient between electrical and optical fluctuations could be: positive, negative or transiting from positive to negative. Positive cross-correlation indicates that electrical and optical $1/f^{\alpha}$ fluctuations are caused by defects in the active area. These defects randomly modulate the free charge carrier number and, as a consequence, lead to photon number fluctuations at the same phase. Negative correlation indicates a leakage current out of the active layer when majority of defects are at the interface of active region.

Noise measurements of reverse biased LDs are important for the comparison of similar quality samples. Two groups of very similar LDs from the same batch grown on the same wafer were selected: one with facet coatings and the other – without (left as-cleaved). No obvious differences in noise characteristics between these two groups were observed at forward bias. Cleavage process of the LD when a periodic crystal potential breaks off

at a semiconductor surface, leads to the origin of surface states and capture centers formation [90, 91]. Appropriate passivation is attributed to lower the noise level [55]. However, our results indicate that LDs with facet coating distinguish by higher $1/f^{\alpha}$ electrical fluctuations at reverse bias than samples without it, and this indicates non-optimal facet passivation process.

Low-frequency noise investigation of GaAsBi laser diodes

Low-frequency noise characteristics of 1.09 μm LDs with 5 $GaAs_{1-x}Bi_x$ (x = 8 %) type-I QWs have been investigated in the current range far below the lasing threshold in order to avoid the self-heating effect and the damage of an active layer. The main results are published in the publication [P3].

Considering different voltage fluctuation spectral density dependencies on the forward current, the investigated samples are classified into two groups: A and B. There equivalent noise circuits of these LDs are proposed and the comparison between experimental and calculated voltage fluctuation spectral densities is also presented.

Laser diodes of group A distinguish by two bumps (maxima) in the electrical noise dependence on the current. The first one is characterized by $1/f^{\alpha}$-type electrical fluctuations, the second one – by Lorentzian-type spectra with the activation energy (0.16 – 0.18) eV. Similar activation energy has been observed in *n*-type GaAsBi layer by deep level transient spectroscopy (DLTS) as described in [44]. Our analysis of the *I-V* characteristics and the equivalent noise circuits has shown that the origin of the first electrical noise bump is determined by the overall LDs defectiveness (the active and the peripheral areas) as these LDs are much more sensitive for defect formation due to low-temperature growth. The second bump in electrical noise dependence on the current is due to large density of g-r centers created by defects involving Bi atoms in their structure. These Bi-related defects are mainly located in the active MQW layer of LDs.

Meanwhile, group B LDs have one steep electrical noise bump in the dependence on the forward current with $1/f^{\alpha}$-type electrical fluctuations in the whole investigated current range. In this case, similarly to the case of high power GaSb-based LDs, the leakage resistance is independent of the applied bias. The corresponding ohmic part of *I-V* characteristic of group B LDs is much higher compared to that of the group A samples. The origin of these fluctuations is the leakage channel formed at the surface of LD due to high density defects and capture centers. The formation of such defects is very sensitive to the quality of cleavage process. Compared to GaSb-based LDs, the main difference is that these g-r centers, located on GaAsBi LDs

surface, have widely distributed relaxation times leading to $1/f^{\alpha}$-type noise spectrum.

Low-frequency noise characteristics of InGaN-based light-emitting diodes

The last group of investigated samples is high power (1 W) InGaN-based LEDs. Low-frequency electrical and optical noise characteristics of near UV LEDs with InGaN QWs and peak radiative wavelength in a range of (380 – 410) nm have been analyzed. Also, a total of 28000 h of phosphor-converted white LED ageing experiment has been performed at room temperature (RT) at maximum allowed current (350 mA). *I-V*, light output power, noise characteristics, cross-correlation coefficient, and optical spectra have been measured upon interrupting the ageing procedure. In order to separate the physical processes taking place in the different LED parts: in the semiconductor chip and in the phosphor layer, the optical characteristics were measured by a photodiode matrix, where the blue light-sensitive area was used for the detection of the InGaN chip radiation and the red light-sensitive area – for the phosphor layer. The main results are published in publications [P4] and [P5].

Analysis of conduction mechanism in near UV LEDs shows that some 380 nm peak wavelength LEDs have a dominant tunneling current component at low bias. Such samples distinguish by the Lorentzian-type electrical noise spectra in the whole investigated current range and the strong cross-correlation between electrical and optical fluctuations. This identifies the location of trap level responsible for observed g-r fluctuations to be in the active area of LED and also the defect assisted tunneling process.

Other LEDs with peak wavelength of 390 nm, 400 nm, 410 nm are characterized by the $1/f^{\alpha}$-type electrical fluctuations with Lorentzian-type noise components appearing at the series resistance-limited currents. G-r noise spectroscopy has been applied and defect levels with the activation energy in the range of (0.03 – 0.045) eV has been determined to be responsible for these Lorentzian fluctuations. Some of 390 nm peak wavelength LEDs distinguish by an additional g-r noise component in the current range of (0.5 – 10) mA with the activation energy of 0.19 eV. In order to identify the location of these noise sources, i. e., active or peripheral area of LED, the analysis of cross-correlation coefficient between electrical and optical fluctuations has been performed.

Both – white LED and near UV LEDs (except those with tunneling current component) – are characterized by "V"-shape electrical noise dependences on the forward current. This characteristic is completely

different from the voltage fluctuation spectral densities dependences on the current of GaSb-based and GaAsBi LDs.

Two main stages of ageing experiment of white LED can be distinguished considering rapid changes of noise characteristics. At the initial stage (after 1100 h), an increase of light output and a decrease of the electrical noise at the small forward current region is related to the annealing, reordering or migration of some defects leading to the potential barrier changes. The growth of the electrical noise at large currents is mostly caused by the contacts' degradation which is related to the serial resistance of the LED increase. This is also supported by the change of cross-correlation coefficient: from positive to negative, indicating flowing current redistribution.

Between the initial and the final stages of ageing, no sudden changes are observed in noise characteristics.

The final stage (after 28000 h) of the ageing is characterized by a sudden noise level growth and a decrease in light output power. A strong positive cross-correlation between electrical and optical fluctuations indicates an increase of non-radiative recombination centers in the active area of the LED. Also, the part of fluctuations generated by the low-frequency $1/f$ and $1/f^{\alpha}$ noise components has been evaluated during the whole ageing experiment. The most presumable reason of the increased defectiveness of the active LED area is an increased device self-heating which led to the rapid defect formation and clustering.

A good coincidence between the cross-correlation coefficient measured with blue light-sensitive area of photodiode and with red light-sensitive area, shows that the phosphor layer does not act as a noise source at a given ageing conditions and time. This layer only reemits part of the blue InGaN chip radiation and this affects only the level of the optical fluctuations. However, phosphor layer contributes to the shift of the correlated color temperature (CCT) of the LED as separate LED parts (chip, the phosphor layer and the encapsulating material) have different kinetic rates of the degradation.

Usually, it is assumed that the comparison of the electrical fluctuations level of different samples is sufficient in order to assess their defectiveness. The performed studies reveal that the form of the dependence of electrical noise spectral density on the forward current $S_{U\,\mathrm{el}}(I)$, i. e. whether this dependence has bumps (maxima) or is "V"-shaped, is a much more informative characteristic that provides an initial knowledge of the current paths in a sample. So, if a clear noise maximum or a pair of them is observed

in this dependence, then the fluctuations are caused by the leakage resistance, and the *I-V* characteristic distinguish by a significant linear (ohmic) part. In some cases, such as in the case of LD with quinternary AlGaInAsSb waveguide and with a high density of defects, this $S_{U\,\mathrm{el}}(I)$ dependence may not be similar to any of those discussed. The comparison of the electrical noise level is more meaningful when the samples under comparison have the same form of the noise spectral density dependence on the current.

From the observed results it can be stated that the quality of LD surface and facet coatings strongly influences electrical and optical properties of IR laser diodes (both GaSb-based and bismuth containing GaAs), primarily due to the existence of surface leakage channels formed by defects. What is more, they result in a higher lasing threshold and lower output power during laser generation. This problem is less critical for LEDs with InGaN QWs, but another phenomenon, tunneling through deep-level defects, also degrades device performance and limits the efficiency of radiative recombination.

Sudden changes in electrical and optical noise characteristics, and, especially, the change of the cross-correlation from the positive to the negative after the initial ageing stage, are not inherent to InGaN LEDs only. The change of the cross-correlation coefficient from the positive to the negative after the first 690 hours of performance was also observed in LDs with GaInAsSb QWs [103]. However, in each case, it is necessary to determine the physical processes that impact on the phase change between electrical and optical fluctuations.

The long-term ageing experiment reveals that the cross-correlation coefficient between electrical and optical fluctuations is the most sensitive characteristic indicating the changes in the LED performance. After the initial ageing stage, the level of electrical noise generated by the leakage resistance increases slightly, but at high flowing current the noise level remains practically the same during the whole experiment until the final stage. A significant change in the noise level is only observed after 28000 hours. Meanwhile, the cross-correlation coefficient at high flowing current begins to change much earlier – after 15000 hours and the coefficient is approaching to zero (slowly becoming positive), which indicates the onset of the active layer failure.

Thus, the presented results show that the investigation of low-frequency noise characteristics, supplemented with the analysis of principal electrical

and optical characteristics (such as *I-V* and output power), allow us to properly identify the ongoing physical processes and their origin in the samples.

Conclusions

1. The origin of fluctuations of GaInSb and GaAsBi laser diodes, which distinguish by one characteristic electrical noise maximum (bump) in the dependence on the forward current and a linear part in *I-V* characteristics, is the leakage channel at a surface of LDs formed by defects. Depending on the distribution of charge carrier relaxation times, the spectral density of electrical fluctuations can be observed of both types: $1/f^{\alpha}$ and Lorentzian.
2. GaAsBi LDs, whose *I-V* characteristics do not have a linear part, are characterized by two maxima (bumps) in the electrical noise dependence on the current. G-r noise spectroscopy has identified that the origin of the second noise maximum with characteristic Lorentzian-type fluctuations is due to Bi-related defects in the QWs. The first electrical noise maximum with characteristic $1/f^{\alpha}$-type fluctuations is determined by the overall sample (active and peripheral areas) defectiveness.
3. The detected surface leakage channel of GaInSb LDs distinguishes by the same type noise spectra (Lorentzian-type) at the forward and reverse biases with the same relaxation time and the same activation energy of the corresponding g-r process.
4. Investigation of reverse electrical noise characteristics of the GaInAsSb LDs has shown that the passivation process of LDs facets is non-optimal.
5. Near UV 380 nm InGaN LEDs with dominant tunneling current component in the low voltage range are characterized by Lorentzian-type noise spectra. The analysis of the cross-correlation coefficient between electrical and optical fluctuations reveals that the trap level in the active LED area is responsible for these fluctuations and participates in the tunneling process. Samples without a tunneling current component have $1/f^{\alpha}$ electrical fluctuations with g-r noise components appearing only at the series resistance-limited currents.
6. The dependence of electrical noise on the current of InGaN (UV and white) LEDs has a characteristic “V”-shape that is in contrast to the GaAsBi and GaSb-based IR LDs electrical fluctuation dependence on the current, which is characterized by higher or lower noise bumps.
7. The long-term ageing experiment of the InGaN white LED has shown that two main stages were distinguished considering sudden changes of

noise characteristics. The initial stage (after 1100 h) is characterized by an increase in light power, a decrease in the electrical noise caused by the leakage resistance and a rise in the electrical fluctuation level at high currents. This is due to defect migration or annealing effects. The final stage (after 28000 h) is distinguished by rapid growth of low-frequency noise and a decrease in light power. The increased correlated part of electrical noise with optical fluctuations indicates the formation of a high number of non-radiative recombination centers in the active LED area.

8. The phosphor layer during long-term ageing (28000 h) does not act as an additional noise source but contributes to the variation of chromatic properties of the LED.

LITERATŪROS SĄRAŠAS / REFERENCES

[1] B. Gayral, LEDs for lighting: Basic physics and prospects for energy savings, C. R. Physique **18**, 453–461 (2017).

[2] H. Nasim, Y. Jamil, Diode lasers: From laboratory to industry, Opt. Laser Technol. **56,** 211–222 (2014).

[3] L. S. Rothman, I. E. Gordon, A. Barbe, D. C. Benner, P. F. Bernath, M. Birk, V. Boudon, L. R. Brown, A. Campargue, J. P. Champion, K. Chance, L. H. Coudert, V. Dana, V. M. Devi, S. Fally, J. M. Flaud, R. R. Gamache, A. Goldman, D. Jacquemart, I. Kleiner, N. Lacome, W. J. Lafferty, J. Y. Mandin, S. T. Massie, S. N. Mikhailenko, C. E. Miller, N. Moazzen-Ahmadi, O. V. Naumenko, A. V. Nikitin, J. Orphal, V. I. Perevalov, A. Perrin, A. Predoi-Cross, C. P. Rinsland, M. Rotger, M. Šimečková, M. A. H. Smith, K. Sung, S. A. Tashkun, J. Tennyson, R. A. Toth, A. C. Vandaele, J. Vander Auwera, The HITRAN 2008 molecular spectroscopic database, J. Quant. Spectrosc. Radiat. Transf. **110**, 533–572 (2009).

[4] K. Vizbaras, M. C. Amann, Room-temperature 3.73 μm GaSb-based type-I quantum-well lasers with quinternary barriers, Semicond. Sci. Technol. **27,** 032001 (2012).

[5] A. Joullie, P. Christol, GaSb-based mid-infrared 2–5 μm laser diodes, C. R. Physique **4**, 621–637 (2003).

[6] M. T. Kelemen, J. Gilly, M. Rattunde, J. Wagner, S. Ahlert, J. Biesenbach, Mid-infrared high-power diode lasers and modules, Proc. SPIE **7583**, 75830O (2010).

[7] K. Scholle, S. Lamrini, P. Koopmann, P. Fuhrberg, 2 μm laser sources and their possible applications. *Frontiers in Guided Wave Optics and Optoelectronics* (InTech, 2010) pp. 471–500.

[8] T. Hosoda, J. Chen, G. Tsvid, D. Westerfeld, R. Liang, G. Kipshidze, L. Shterengas, G. Belenky, Development of room temperature CW GaSb based diode lasers, Int. J. High Speed Electron. Syst. **20**, 43–49 (2011).

[9] S. Sprengel, A. Andrejew, K. Vizbaras, T. Gruendl, K. Geiger, G. Boehm, C. Grasse, M. C. Amann, Type-II InP-based lasers emitting at 2.55 μm, Appl. Phys. Lett. **100**, 041109 (2012).

[10] R. Q. Yang, J. L. Bradshaw, J. D. Bruno, J. T. Pham, D. E. Wortman, Room temperature type-II interband cascade laser, Appl. Phys. Lett. **81**, 397–399 (2002).
[11] R. Q. Yang, C. J. Hill, B. Yang, J. K. Liu, Room-temperature type-II interband cascade lasers near 4.1 μm, Appl. Phys. Lett. **83**, 2109–2111 (2003).
[12] S. D. Sifferman, H. P. Nair, R. Salas, N. T. Sheehan, S. J. Maddox, A. M. Crook, S. R. Bank, Highly strained mid-infrared type-I diode lasers on GaSb, IEEE J. Sel. Top. Quantum Electron. **21**, 1502410 (2015).
[13] A. Vizbaras, M. Greibus, E. Dvinelis, A. Trinkūnas, D. Kovalenkovas, I. Šimonytė, K. Vizbaras, Ultra-low input power long-wavelength GaSb type-I laser diodes at 2.7–3.0 μm, Proc. SPIE **9002**, 900214 (2014).
[14] K. Vizbaras, M. C. Amann, 3.6 μm GaSb-based type-I lasers with quinternary barriers, operating at room temperature, Electron. Lett. **47**, 980 (2011).
[15] O. Dier, S. Dachs, M. Grau, C. Lin, C. Lauer, M. C. Amann, Effects of thermal annealing on the band gap of GaInAsSb, Appl. Phys. Lett. **86**, 151120 (2005).
[16] G. Rainò, A. Salhi, V. Tasco, R. Intartaglia, R. Cingolani, Y. Rouillard, E. Tournié, M. De Giorgi, Subpicosecond timescale carrier dynamics in GaInAsSb/AlGaAsSb double quantum wells emitting at 2.3 μm, Appl. Phys. Lett. **92**, 101931 (2008).
[17] I. P. Marko, S. R. Jin, K. Hild, Z. Batool, Z. L. Bushell, P. Ludewig, W. Stolz, K. Volz, R. Butkute, V. Pačebutas, A. Geizutis, A. Krotkus, S. J. Sweeney, Properties of hybrid MOVPE/MBE grown GaAsBi/GaAs based near-infrared emitting quantum well lasers. Semicond. Sci. Technol. **30**, 1–10 (2015).
[18] P. K. Patil, E. Luna, T. Matsuda, K. Yamada, K. Kamiya, F. Ishikawa, S. Shimomura, GaAsBi/GaAs multi-quantum well LED grown by molecular beam epitaxy using a two-substrate-temperature technique, Nanotechnology **28**, 105702 (2017).
[19] W. Pan, L. Zhang, L. Zhu, Y. Li, X. Chen, X. Wu, F. Zhang, J. Shao, S. Wang, Optical properties and band bending of InGaAs/GaAsBi/InGaAs type-II quantum well grown by gas source molecular beam epitaxy, J. Appl. Phys. **120**, 105702 (2016).
[20] A. R. Mohmad, F. Bastiman, C. J. Hunter, R. D. Richards, S. J. Sweeney, J. S. Ng, J. P. R. David, B. Y. Majlis, Localization effects

and band gap of GaAsBi alloys, Phys. Status Solidi B **251**, 1276–1281 (2014).

[21] A. R. Mohmad, B. Y. Majlis, F. Bastiman, C. J. Hunter, R. D. Richards, J. S. Ng, J. P. R. David, Photoluminescence from localized states in GaAsBi epilayers. *Proc. International Conference on Semiconductor Electronics (ICSE)* (IEEE, 2014) pp. 354–357.

[22] L. Gelczuk, J. Kopaczek, T. B. O. Rockett, R. D. Richards, R. Kudrawiec, Deep-level defects in n-type GaAsBi alloys grown by molecular beam epitaxy at low temperature and their influence on optical properties, Sci. Rep. **7**, 12824 (2017).

[23] R. Butkute, A. Geižutis, V. Pačebutas, B. Cechavičius, V. Bukauskas, R. Kundrotas, P. Ludewig, K. Volz, A. Krotkus, Multi-quantum well Ga(AsBi)/GaAs laser diodes with more than 6 % of bismuth, Electron. Lett. **50**, 1155–1157 (2014).

[24] J. Liu, W. Pan, X. Wu, C. Cao, Y. Li, X. Chen, Y. Zhang, L. Wang, J. Yan, D. Zhang, Y. Song, J. Shao, S. Wang, Electrically injected GaAsBi/GaAs single quantum well laser diodes, AIP Advances **7**, 115006 (2017).

[25] S. Nakamura, G. Fasol, *The Blue Laser Diode: GaN Based Light Emitters and Lasers* (Springer, Berlin/Heidelberg, Germany, 1997) 335 p.

[26] X. Li, T. Yu, Y. Tao, J. Deng, C. Xu, G. Zhang, Epitaxial lateral overgrowth of InGaN/GaN multiple quantum wells on HVPE GaN template, Phys. Status Solidi C **9**, 445–448 (2012).

[27] H. Y. Shin, Y. I. Chang, S. K. Kwon, K. T. Lee, M. J. Cho, K. H. Park, The growth characteristics of a GaN layer on a cone-shaped patterned sapphire substrate by TEM observation, J. Korean Phys. Soc. **50**, 1147–1151 (2007).

[28] S. Ishimoto, D. P. Han, K. Yamamoto, R. Mano, S. Kamiyama, T. Takeuchi, M. Iwaya, I. Akasaki, Enhanced device performance of GaInN-based green light-emitting diode with sputtered AlN buffer layer, Appl. Sci. **9**, 788 (2019).

[29] Y. H. You, V. C. Su, T. E. Ho, B. W. Lin, M. L. Lee, A. Das, W. C. Hsu, C. H. Kuan, R. M. Lin, Influence of patterned sapphire substrates with different symmetry on the light output power of InGaN-based LEDs, Nanoscale Res. Lett. **9**, 596 (2014).

[30] P. Ruterana, S. Kret, A. Vivet, G. Maciejewski, P. Dluzewski, Composition fluctuation in InGaN quantum wells made from molecular beam or metalorganic vapor phase epitaxial layers, J. Appl. Phys. **91**, 8979–8985 (2002).

[31] Y. Muramoto, M. Kimura, S. Nouda, Development and future of ultraviolet light-emitting diodes: UV-LED will replace the UV lamp, Semicond. Sci. Technol. **29**, 084004 (2014).
[32] J. T. Oh, Y. T. Moon, D. S. Kang, C. K. Park, J. W. Han, M. H. Jung, Y. J. Sung, H. H. Jeong, J. O. Song, T. Y. Seong, High efficiency ultraviolet GaN-based vertical light emitting diodes on 6-inch sapphire substrate using ex-situ sputtered AlN nucleation layer, Opt. Express. **26**, 5111–5117 (2018).
[33] Y. Muramoto, M. Kimura, A. Dempo, S. Nouda, Y. Fukawa, 66.1: Application of UV-LED to the LCD Backlight, SID Dig. Tech. Pap. **41**, 982–984 (2012)
[34] M. Yazdan Mehr, W. D. van Driel, G. Q. Zhang, Reliability and lifetime prediction of remote phosphor plates in solid-state lighting applications using accelerated degradation testing, J. Electron. Mater. **45**, 444–452 (2016).
[35] B. K. Jones, Low-frequency noise spectroscopy, IEEE Trans. Electron Devices **41**, 2188–2197 (1994).
[36] L. K. J. Vandamme, Noise as a diagnostic tool for quality and reliability of electronic devices, IEEE Trans. Electron Devices, **41**, 2176–2187 (1994).
[37] B. K. Jones, Electrical noise as a reliability indicator in electronic devices and components, IEE Proc.-Circuits Devices Syst. **149**, 13–22 (2002).
[38] C. Claeys, E. Simoen, Noise as a diagnostic tool for semiconductor material and device characterization, J Electrochem. Soc. **145**, 2058–2067 (1998).
[39] D. Ursutiu, B. K. Jones, Low-frequency noise used as a lifetime test of LEDs, Semicond. Sci. Technol. **11**, 1133–1136 (1996).
[40] S. L. Jang, J. Y. Wu, Low-frequency current and intensity noise in AlGaAs laser diodes, Solid-State Electron. **36**, 189–196 (1993).
[41] S. Yang, T. Sasaki, T. Mizunami, K. Takagi, Measurements on low-frequency fluctuation in the laser diodes, IEEE Trans. Electron Dev. **41**, 2162–2164 (1994).
[42] S. Pralgauskaitė, V. Palenskis, J. Matukas, J. Glemža, G. Muliuk, B. Šaulys, A. Trinkūnas, Reliability investigation of light-emitting diodes via low frequency noise characteristics, Microelectron. Reliab. **55**, 52–61 (2015).
[43] V. Palenskis, J. Matukas, S. Pralgauskaitė, B. Šaulys, A detail analysis of electrical and optical fluctuations of green light-emitting diodes by correlation method, Fluctuation Noise Lett. **9**, 179–192 (2010).

[44] V. Palenskis, J. Matukas, B. Šaulys, A detailed analysis of electrical and optical fluctuations of light-emitting diodes by correlation method, Lith. J. Phys. **49**, 453–460 (2009).
[45] V. Palenskis, J. Matukas, S. Pralgauskaitė, Light-emitting diode quality investigation via low-frequency noise characteristics, Solid State Electron. **54**, 781–786 (2010).
[46] S Pralgauskaitė, V Palenskis, J. Matukas, B. Šaulys, V. Kornijčuk, V. Verdingovas, Analysis of mode-hopping effect in Fabry–Pérot multiple-quantum well laser diodes via low frequency noise investigation, Solid-State Electron. **79**, 104–110 (2013).
[47] V. Palenskis, J. Matukas, S. Pralgauskaitė, J. G. Simmons, S. Smetona, R. Sobiestianskas, Experimental investigations of the effect of the mode-hopping on the noise properties of InGaAsP Fabry–Pérot multiple-quantum-well laser diodes, IEEE Trans. Electron Devices **50,** 366–371 (2003).
[48] J. Glemža, V. Palenskis, A. Geižutis, B. Cechavičius, R. Butkutė, S. Pralgauskaitė, J. Matukas, Low-frequency noise investigation of 1.09 μm GaAsBi laser diodes, Materials **12**, 673 (2019).
[49] J. Guan, S. Guo, J. Wang, M. Tao, J. Cao, F. Gao, Analysis of origin of measured 1/*f* noise in high-power semiconductor laser diodes far below threshold current, Microelectron. Reliab. **59**, 55–59 (2016).
[50] M. Behringer, High-power diode laser technology and characteristics. *High Power Diode Lasers. Springer Series in Optical Sciences, vol 128* (Springer, New York, NY, 2007) pp. 5–74.
[51] L. Liu, J. Yang, G. Wang, The investigation of LED's reliability through highly accelerated stress testing methods. *Proc. 14th International Conference on Electronic Materials and Packaging (EMAP)* (IEEE, 2012) pp. 1–3.
[52] L. Trevisanello, M. Meneghini, G. Mura, M. Vanzi, M. Pavesi, G. Meneghesso, E. Zanoni, Accelerated life test of high brightness light emitting diodes, IEEE Trans. Device Mater. Reliab. **8**, 304–311 (2008).
[53] P. Del Vecchioa, A. Curutcheta, Y. Deshayesa, M. Bettiatib, F. Laruelleb, N. Labata, L. Béchoua, Correlation between forward-reverse low-frequency noise and atypical I–V signatures in 980 nm high-power laser diodes, Microelectron. Reliab. **55**, 1741–1745 (2015).
[54] A. Jayawardena, N. Narendran, Analysis of electrical parameters of InGaN-based LED packages with aging, Microelectron. Reliab. **66**, 22–31 (2016).

[55] R. Hakimi, M. C. Amann, Reduction of 1/*f* carrier noise in InGaAsP/InP heterostructures by sulphur passivation of facets, Semicond. Sci. Technol. **12**, 778–780 (1997).
[56] J. Jiménez, Laser diode reliability: crystal defects and degradation modes, C. R. Physique **4,** 663–673 (2003).
[57] M. Hempel, J. W. Tomm, M. Ziegler, T. Elsaesser, N. Michel, M. Krakowski, Catastrophic optical damage at front and rear facets of diode lasers, Appl. Phys. Lett. **97**, 231101 (2010).
[58] J. Glemža, S. Pralgauskaitė, V. Palenskis, J. Matukas, Low-frequency noise investigation of 2–3 μm GaSb-based laser diodes, Solid State Electron. **133**, 70–77 (2017).
[59] J. Glemža, J. Matukas, S. Pralgauskaitė, V. Palenskis, Low-frequency noise characteristics of high-power white LED during long-term aging experiment, Lith. J. Phys. **58**, 194–203 (2018).
[60] J. A. Copeland, Semiconductor impurity analysis from low-frequency noise spectra, IEEE Trans. Electron Devices **18**, 50–53 (1971).
[61] V. Palenskis, K. Maknys, Nature of low-frequency noise in homogeneous semiconductors, Sci. Rep. **5**, 18305 (2016).
[62] V. Palenskis, J. Glemža, J. Vyšniauskas, J. Matukas, Carrier density and mobility fluctuations due to carrier retrapping process in homogeneous semiconductors. *Proc. International Conference on Noise and Fluctuations (ICNF)* (IEEE, 2017) pp. 1–4.
[63] S. V. Melkonyan, V. M. Aroutiounian, F. V. Gasparyan, H. V. Asriyan, Phonon mechanism of mobility equilibrium fluctuation and properties of 1/*f*-noise, Physica B **382**, 65–70 (2006).
[64] V. Palenskis, Flicker noise problem (review), Lith. Phys. J. **30**, 107–152 (1990).
[65] B. Pellegrini, A general model of $1/f^{\gamma}$ noise, Microelectron. Reliab. **40**, 1775–1780 (2000).
[66] V. Palenskis, J. Vyšniauskas, J. Glemža, J. Matukas, Charge carrier mobility fluctuations due to the capture–emission process, Lith. J. Phys. **58**, 261–266 (2018).
[67] V. Palenskis, The charge carrier capture-emission process – the main source of the low-frequency noise in homogeneous semiconductors, Lith. J. Phys. **56**, 200–206 (2016).
[68] S. Pralgauskaitė, V. Palenskis, J. Matukas, Low frequency noise characteristics of multimode and singlemode laser diodes. *Semiconductor Laser Diode Technology and Applications* (InTech, 2012) pp. 133–160.

[69] A. Mahmoud, S. W. Z. Mahmoud, K. Abdelhady, Modeling and simulation of dynamics and noise of semiconductor lasers under NTSC modulation for use in the CATV technology, Beni-Suef Univ. J. Basic Appl. Sci. **4**, 99–108 (2015).

[70] H. Li, J. Ye, J. G. McInerney, Detailed analysis of coherence collapse in semiconductor lasers, IEEE J. Quantum Electron., **29**, 2421–2432 (1993).

[71] M. F. Ahmed, S. Abdulrhmann, M. Yamada, Optical feedback-induced noise in laser diodes in optical-disc systems. *Proc. 46th Midwest Symposium on Circuits and Systems* (MWSCAS) (IEEE, 2003) pp. 1331–1336.

[72] S. Schilt, L. Tombez, C. Tardy, A. Bismuto, S. Blaser, R. Maulini, R. Terazzi, M. Rochat, T. Südmeyer, An experimental study of noise in mid‑infrared quantum cascade lasers of different designs, Appl. Phys. B **119**, 189–201 (2015).

[73] L. D. Turner, K. P. Weber, C. J. Hawthorn, R. E. Scholten, Frequency noise characterisation of narrow linewidth diode lasers, Opt. Commun. **201**, 391–397 (2002).

[74] Z. Chobola, M. Luňák, J. Vaněk, E. Hulicius, I. Kusák, Low-frequency noise measurements used for quality assessment of GaSb based lasers diodes prepared by molecular beam epitaxy, J. Electr. Eng. **66**, 226–230 (2015).

[75] Z. Chobola, J. Vaněk, E. Hulicius, T. Šimeček, Noise as a diagnostic tool for quality of GaSb laser diodes. *Proc. 25th International Conference on Microelectronics (MIEL)* (IEEE, 2006) pp. 288–289.

[76] Z. Chobola, M. Luňák, J. Vaněk, E. Hulicius, Noise as characterization for GaSb based laser diodes prepared by molecular beam epitaxy, Proc. SPIE **7720**, 77202C-1 (2010).

[77] J. Glemža, V. Palenskis, S. Pralgauskaitė, J. Vyšniauskas, J. Matukas, Properties of the surface generation-recombination noise in 1.94 μm GaSb-based laser diodes, Infrared Phys. Technol. **91**, 101–106 (2018).

[78] J. Glemža, S. Pralgauskaitė, V. Palenskis, J. Matukas, Low-frequency noise of near UV LEDs, Lith. J. Phys. **59**, 146–155 (2019).

[79] M. E. Levinshtein, S. L. Rumyantsev, Noise spectroscopy of local levels in semiconductors, Semicond. Sci. Technol. **9**, 1183–1189 (1994).

[80] G. Bosman, R. J. J. Zijlstra, Generation-recombination noise in p-type silicon, Solid State Electron. **25**, 273–280 (1982).

[81] S. L. Rumyantsev, N. Pala, M. S. Shur, M. E. Levinshtein, R. Gaska, M. A. Khan, G. Simin, Generation-recombination noise in GaN-based devices, Int. J. High Speed Electron. Syst. **14**, 175–195 (2004).

[82] F. N. Hooge, T. G. M. Kleinpenning, L. K. J. Vandamme, Experimental studies on 1/*f* noise, Rep. Prog. Phys. **44**, 479–532 (1981).

[83] S. Bychikhin, D. Pogany, L. K. J. Vandamme, G. Meneghesso, E. Zanoni, Low-frequency noise sources in as-prepared and aged GaN-based light-emitting diodes, J. Appl. Phys. **97**, 123714 (2005).

[84] S. Sawyer, S. L. Rumyantsev, M. S. Shur, N. Pala, Yu. Bilenko, J. P. Zhang, X. Hu, A. Lunev, J. Deng, R. Gaska, Current and optical noise of GaN⁄AlGaN light emitting diodes, J. Appl. Phys. **100**, 034504 (2006).

[85] X. J. Liang, Z. Yu, X. Y. Qiang, W. G. Wei, W. Juan, X. Wei, N. H. Qiao, R. Z. Wei, H. Z. Hong, N. Z. Chuan, High quality above 3-μm mid-infrared InGaAsSb/AlGaInAsSb multiple-quantum well grown by molecular beam epitaxy, Chin. Phys. B **23,** 017805 (2014).

[86] L. J. Olafsen, I. Vurgaftman, J. R. Meyer, Antimonide mid-IR lasers. *Long-Wavelength Infrared Semiconductor Lasers* (John Wiley & Sons, Inc., Hoboken, New Jersey, USA, 2005) pp. 69–143.

[87] A. E. Chernyakov, M. E. Levinshtein, N. A. Talnishnikh, E. I. Shabunina, N. M. Shmidt, Low-frequency noise in diagnostics of power blue InGaN/GaN LEDs, J. Cryst. Growth **401**, 302–304 (2014).

[88] J. Park, T. Kang, D. Woo, J. K. Son, J. H. Lee, B. G. Park, H. Shin, Non-ideal characteristic analysis of GaN-based light-emitting diode using current-voltage (I–V) and low-frequency noise experiment. *Proc. 18th International Symposium on the Physical and Failure Analysis of Integrated Circuits (IPFA)* (IEEE, 2011) pp. 408–411.

[89] V. Palenskis, J. Matukas, J. Vyšniauskas, S. Pralgauskaitė, H. Shtrikman, D. Seliuta, I. Kašalynas, G. Valušis, Analysis of noise characteristics of GaAs tunnel diodes, Fluct. Noise Lett. **12**, 1350014 (2013).

[90] R. W. Lambert, T. Ayling, A. F. Hendry, J. M. Carson, D. A. Barrow, S. McHendry, C. J. Scott, A. McKee, W. Meredith, Facet-passivation processes for the improvement of Al-containing semiconductor laser diodes, J. Light. Technol. **24**, 956–961 (2006).

[91] V. N. Bessolov, M. V. Lebedev, Y. M. Shernyakov, B. V. Tsarenkov, Sulfur passivation of InGaAs/AlGaAs SQW laser (977 nm) facets in alcohol-based solutions, Mater. Sci. Eng. B **44**, 380–382 (1997).

[92] J. Kim, Y. Tak, J. Kim, S. Chae, J. Y. Kim, Y. Park, Analysis of forward tunneling current in InGaN/GaN multiple quantum well light-emitting diodes grown on Si (111) substrate, J. Appl. Phys. **114**, 013101 (2013).

[93] X. A. Cao, E. B. Stokes, P. M. Sandvik, S. F. LeBoeuf, J. Kretchmer, D. Walker, Diffusion and tunneling currents in GaN/InGaN multiple quantum well light-emitting diodes, IEEE Electron Device Lett. **23**, 535–537 (2002).

[94] L. Hirsch, A. S. Barrière, Electrical characterization of InGaN/GaN light emitting diodes grown by molecular beam epitaxy, J. Appl. Phys. **94**, 5014 (2003).

[95] M. Lee, H. Lee, K. M. Song, J. Kim, Investigation of forward tunneling characteristics of InGaN/GaN blue light-emitting diodes on freestanding GaN detached from a Si substrate, Nanomaterials **8**, 543 (2018).

[96] X. A. Cao, K. Topol, F. Shahedipour-Sandvik, J. Teetsov, P. M. Sandvik, S. F. LeBoeuf, A. Ebong, J. Kretchmer, E. B. Stokes, S. Arthur, A. E. Kaloyeros, D. Walker, Influence of defects on electrical and optical characteristics of GaN/InGaN-based light-emitting diodes, Proc. SPIE **4776**, 105–113 (2002).

[97] J. Hu, L. Yang, L. Kim, M. W. Shin, The ageing mechanism of high-power InGaN/GaN light-emitting diodes under electrical stresses, Semicond. Sci. Technol. **22**, 1249–1252 (2007).

[98] Illuminating Engineering Society, TM-21-11 Projecting Long Term Lumen Maintenance of LED Light Sources, (USA, 2012).

[99] M. Yazdan Mehr, W. D. van Driel, G. Q. Zhang, Accelerated life time testing and optical degradation of remote phosphor plates, Microelectron. Reliab. **54**, 1544–1548 (2014).

[100] C. S. McCamy, Correlated color temperature as an explicit function of chromaticity coordinates, Color Res. Appl. **17**, 142–144 (1992).

[101] Z. Qin, J. Feng, C. Zhaohui, X. Ling, W. Simin, L. Sheng. Effect of temperature and moisture on the luminescence properties of silicone filled with YAG phosphor, J. Semicond. **32**, 012002 (2011).

[102] M. Meneghini, L. R. Trevisanelloa, F. de Zuania, N. Trivellin, G. Meneghesso, E. Zanoni, Extensive analysis of the degradation of phosphor-converted LEDs, Proc. SPIE **7422**, 74220H (2009).

[103] J. Glemža, J. Matukas, S. Pralgauskaitė, V. Palenskis, Mid-infrared laser diodes investigation via low-frequency noise spectroscopy and electrical derivative characteristics. *Proc. International Conference on Noise and Fluctuations (ICNF)* (IEEE, 2017) pp. 1–4.

PADĖKA

Didžiausią padėką skiriu savo mokslinio darbo vadovui prof. dr. (HP) Jonui Matukui už suteiktas teorines ir praktines žinias ir galimybę tobulėti, už nuoširdų palaikymą ir paskatinimą, už visokeriopą pagalbą bet kokiu klausimu ir optimizmą.

Širdingai dėkoju prof. dr. (HP) Viliui Palenskiui už vertingas mokslines diskusijas, pasidalinimą žiniomis ir idėjomis.

Labai ačiū doc. dr. Sandrai Pralgauskaitei už pagalbą ir patarimus rengiant publikacijas.

Nuoširdžiai dėkoju Kristijonui ir Augustinui Vizbarams (UAB Brolis Semiconductors, Vilnius, Lietuva) už suteiktus bandinius, jų specifikacijas ir naudingas konsultacijas.

Didelę padėką skiriu dr. Renatai Butkutei ir Fizinių ir technologijos mokslų centro Optoelektronikos technologijos laboratorijos kolektyvui už suteiktus bandinius, bendradarbiavimą ir naudingas diskusijas.

Dėkoju visam Taikomosios elektrodinamikos ir telekomunikacijų instituto Triukšmų ir terahercinės elektronikos grupės kolektyvui.

Ačiū visai savo šeimai už visapusišką palaikymą, kantrybę ir supratingumą visus metus kelyje iki šio darbo.

CURRICULUM VITAE

Vardas, pavardė: Justinas Glemža
Gimimo data: 1991-11-27
El. paštas: justinas.glemza@ff.vu.lt

Išsilavinimas

2016–2020 m. Vilniaus universitetas, Fizikos fakultetas, Taikomosios elektrodinamikos ir telekomunikacijų institutas, Vilnius, Lietuva
Doktorantūros studijos

2014–2016 m. Vilniaus universitetas, Fizikos fakultetas, Vilnius, Lietuva
Elektronikos inžinerijos magistro laipsnis, Magna Cum Laude diplomas

2010–2014 m. Vilniaus universitetas, Fizikos fakultetas, Vilnius, Lietuva
Elektronikos inžinerijos bakalauro laipsnis, Cum Laude diplomas

Darbo patirtis

2019–dabar Laborantas, Vilniaus universitetas, Fizikos fakultetas, Taikomosios elektrodinamikos ir telekomunikacijų institutas, Vilnius, Lietuva

2015–2019 m. Inžinierius, Vilniaus universitetas, Fizikos fakultetas, Radiofizikos katedra/Taikomosios elektrodinamikos ir telekomunikacijų institutas, Vilnius, Lietuva

Gauti apdovanojimai

2015 m. gauta vienkartinė tikslinė stipendija, kuri skiriama studentams, pasiekusiems gerų rezultatų mokslinėje veikloje.
2014 m. paskirta dr. Remio Gaškos ir „Sensor Electronic Technology, Inc.“ vardinė stipendija, kuri skiriama pirmosios pakopos baigiamųjų kursų studentams už tais metais apgintus geriausius bakalauro baigiamuosius darbus.

PUBLIKACIJŲ KOPIJOS / COPIES OF PUBLICATIONS

P1

J. Glemža, S. Pralgauskaitė, V. Palenskis, J. Matukas,

Low-frequency noise investigation of 2–3 μm GaSb-based laser diodes,

Solid State Electron. **133**, 70–77 (2017).
doi: 10.1016/j.sse.2017.05.002.

Copyright © 2017 Elsevier Ltd. All rights reserved.

Leidimas perspausdinti disertacijoje nereikalingas

Permission to reprint in a dissertation is not required

Solid-State Electronics 133 (2017) 70–77

Contents lists available at ScienceDirect

Solid-State Electronics

journal homepage: www.elsevier.com/locate/sse

Low frequency noise investigation of 2–3 μm GaSb-based laser diodes

Justinas Glemža *, Sandra Pralgauskaitė, Vilius Palenskis , Jonas Matukas

Radiophysics Dep. Vilnius University, Sauletekio 9 (III), LT-10222 Vilnius, Lithuania

ARTICLE INFO

Article history:
Received 21 February 2017
Received in revised form 13 April 2017
Accepted 4 May 2017
Available online 6 May 2017

The review of this paper was arranged by Prof. E. Calleja

Keywords:
Cross-correlation coefficient
Electrical noise
Fluctuation
GaSb
Mid-infrared laser diode
Optical noise

ABSTRACT

A detailed noise study of mid-infrared 2–3 μm wavelenght GaSb-based type-I ridge-waveguide laser diodes (LDs) has been carried out using the low frequency noise spectroscopy. Different samples having slightly different heterostructures, differently packaged, with and without facet passivation have been investigated. The activation energies of trap levels, associated with additional generation-recombination (g–r) noise components in noise spectra at small current region before the threshold, have been determined. It was shown that at particular forward currents the mode-hopping effect dominates during LD lasing operation. It was demonstrated that small differences in LD heterostructure and waveguide layers have got the largest influence to LD noise characteristics while influence of the absence of facet passivation, linking to noise generation centers at the cleaved semiconductor interface, and package type is much weaker.

© 2017 Elsevier Ltd. All rights reserved.

1. Introduction

High performance semiconductor laser diodes (LD) emitting in the mid-infrared (MIR) 2–4 μm spectral region are attractive for a plurality of applications, such as gas sensing, defense and many other due to their compactness, low electrical power consumption and potential low-cost. Efficient and high-power MIR laser diodes are interesting for free-space communications, LIDAR and infrared countermeasures due to presence of water absorption-free atmospheric windows [1,2]. The above mentioned applications typically require efficient emitters, operating at room-temperature. There are three main approaches on how to achieve laser emission in the required 2–4 μm wavelength range, such as GaSb-based interband cascade lasers (ICLs) [3], InP-based type-II lasers [4] and GaSb-based type-I lasers. The latter – GaSb-based type-I quantum-well (QW) laser diodes, utilizing direct interband optical transition are the most popular, robust and the most developed approach for making efficient light sources and, also, the only ones that cover whole spectral range. Room-temperature lasing from 2 μm to 3.73 μm [5–7], extremely low threshold currents comparing to those of near-infrared GaAs-based lasers [8] and high-power continuous-wave operation of GaSb-based type-I QW have been demonstrated. Despite successful demonstration, manufacturing of these laser diodes is less mature compared to GaAs-based near-infrared (NIR) ones. This is related to complexity in epitaxial growth that involves multinary mixed group-V alloys [6,7] and, also, because narrow-gap semiconductors suffer much more from non-radiative Auger recombination, and the internal losses associated with free carrier absorption also strongly increase with wavelength [9]. Due to the above mentioned reasons, various processes related to device lifetime, defect migration, leakage currents, etc. are of interest to the scientific community.

In order to improve LDs operation and their lifetime it is essential to understand physical processes that affect the device reliability and accelerate device degradation most. There are several methods for evaluation of processes of interest, related to reliability of the devices. Such as highly accelerated stress testing (HAST) [10] or electrical derivative measurements [11] could be mentioned. Also low frequency noise spectroscopy is highly informative method for physical processes and device reliability revealing [12]. The essential feature of the investigation of semiconductor device noise characteristics for diagnostic purposes is the sensitivity: the noise measurements are carried out near the equilibrium state and are non-destructive, since they are performed under normal bias condition. Measurement data of low frequency noise can indicate the presence of intrinsic defects as well as fabrication imperfections that act as deep traps in the active region of LDs [13].

* Corresponding author.
E-mail addresses: justinas.glemza@ff.vu.lt (J. Glemža), sandra.pralgauskaite@ff.vu.lt (S. Pralgauskaitė), vilius.palenskis@ff.vu.lt (V. Palenskis), jonas.matukas@ff.vu.lt (J. Matukas).

http://dx.doi.org/10.1016/j.sse.2017.05.002
0038-1101/© 2017 Elsevier Ltd. All rights reserved.

To date, despite the fact that first attempts to create a room temperature continuous-wave (CW) mid-infrared laser diode reach the ninth decade of the last century, there are only few articles on electrical low frequency noise investigation in GaSb-based MIR laser diodes [14,15]. Noise behavior of ohmic contacts on GaSb was reported in [16]. There are several works, where the excess noise in mid-infrared avalanche photodiodes of AlInAsSb grown on GaSb and InAs/GaSb strained layer superlattice has been investigated [17,18]. Therefore, noise behavior in antimonide-based heterostructures is in general very little studied and of high interest.

In this paper, we present an experimental study of noise characteristics (electrical and optical fluctuations) and cross-correlation coefficient between electrical and optical fluctuations of different 2–3 μm GaSb-based laser diodes. The aim of the work is to identify physical processes that take place during LD operation, to determine possible noise sources in the investigated devices and to assess their impact to overall reliability of the device.

This article is structured as follows: in Sections 2 and 3 the noise measurement technique and the main properties of the investigated devices are described; in Section 4.1 the noise behavior of forward biased LDs below lasing threshold is presented; Section 4.2 describes the electrical and optical noise characteristics at lasing operation and their cross-correlation coefficient; Section 4.3 is devoted to analysis of noise characteristics at reverse bias for selected LDs with and without facet passivation.

2. Measurement technique

Low-frequency 10 Hz–250 kHz voltage noise spectral density (optical noise – the emitted light power fluctuations; electrical noise – the laser diode voltage fluctuations) and cross-correlation coefficient between optical and electrical fluctuations have been measured under CW operation at room temperature using a thermoelectric cooler for stabilization of the sample temperature. Laser diode emitted light and its power fluctuations were registered by PbSe photodetector, which is suitable for 1.5–4.8 μm wavelength radiation detection. Fig. 1 shows a measurement circuit for simultaneous investigation of two noise sources: optical and electrical. Each noise measurement channel has the low-noise amplifier, the filter system and the analogue-to-digital converter NI PCI-6115. Current generator mode is guaranteed for LDs by choosing appropriate bias voltage and load resistance. The spectral density of voltage fluctuations is estimated by using Fast Fourier Transform (FFT). Absolute value of the measured noise voltage spectral density is calculated by comparing with thermal noise of the reference resistance, R_{ref}:

$$S_U = \frac{\overline{\Delta u_{LD}^2} - \overline{\Delta u_{syst}^2}}{\overline{\Delta u_{ref}^2} - \overline{\Delta u_{syst}^2}} 4kT_0R_{ref}; \quad (1)$$

where $\overline{\Delta u_{LD}^2}$, $\overline{\Delta u_{syst}^2}$ and $\overline{\Delta u_{ref}^2}$ are, respectively, the variances of the laser diode, the measuring system, and the reference resistor thermal noises in the narrow frequency band Δf; T_0 is the absolute temperature of the reference resistor. Specially designed low-noise amplifier (LNA in Fig. 1) with noise equivalent resistance of 13 Ω (at 1 kHz) was used for electrical noise measurements. The floor of the optical noise was determined by the thermal noise of the load resistor $R_{PD\ load}$ of the photodetector.

Two identical channels for noise measurement that operate simultaneously enable to measure the cross-correlation coefficient between optical and electrical fluctuations. Simultaneous cross-correlation coefficient was directly measured not only over frequency region from 10 Hz to 20 kHz, but also in every one-octave frequency range by using digital filters and computed by the following expression:

$$k = \frac{\langle u_{el}(t) \cdot u_{op}(t) \rangle}{(\sigma_{el}^2 \cdot \sigma_{op}^2)^{1/2}}; \quad (2)$$

where brackets $\langle \ldots \rangle$ mean averaging both on time and on number of realizations, $\sigma_{el}^2 = \langle u_{el}^2(t) \rangle$, $\sigma_{op}^2 = < u_{op}^2(t) >$ are the variances of electrical and optical fluctuations in investigated frequency range, respectively. Positive cross-correlation factor indicates that optical and electrical noise signals change simultaneously in phase, while negative correlation indicates a change in opposite phases. Evaluation of the error of cross-correlation coefficient did not exceed 1%.

Noise characteristic measurements were carried out in a special Lab room screened by iron and copper sheets (Faraday cage) in order to avoid interferences from extrinsic electromagnetic field. All measurements have been performed at room temperature (293 K).

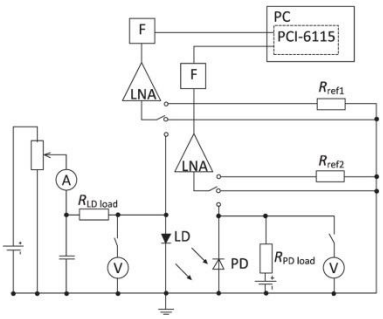


Fig. 1. Two channel noise measurement system: LD – laser diode, PD – photodetector, $R_{LD\ load}$, $R_{PD\ load}$ – load resistances, R_{ref1}, R_{ref2} – reference resistors, LNA – low-noise amplifier, F – filter system, PC – personal computer, PCI-61115 – analogue-to-digital converter.

3. Electrical and optical properties of investigated LDs

The main features of the devices presented in this paper are summarized in the Table 1. In general, investigated samples could be classified in three main groups by: (1) different structure: number of QWs, waveguide layer and composition; (2) package type: C–mount or TO5; (3) facet coating: with or without anti-reflective/high-reflective (AR/HR) coating. In this section epitaxial structure and the main electrical and optical characteristics of investigated specimens will be introduced.

3.1. Device structure and growth

Investigated devices were grown by means of solid-source molecular beam epitaxy (MBE). All of the investigated devices contain doped $Al_{0.5}Ga_{0.5}As_{0.04}Sb_{0.96}$ claddings, LDs 1, 2, 4, 5 have nominally undoped $Al_{0.1}Ga_{0.9}As_{0.01}Sb_{0.99}$ waveguide layers and barriers, where two GaInAsSb compressively strained QWs are embedded. LD 3 has a quinary AlGaInAsSb waveguide layer and three QWs in the active region (Fig. 2). After MBE growth devices were fabricated into narrow ridge-waveguide lasers for single spatial mode emission. Cavities of 1 mm length were formed by cleaving. Cleaved facets were either left as-cleaved (LD 3 and LD 5) or coated with high-reflective (95%) and anti-reflective coatings (up to 5%), where Ta_2O_5 was used for AR side and a multi stack of Si/SiO_2 for HR one.

Table 1
Features of investigated devices.

Sample	LD 1	LD 2	LD 3	LD 4	LD 5
Number of QW	2	2	3	2	2
QW/barrier	GaInAsSb/AlGaAsSb		GaInAsSb/AlGaInAsSb	GaInAsSb/AlGaAsSb	
Threshold current (mA)	68	36	96	100	67
Central wavelength (nm)	2442 (400 mA)	2101 (300 mA)	2927 (200 mA)	2432 (300 mA)	2430 (250 mA)
Package	TO5	C–mount	C–mount	TO5	TO5
AR/HR coating	Yes	Yes	No	Yes	No

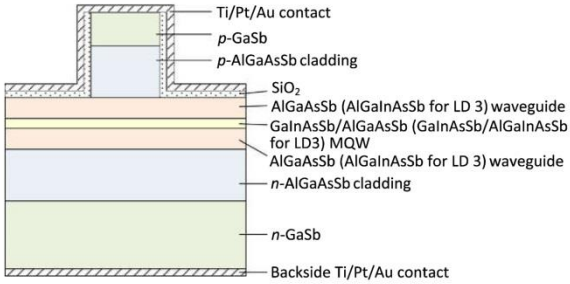


Fig. 2. Schematic structure of investigated LDs.

LD 4 and LD 5 were very similar samples from the same batch grown on the same wafer except that one is with facet coating and the other without it.

Finally, laser bars were chipped and mounted onto respective packages: indium soldering to a C–mount was used for LD 2 and LD 3 and indium soldering to full-copper body TO5 headers in case of the remaining samples was used (Table 1).

In Fig. 3(a) there is presented the light emission spectrum for LD 2, which is similar to other specimens with several intensive competing longitudinal modes. Due to formed waveguide structure all investigated samples demonstrate single-spatial mode operation. An example of far-field profile for the LD is presented in Fig. 3(b).

3.2. Electrical and optical characteristics of investigated devices

The current–voltage (I–V) characteristics for all investigated specimens are presented in Fig. 4(a). The latter characteristics can give some information on semiconductor laser diode quality: ideality factor η of I–V characteristic ($I = I_0[\exp(eU/\eta kT) - 1]$) in small current region larger than 2 indicates that there is leakage current through the channels formed by defects in the diode structure. In the investigated specimens in small current region (up to approx. 1 mA) the ideality factor varies from 1.8 to 2 that indicates to generation-recombination (g–r) processes in p–n junction. The deviation from exponential law at higher currents is due to the series resistance including contact resistances of the device. There is no evident influence to I–V characteristics caused by package type and facet coatings of LDs.

Characteristics of the normalized light output power (which is proportional to the photovoltage U_{photo} on the load resistance of photodetector) are presented in Fig. 4(b). The light output power gradually saturates as the injected current increases due to heating of the device. Influence of structure difference to the LDs optical characteristics could be observed from characteristics of samples with different composition, e. g. LD 2 ($\lambda \approx 2.1$ μm) and LD 3 ($\lambda \approx 2.9$ μm). The threshold current value of LD 2 sample is smaller due to the smaller Auger recombination, while larger threshold can

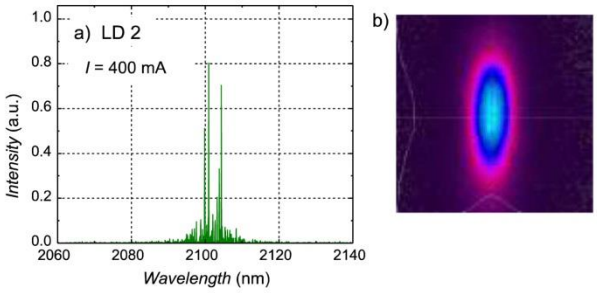


Fig. 3. (a) Light emission spectrum for LD 2 at stable lasing operation and (b) far-field profile at 400 mA forward current for LD 1.

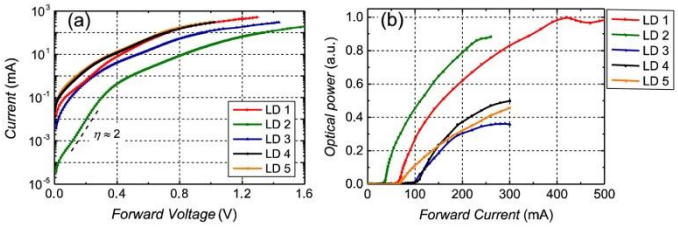


Fig. 4. (a) The current–voltage characteristics and (b) the emitted light output power dependences on forward current (normalized to maximum optical power of LD 1).

be attributed to increased Auger recombination (which is dominant at room temperature for long wavelength lasers) [9] and free carrier absorption losses. The influence of the AR/HR coating to laser diode threshold current could be evaluated comparing two identical samples: one with facet coating and the other without it. In our experiment LD 4 and LD 5 follow these conditions and could be compared (see Section 3.1). Internal losses due to AR/HR coating are larger ($\sim$10 cm^{-1}) than losses of specimen without coating ($\sim$7.8 cm^{-1}) and this explains why threshold current of LD 4 is larger than LD 5 (Fig. 4b). Also, a small kink is observed in light output dependency on current in case of LD 1 (Fig. 4b) due to spatial hole burning phenomenon [19], that is a consequence of formed ridge waveguide structure.

4. Results and discussion of noise measurements

In order to evaluate the impact of different growth structure, package type and facet passivation on laser diode performance and reliability, the low frequency noise measurements have been performed. Low frequency fluctuations were investigated at forward bias below the laser threshold, i.e. where only spontaneous emission appears, and above the threshold current at lasing operation.

4.1. Noise characteristics at forward current below the lasing threshold

Low-frequency noise characteristics in small current region (below the lasing threshold) are much more informative than regular *I–V* characteristics. Processes, observed at the currents far below laser diode threshold, could be used as precursors of device quality and degradation mechanism which affects LD reliability. Nowadays such measurements are of a great importance especially for high-power laser diodes as a non-destructive testing method, as in this case the bias current is far below the threshold and does not damage the internal specimen structure [20].

The electrical noise spectra of the investigated LDs are close to $1/f^{\alpha}$-type over all investigated frequency range with some appearances of Lorentzian-type components (graph (a) in Fig. 5). In the majority of the semiconductor devices $1/f^{\alpha}$-type fluctuations are originating from a superposition of charge carrier capture and release processes in the capture centers with widely distributed relaxation times [21]. These centers are formed by various defects in the device structure that were obtained during its fabrication or due to degradation.

Usually for various diode type optoelectronic devices spectral density of electrical noise decreases with forward current increasing, i. e. spectral density of the current fluctuation, S_I, in *p–n* junction is approximately proportional to the forward current I, thus voltage spectral density $S_U \sim S_I \cdot R_d^2 \sim 1/I$ (as differential resistance of the diode $R_d \sim 1/I$). Such behavior was observed in many GaN or InGaN light-emitting diodes (LEDs) and also in InGaAsP laser diodes before threshold [22,23]. However, additional features have been observed for GaSb-based laser diodes. One could be seen in Fig. 5(b): a local increase of electrical noise spectral density as the current is increased from 10 μA to 1 mA for all investigated devices (for LD 2 sample this increase is slightly shifted to smaller current values). In this current region the calculated electrical noise spectral density of the current fluctuation ($S_I = S_U/R_d^2$) also has a bump and is proportional to the square of the forward current. This means that the occupancy of the trap levels increases with current increase [24]. This may lead to the additional generation-recombination noise components in noise spectra (LD 1 in Fig. 5 a). In order to observe a single Lorentzian type spectrum, a certain *g–r* center density must be much larger than others, because superposition of Lorentzians with comparable densities of traps and different cut-off frequencies lead to the $1/f^{\alpha}$-type spectrum.

Additional *g–r* noise components were detected not only in LD 1 sample characteristics, but also for the LD 4 and LD 5 at I = 0.02 mA. Dependence of the relaxation time τ, on temperature

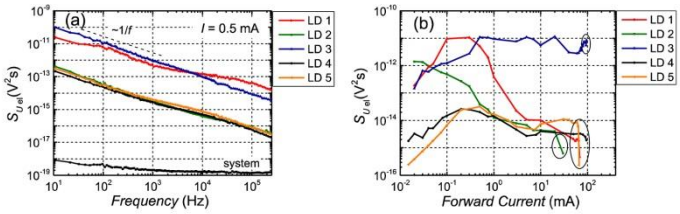


Fig. 5. (a) Typical electrical noise spectra of the investigated samples at forward current 0.5 mA ("system" represents the measurement system electrical noise floor); (b) dependencies of voltage spectral density of electrical noise on forward current at 108 Hz frequency (circles denote the subthreshold regions).

for the observed g–r processes (Fig. 6) was estimated ($\tau = 1/[2\pi f_0]$). Using equation $\tau = \tau_0 \exp(\Delta E/kT)$ [24], the activation energy ΔE of these trap levels has been determined (Fig. 6).

Experimentally determined activation energies are distributed from low energies (0.1 eV) up to approximately half of the barrier bandgap (0.4 eV), which in this case suggests that these noise sources are related to the recombination processes in the barrier (in the QWs structure) layers.

It must be pointed that low frequency noise intensity at current $I > 1$ mA for LD 3 is remarkably higher than for other ones (Fig. 5). This indicates higher defectiveness which is possibly related with different than other samples quinary waveguide layer of LD 3 as a possible noise source. Differences in local maxima level for the remaining LDs could be related to different density of trap levels which are a consequence of different growing conditions, e. g. slight variation in growing optimum temperature. For the same fabrication samples (LD 4 and LD 5) noise characteristics look similar.

Absence of facet coating can lead to the higher density of the interfacial states and higher number of point defects [25]. Two uncoated samples (LD 3 and LD 5) were investigated. However, we attribute to different LD 3 structure as a main reason of high electrical noise level, because the other specimen without facet coating (LD 5) do not show any noticeable difference in the noise characteristics compared with coated sample LD 4.

Due to the above mentioned reasons a sudden drop up to 1.5 order of magnitude in the electrical noise spectral density at forward current just before the threshold value (marked with circles in Fig. 5b) is concealed for LD 3 because of additional defects and higher electrical noise level. This drop is related to the quasi-Fermi level clamping at the lasing threshold when stimulated emission process take place and also a kink in electrical derivative ($Id U/dI$) characteristic appears due to p–n junction voltage saturation [26].

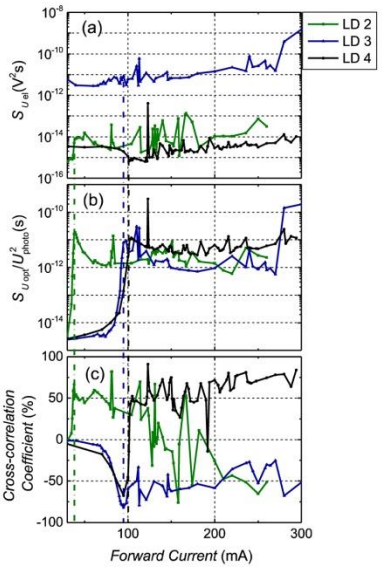


Fig. 7. Dependencies of (a) the spectral density of electrical noise and (b) the normalized spectral density of optical noise at 108 Hz frequency and (c) their cross-correlation coefficient over all frequency range 10 Hz–20 kHz on forward current at the lasing operation. Dashed lines denote different threshold current values for presented LDs.

4.2. Noise characteristics at the lasing operation

High level of the laser diode terminal voltage fluctuations does not always indicate high defectiveness of the LD active layer, it can be related with the physical processes outside the active region (peripheral regions or contact areas) that weakly influence the light emission process [27] or with high interfacial state density [28]. Cross-correlation coefficient between optical and electrical fluctuations is much more sensitive indicator of defectiveness of the active region and its interfaces. So, in order to evaluate this coefficient, optical noise at the lasing operation was measured.

At lasing operation correlated noise peaks are observed in electrical and optical noise dependencies on forward current (Fig. 7).

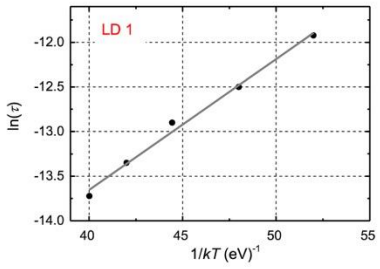


Fig. 6. Dependency of relaxation time on temperature for ΔE evaluation for sample LD 1 at forward current I = 0.5 mA.

These peaks, where noise intensity increases up to 2 orders of magnitude, are caused by the mode-hopping effect [29]. The resonator of investigated lasers was long (1 mm), so the distance between adjacent longitudinal modes is small (graph (a) in Fig. 3). During the mode-hopping the peak longitudinal mode hops to the neighboring one when optical gain of the adjacent mode exceeds the gain of the peak one.

Results for samples LD 2, LD 3 and LD 4 are presented in Fig. 7 as three types of cross-correlation coefficient dependency on forward current could be distinguished for investigated devices. Noise level at the lasing and cross-correlation coefficient behavior for specimens LD 1 and LD 5 are very similar to the sample LD 4. Main results at lasing operation are summarized in Table 2.

Despite the mode-hopping peaks, cross-correlation coefficient could be: (1) positive as for sample LD 4 (and also for LD 1, LD 5), (2) negative as for LD 3 and (3) as for LD 2 – transiting from positive to negative. Positive cross-correlation indicates that optical and electrical $1/f^{\alpha}$-type fluctuations are caused by the defects in the active region of LD and these defects randomly modulate the free charge carrier number in the active layer and, as a consequence, lead to the photon number fluctuations that have the same phase as the carrier number fluctuations. Negative correlation, as in the case of LD 3 and LD 2 at current above 200 mA, indicates that there is leakage current out of the active region when majority of the active defects are at the interface of the active region and modulate potential height of the barrier leading to the current redistribution between the active region and the neighbor layers. This, especially in the case of LD 3, is concomitant with non-radiative recombination in facets forming leakage current channels that also can modulate and increase light losses in facets.

Table 2
Main results and features of investigated LDs at lasing (despite mode-hopping peaks).

Sample characteristic	LD 1 LD 4 LD 5 LD 2		LD 3
Electrical noise level at I = 200 mA and f = 108 Hz	Similar (difference up to 1 order)		Highest (up to 3 orders higher than remaining LDs)
Normalized optical noise level at I = 200 mA and f = 108 Hz	Differences are less than 1 order		
Cross-correlation coefficient	Positive	Transiting from positive to negative	Negative

Optical and electrical noise spectra during mode-hopping are Lorentzian-type (Fig. 8a and b) and this type fluctuations at mode-hopping prevails $1/f^{\alpha}$-type noise level. Lorentzian-type spectra are characteristic for the g–r processes in carrier capture centers that are formed by defects and imperfections in LD layers. More about mode-hopping effect on the noise properties could be found in our previous works [27,29].

During the mode-hopping electrical fluctuations of specimen LD 3 remains $1/f^{\alpha}$-type in our investigated frequency range over all investigated current range (Fig. 8c). From Fig. 7(a) it is seen that electrical noise level of LD 3 at the lasing operation is the highest comparing to other samples. We attribute that in this case Lorentzian-type fluctuations, originated from the charge carrier retrapping during the mode-hopping, do not prevail the high level of electrical $1/f^{\alpha}$-type noise. This can be proved by the fact that in optical noise spectra of LD 3 Lorentzian-type spectra are observed during mode-hopping (Fig. 8d). The highest noise level of sample LD 3 is related to complexity in manufacturing of longer wavelength (λ = 2.9 μm) LDs. In case of LD 3, quinary waveguide is the main difference of the remaining devices. The fact that noise arises mainly from the active layer structure is confirmed by the lowest light output, high threshold current value (facets of this LD are uncoated) and negative cross-correlation coefficient at lasing. Higher defectiveness (caused by quinary waveguide of LD 3) leads to that more charge carries are redistributed between the active and the cladding layers and less charge carriers recombine radiatively, i.e. generate photons.

It was obtained that different LDs package types do not directly influence the device performance characteristics. Electrical noise characteristics before and during lasing of C–mounted samples for LD 2 and LD 3 strongly differ while LD 2 noise characteristic is similar to other samples in TO5 packages.

Mode-hopping effect dominates at the lasing, but no remarkable differences in noise characteristics were observed between the samples with AR/HR coating and without it. For this reason, noise characteristics of samples LD 4 and LD 5 were measured also in reverse bias to evaluate influence of coating process.

4.3. Noise characteristics of reverse biased LD 4 and LD 5 samples

Noise measurements of reverse biased devices mostly are used to analyze physical processes in photodiodes or avalanche breakdown p–n junction diodes [30]. Such measurements applied to laser diodes are especially important for the comparison of similar quality samples [31].

Reverse I–V and noise characteristics were measured safely in order to avoid the breakdown and p–n junction damaging: the current and the bias voltage have the restriction circuits. In the

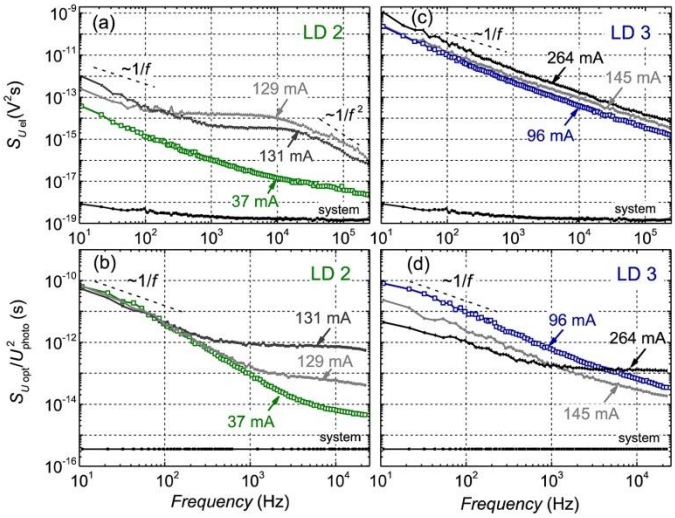


Fig. 8. (a and c) Electrical and (b and d) optical noise spectra dependencies on frequency at the mode-hopping peak at different injection currents for sample LD 2 (left) and for LD 3 (right) (current values 37 mA (LD 2) and 96 mA (LD 3) represent the threshold currents).

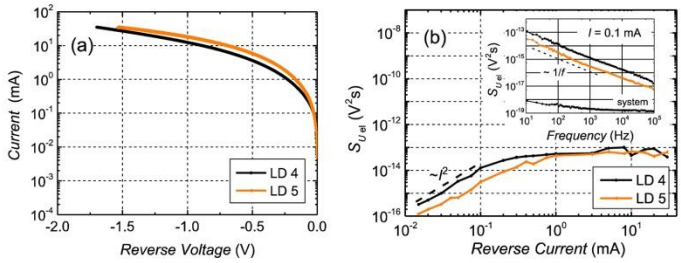


Fig. 9. (a) Reverse current–voltage characteristics; (b) dependencies of voltage spectral density of electrical noise on reverse current at $f = 108$ Hz and electrical noise spectra of LD 4 and LD 5 samples at reverse current $I_R = 0.1$ mA (in the inset).

breakdown region reverse current ($I_R = I_d + I_g$) is caused by diffusion (I_d) and generation of carriers (I_g), and depends on p–n junction depletion width (Fig. 9a).

Reverse electrical noise spectra for both LDs are $1/f^{\alpha}$-type in whole investigated frequency range (Fig. 9b). In small current region electrical noise increases as $S_U \sim I^2$ what indicates that the main noise source is fluctuations of parasitic leakage resistance. Saturation of electrical noise spectral density is related with a shunting effect caused by differential resistance R_{diff}.

No significant difference in noise level measured in forward (Fig. 5b) and reverse (Fig. 9b) directions for coated LD 4 and uncoated LD 5 devices indicates poor facet passivation as it could be expected that appropriate passivation is attributed to decrease of the surface state density and as a consequence to lower noise level [28]. In contrast, slightly higher noise level of coated LD 4 sample up to $I_R \approx 0.2$ mA possibly is a consequence of a non-optimum coating process.

Also, in case of the investigated samples, influence of non-radiative recombination at the interfacial states located at the uncoated laser facets to noise characteristics is rather weak and this is not a dominant noise source. However, measurements of negative cross-correlation coefficient show that it could not be completely rejected as a possible noise source (sample LD 3).

5. Conclusions

A comprehensive investigation of noise characteristics of the mid-infrared 2–3 μm GaSb-based type-I laser diodes has been performed at forward (below the threshold and at lasing) and reverse biases for selected samples.

Investigated LDs in low frequency region exhibit $1/f^{\alpha}$-type and Lorentzian-type electrical fluctuation spectra at operation below the threshold. A bump in LDs electrical noise characteristics in small current region indicates the presence of high density trap. At the lasing operation mode-hopping effect is dominant and causes intensive highly positively or negatively correlated Lorentzian-type electrical and optical fluctuations. No major differences in noise level in forward and reverse biases might indicate non-optimum LDs facet passivation process.

Differences in internal LD structure, i. e. waveguide layer and slightly different composition, have got the largest influence to LD noise characteristics and influence of other factors, such as absence of facet coating and packaging type, is much weaker.

Obtained measurement results and analysis could be used for device design, technological improvement and device reliability evaluation.

Acknowledgements

The authors would like to thank Kristijonas Vizbaras and Augustinas Vizbaras (Brolis Semiconductors UAB, Vilnius, Lithuania) for providing samples, their specifications and valuable consultations.

References

[1] Rothman LS, Gordon IE, Babikov Y, et al. The HITRAN2012 molecular spectroscopic database. J. Quant. Spectrosc. Radiat. Transf. 2013;130:4–50.
[2] Dvinelis E, Trinkūnas A, Greibus M, et al. High-performance GaSb laser diodes and diode arrays in the 2.1-3.3 micron wavelength range for sensing and defense applications. In: Proc. of SPIE, 2015. 9370:93702E.
[3] Yang RQ, Bradshaw JL, Bruno JD, et al. Appl Phys Lett 2002;81:397–9.
[4] Sprengel S, Andrejew A, Vizbaras K, et al. Type-II InP lasers emitting at 2.55 μm. Appl Phys Lett 2012;100:041109.
[5] Hosoda T, Chen J, Tsvid G, et al. Int J Hi Spe Ele Syst 2011;20(1):43–9.
[6] Vizbaras K, Amann M-C. 3.6 μm GaSb-based type-I lasers with quinternary barriers, operating at room-temperature. Electron Lett 2011;47:980–1.
[7] Vizbaras K, Amann M-C. Room-temperature 3.73 μm GaSb-based type-I quantum-well lasers with quinternary barriers. Semicond Sci Technol 2012;27:032001.
[8] Kashani-Shirazi K, Vizbaras K, Bachmann A, et al. Low threshold strained quantum-well gasb-based lasers emitting in the 2.5–2.7 μm wavelength range. IEEE Photon Technol Lett 2009;21(16):1106–8.
[9] Joullié A, Christol P. GaSb-based mid-infrared 2–5 μm laser diodes. C R Phys 2003;4:621–37.
[10] C.D. Theis, D.J. Siconolfi, R.B. IEEE Proc. 50th comizzoli, highly accelerated life testing for non-hermetic laser modules, electronic components & technology conference 2000; 2000. p. 955–961.
[11] Lu G, Xie S, Huang Y, Cao J. Effective methods for evaluation of high power laser diode quality and reliability. In: Proceedings of the international conference on reliability, maintainability and safety (ICRMS), IEEE; 2014. p. 874–877.
[12] Vandamme LKJ. Noise as diagnostic tool for quality and reliability of electronic devices. IEEE Trans Electron Dev 1994;41:2176–87.
[13] Jones BK. Electrical noise as a reliability indicator in electronic devices and components. IEEE Proc Circ Dev Syst 2002;149:13–22.
[14] Chobola Z, Vaněk J, Hulicius E, Šimeček T. Noise as a diagnostic tool for quality of gasb laser diodes. In: Proceedings of the international conference on microelectronics (MIEL 2006), IEEE; 2006.
[15] Chobola Z, Luňák M, Vaněk J, et al. Low-frequency noise measurements used for quality assessment of GaSb based lasers diodes prepared by molecular beam epitaxy. J Electr Eng 2015;66(4):226–30.
[16] Rolland M, Gaillard S, Villemain E, et al. Low-noise ohmic contacts on n and p type GaSb. J Phys III France 1993;3:1825–32.
[17] Woodson M, Ren M, Maddox SJ, et al. Low-noise AlInAsSb avalanche photodiode. Appl Phys Lett 2016;108(081102):1–4.
[18] Ghosh S, Mallick S, Banerjee K, et al. Low-noise mid-wavelength infrared avalanche photodiodes. J Electron Mater 2008;37(12):1764–9.
[19] Shigihara K, Kawasaki K, Yoshida Y, et al. High-power 980-nm ridge waveguide laser diodes including an asymmetrically expanded optical field normal to the active layer. IEEE J Quantum Electron 2002;38(8):1081–8.
[20] Guan J, Guo S, Wang J, et al. Analysis of origin of measured $1/f$ noise in high-power semiconductor laser diodes far below threshold current. Microelectron Reliab 2016;59:55–9.
[21] Palenskis V, Maknys K. Nature of low-frequency noise in homogenous semiconductors. Sci Rep 2015;5(18305):1–7.

[22] Pralgauskaite S, Palenskis V, Matukas J. Reliability investigation of light-emitting diodes via low frequency noise characteristics. Microelectron Reliab 2015;55(1):52–61.
[23] Palenskis V, Matukas J, Pralgauskaite S. Light-emitting diode quality investigation via low-frequency noise characteristics. Solid State Electron 2010;54(8):781–6.
[24] Levinshtein ME, Rumyantsev SL. Noise spectroscopy of local levels in semiconductors. Semicond Sci Technol 1994;9(6):1183–9.
[25] Fukuda M. Optical semiconductor device reliability. Microelectron Reliab 2002;42:679–93.
[26] Schilt S, Tombez L, Tardy C, et al. An experimental study of noise in mid-infrared quantum cascade lasers of different designs. Appl Phys B 2015;119:189–201.
[27] Pralgauskaitė S, Palenskis V, Matukas J. Low frequency noise characteristics of multimode and single mode laser diodes. In: Semiconductor laser diode technology and applications; 2012. p. 133–60 [chap. 8].
[28] Hakimi R, Amann M-C. Reduction of 1/f carrier noise in InGaAsP/InP heterostructures by sulphur passivation of facets. Semicond Sci Technol 1997;12:778–80.
[29] Palenskis V, Matukas J, Pralgauskaitė S, et al. Experimental investigations of the effect of the mode-hopping on the noise properties of InGaAsP fabry-pérot multiple-quantum-well laser diodes. IEEE Trans Electron Dev 2003;50:336–71.
[30] Marinov O, Jamal Deen M. Low frequency noise in avalanche breakdown of pn junction diodes. In: Proc. 16th int. conf. noise in physical systems and 1/f fluctuations. World Scientific; 2001.
[31] Del Vecchioa P, Curutcheta A, Deshayesa Y, et al. Correlation between forward-reverse low-frequency noise and atypical I-V signatures in 980 nm high-power laser diodes. Microelectron Reliab 2015;55:1741–5.



Justinas Glemža was born in Vilnius, Lithuania, in 1991. He received BSc and MSc degree in Telecommunication physics and Electronics at Vilnius University, Faculty of Physics, Vilnius, Lithuania, in 2014 and 2016, respectively. Currently, he is a PhD student at the Noise Research Laboratory, Vilnius University, Lithuania. His main interests are low-frequency noise of optoelectronic devices: semiconductor laser and light-emitting diodes, their reliability assessment and noise origin in semiconductors phenomenon. *Main publications:* 1. J. Glemža, J. Matukas, S. Pralgauskaitė, Low Frequency Noise Spectroscopy and Threshold Characteristics of Laser Diodes, IEEE Proc. of 21st International Conference on Microwaves, Radar and Wireless Communications (MIKON), (2016) Electronic ISBN: 978-1-5090-2214-4, DOI: 10.1109/MIKON.2016.7491951. 2. S. Pralgauskaitė, V. Palenskis, J. Matukas, J. Glemža, G. Muliuk, B. Šaulys, A. Trinkūnas, Reliability investigation of light emitting diodes via low frequency noise characteristics, Microelectron. Reliab. 55 (1) (2015) 52-61.

P2

J. Glemža, V. Palenskis, S. Pralgauskaitė, J. Vyšniauskas, J. Matukas,

Properties of the surface generation-recombination noise in 1.94 μm GaSb-based laser diodes,

Infrared Phys. Technol. **91**, 101–106 (2018).
doi: 10.1016/j.infrared.2018.04.002.

Copyright © 2018 Elsevier B.V. All rights reserved.

Leidimas perspausdinti disertacijoje nereikalingas

Permission to reprint in a dissertation is not required

Infrared Physics & Technology 91 (2018) 101–106

Contents lists available at ScienceDirect

Infrared Physics & Technology

journal homepage: www.elsevier.com/locate/infrared

Regular article

Properties of the surface generation-recombination noise in 1.94 μm GaSb-based laser diodes

Justinas Glemža *, Vilius Palenskis, Sandra Pralgauskaitė, Juozas Vyšniauskas, Jonas Matukas

Institute of Applied Electrodynamics and Telecommunications, Vilnius University, Saulėtekio av. 3, LT-10257 Vilnius, Lithuania

HIGHLIGHTS

- Generation-recombination noise in the investigated LDs is caused by surface leakage.
- Surface current leakage channel between n^+GaSb and p^+GaSb contacts exists.
- Resistance of the surface leakage channel is independent from the bias direction.

ARTICLE INFO

Article history:
Received 1 February 2018
Revised 5 April 2018
Accepted 8 April 2018
Available online 10 April 2018

Keywords:
Electrical noise
Fluctuation
GaSb laser diode
Generation-recombination noise
Surface leakage

ABSTRACT

A detail investigation of generation-recombination (g-r) noise in 1.94 μm GaSb-based type-I ridge waveguide laser diodes (LDs) has been performed in a temperature range (230–295) K. Lorentzian-type noise spectra have been observed in the current range below the threshold at the forward and reverse biases of the LDs with the same characteristic time (3.7 μs) and activation energy (≈0.37 eV) of charge carriers transitions associated with the g-r processes. An equivalent electrical circuit possessing the voltage noise source is presented, which allows the description of both the current-voltage characteristic and the voltage fluctuation spectral density of the laser diode. Results indicate that the origin of the g-r noise in the investigated samples is the surface recombination caused by the surface leakage current channel between n^+GaSb and p^+GaSb contacts, which is practically independent from the applied bias polarity.

© 2018 Elsevier B.V. All rights reserved.

1. Introduction

Laser diodes (LDs) and their arrays radiating at ~1.9 μm are widely used in pumping the Ho-doped solid state lasers, in military and defense for infrared countermeasures, in "eye-safe" illumination, in medicine for human tissue welding and vascular surgery due to strong optical absorption in tissues, etc. [1,2]. GaSb-based material system is widely used for such LDs manufacturing. These type-I semiconductor lasers, where ternary, quaternary and quinternary alloys are used for quantum wells (QWs) and barrier layers, can cover spectral range from 1.8 μm to 4 μm [3,4]. Due to a large variety of possible applications, there is a huge demand for high reliability and performance laser diodes in this spectral range. With increasing radiation wavelength, some major problems related to the carrier loss arise: Auger recombination and free carrier absorption [4,5]. Also, holes' leakage from the active area due to their poor confinement in the valence band is a common problem [6]. From the point of technology it is difficult to grow quaternary QWs and quinternary barriers due to annealing effects during the growth that lead to an increase in bandgap energy, i.e. to shorten the wavelength [4].

So, an effective and non-destructive characterization method for these emitters is necessary. The low-frequency noise spectroscopy is a promising diagnostic tool for various electronic devices [7,8]. It is well known that fluctuations with $1/f$ spectra dominate in the most semiconductor devices at low-frequencies due to the superposition of different generation-recombination (g-r) or capture-emission of charge carrier processes with very wide distribution of relaxation times [9]. Those g-r centers are formed by defects in the bulk, and by imperfections at the semiconductor surface, where breaking off periodic crystal potential, various adsorbed impurities and oxide layers create surface states [10]. In those cases when the g-r noise component with Lorentzian-type spectrum overheads the level of $1/f$ noise, the g-r noise spectroscopy is enabled. This allows detection and identification of local levels in semiconductors even when the deep level transient spectroscopy (DLTS) fails [7]. G-r and other

* Corresponding author.
E-mail addresses: justinas.glemza@ff.vu.lt (J. Glemža), vilius.palenskis@ff.vu.lt (V. Palenskis), sandra.pralgauskaite@ff.vu.lt (S. Pralgauskaitė), juozas.vysniauskas@ff.vu.lt (J. Vyšniauskas), jonas.matukas@ff.vu.lt (J. Matukas).

https://doi.org/10.1016/j.infrared.2018.04.002
1350-4495/© 2018 Elsevier B.V. All rights reserved.

low-frequency fluctuations are widely investigated in the most III-V group semiconductor lasers, e. g. in AlGaInP LDs [11,12], in AlGaAs LDs [13,14] and in InGaAsP [15,16]. Unfortunately, to our knowledge only a few studies on a low-frequency noise analysis in the GaSb-based laser diodes are published [17,18]. Under the particular circumstances variation of technological process of GaSb-based LDs manufacturing, e. g. change of the growth temperature or post growth annealing, leads to the unexpected high level g-r noise. For the further improving of design and growth technology of GaSb-based LDs, the origin of this g-r noise should be found and examined.

In this paper, we present a comprehensive investigation of 1.94 μm GaSb-based type-I laser diodes through low-frequency noise characteristics at the forward and reverse biases. The aim of this work is to identify the generation-recombination noise source, to relate it to the device structure and an equivalent electrical circuit of such LDs.

2. Experimental details and investigated samples

Low-frequency 10 Hz–500 kHz electrical noise (the laser diode terminal voltage fluctuations) has been measured under constant current operation in the current range below the threshold at the forward and reverse biases. Current-voltage (*I-U*) and noise characteristics at reverse bias were measured safely in order to avoid the damage of the quantum-well region in the LD structure. For *I-U* characteristics measurements a precision source/measure unit Keysight B2901 has been used. A noise measurement circuit is presented in Fig. 1. Current generator mode is guaranteed for the LDs by choosing appropriate feeding voltage and load resistance $R_{\mathrm{LD\ load}}$, which is at least ten times higher than the resistance of the sample under investigation. The used high power load resistor has been tested so that its own $1/f$ noise level in the measured current range would be many times smaller than its thermal noise. The measured fluctuations are amplified by a specially designed low-noise amplifier (LNA in Fig. 1) with a noise equivalent resistance of 13 Ω (at 1 kHz). A filter system confines the bandwidth of the analogue amplified signal which is being converted to the digital one. As an analogue-to-digital converter National Instruments PCI-6115 board has been used. The spectral density of voltage fluctuations is estimated by using Cooley-Tukey Fast Fourier Transform (FFT) and calculated spectral densities have been averaged by using over 300 of realizations in a narrow frequency band $\Delta f = 0.1f$ (here f is the central frequency of Δf). The absolute value

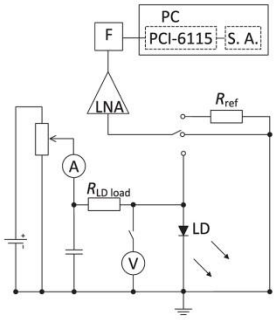


Fig. 1. The noise measurement system: LD – the laser diode under investigation, $R_{\mathrm{LD\ load}}$ – a load resistor, R_{ref} – a reference resistor, LNA – a low-noise amplifier, F – a filter system, PC – a personal computer, PCI-6115 – an analogue-to-digital converter, S. A. – FFT based spectrum analyzer program.

of the measured noise voltage fluctuation spectral density is calculated by comparing it to the thermal noise of the reference resistance, $R_{\mathrm{ref}} = 72\ \Omega$:

$$S_U = \frac{\overline{\Delta u_{\mathrm{LD}}^2} - \overline{\Delta u_{\mathrm{syst}}^2}}{\overline{\Delta u_{\mathrm{ref}}^2} - \overline{\Delta u_{\mathrm{syst}}^2}} 4kT_0R_{\mathrm{ref}}; \quad (1)$$

where $\overline{\Delta u_{\mathrm{LD}}^2}$, $\overline{\Delta u_{\mathrm{ref}}^2}$, and $\overline{\Delta u_{\mathrm{syst}}^2}$ are the variances of voltage fluctuations in the narrow frequency band Δf when the input of the LNA is connected, respectively, to the laser diode, to the reference resistor, and when the input of the LNA is short connected (in order to estimate the own noise level of the measuring system). Considering that all these fluctuations are not correlated, the variances in (1) can be written as $\overline{\Delta u_{\mathrm{LD}}^2} = \overline{\Delta u_{\mathrm{LD0}}^2} + \overline{\Delta u_{\mathrm{syst}}^2}$ and $\overline{\Delta u_{\mathrm{ref}}^2} = 4kT_0R_{\mathrm{ref}}\Delta f + \overline{\Delta u_{\mathrm{syst}}^2}$, where $\overline{\Delta u_{\mathrm{LD0}}^2}$ is the variance of the laser diode voltage fluctuations; k is the Boltzmann's constant, and T_0 is the absolute temperature of the reference resistor. The ratio in the (1) shows how many times the voltage fluctuation spectral density of the LD is larger than the spectral density of the reference resistor thermal noise. The noise measurements have been performed in a laboratory screened by iron and copper sheets (Faraday cage).

The investigated devices have been grown on n^+ GaSb substrate by solid-source molecular beam epitaxy (MBE). Investigated samples contain doped $Al_{0.5}Ga_{0.5}As_{0.04}Sb_{0.96}$ claddings, nominally undoped $Al_{0.25}Ga_{0.75}As_{0.02}Sb_{0.98}$ waveguide layers and barriers, where two 6.2 nm wide $Ga_{0.7}In_{0.3}Sb$ QWs are embedded (Fig. 2). For n cladding layer doping by Te has been used up to $3 \cdot 10^{17}$ cm^{-3}, while for p cladding layer linear Be doping profile varying from $1 \cdot 10^{17}$ cm^{-3} to $1 \cdot 10^{19}$ cm^{-3} has been used. The structure has been finalized with p^+ GaSb contact layer doped to $1 \cdot 10^{20}$ cm^{-3}. After MBE growth the wafers have been fabricated into 5 μm width ridge-waveguide devices for single spatial mode radiation. Cavities of 1 mm length have been formed by cleaving the wafers into laser bars and LDs' facets have been left as-cleaved. After that the laser bars have been chipped into separate emitters.

3. Results and discussion

3.1. Optical and electrical characteristics of forward biased GaSb-based LDs

Investigated samples radiate at 1.94 μm wavelength, and their typical output power characteristic is presented in Fig. 3. There light output power is proportional to the photovoltage U_{photo} on the load resistance of photodetector.

The typical current-voltage characteristic of the investigated LDs at forward current below the threshold is presented in Fig. 4 (the black curve with square symbols). As it is seen from this double logarithmic scale figure, *I-U* characteristic is linear at small currents (<0.5 mA), then quadratic, and at currents larger than 40 mA the index $n > 3$ ($I \sim U^n$). Thus, the obtained *I-U* characteristic can be described by a polynomial:

$$I = aU + bU^2 + cU^n; \quad (2)$$

where a, b and c are coefficients, and index n are determined from the best coincidence with the experimental curve (red curve in Fig. 4). Such current approximation usually is applicable for a double injection space charge limited diode [19]. Additionally, for the better experimental *I-U* characteristic approximation at large currents (>350 mA), the voltage drop caused by the contacts and resistances of the n^+ and p^+ ranges has been accounted. Such *I-U* characteristic description is very useful for the design of the equivalent electrical circuit of the LD and further analysis of its noise characteristics.

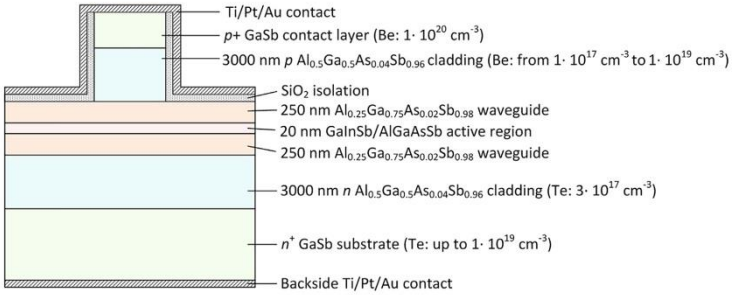


Fig. 2. A schematic structure of the investigated GaSb-based LD with two QWs. Corresponding doping densities are presented in brackets.

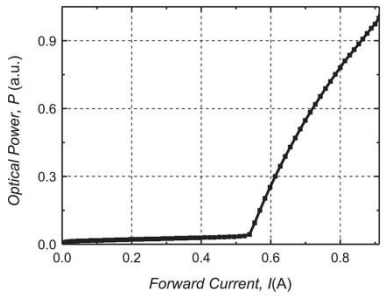


Fig. 3. Typical emitted light output power of the investigated GaSb-based LD.

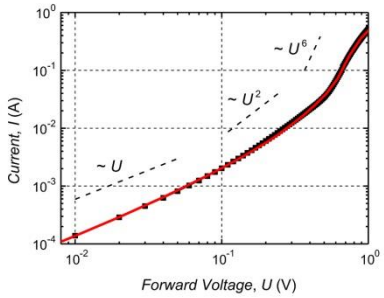


Fig. 4. Typical *I-U* characteristic of the forward biased LD in the current range below the threshold: the black square symbols represent the experimental results and the red curve – the approximation by (2). (For interpretation of the references to colour in this figure legend, the reader is referred to the web version of this article.)

3.2. Electrical noise characteristics at the forward bias

Low-frequency electrical fluctuations of investigated laser diodes at the forward bias distinguish by a clear generation-recombination noise (Lorentzian-type) spectra. Typical electrical noise spectra multiplied by frequency f, $S_{U\,\mathrm{el}}f$ (normalized voltage fluctuation spectral densities), at different forward current values are presented in Fig. 5(a). Such $S_{U\,\mathrm{el}}f$ representation is very useful for the noise spectroscopy [7] as it easily indicates the maximum of the normalized g-r noise voltage spectral density at characteristic frequency $f_0 \approx 43$ kHz, for which $2\pi f_0\tau = 1$. Thus, the relaxation time can be calculated as $\tau = 1/(2\pi f_0)$. From the noise spectra presented in Fig. 5(a) it can be pointed that the relaxation time τ does not depend on the forward current in the investigated current region at room temperature.

Usually the level of the g-r noise in various linear devices is proportional to the square of the direct current [20]. In the case of the investigated samples, this proportionality is satisfied up to 1 mA, at larger currents the spectral density of voltage fluctuation saturates and then the level of the g-r noise level steeply decreases (Fig. 5 (b)). There is no change in noise spectrum at different forward current regions at room temperature – spectra remain Lorentzian-type with the same relaxation time. In order to explain the obtained electrical noise characteristics at the forward current and relate them with the features of the sample *I-U* characteristic, an equivalent electrical noise circuit of the LD should be designed.

3.3. The equivalent electrical circuit of the LD and its g-r noise

An equivalent electrical noise circuit of the LD is presented in Fig. 6. Here resistance R_1 (about 75 Ω) is determined from the linear (ohmic) regime of *I-U* characteristic (Fig. 4) and represents the resistance of the current leakage channel. The meaning of this channel and its relation with the origin of the g-r noise will be explained sequentially. The resistance R_2 in respect of R_1 acts as a shunting differential resistance of the LD and is expressed as $R_2 = (\mathrm{d}U/\mathrm{d}I) - R_3 = \mathrm{d}U_2/\mathrm{d}I$ (here U is the voltage drop on the LD and I is the current corresponding this voltage value). Application of this expression and elimination of the linear regime of the *I-U* characteristic in (2) allows to find the dependence of the resistance R_2 on the forward voltage, which is $R_2 = 1/(0.1\ U + 3.5\ U^5)$. These calculated dependencies of the resistance R_2 and its current $I_2 = (U - U_{R_3})/R_2$ on the forward voltage are represented in Fig. 7. The determined value of series resistance R_3 (caused by the contacts' resistance and resistances of highly doped n^+ and p^+ areas) is more than 35 times lower than R_1 ($R_3 \ll R_1$).

If the source of the g-r noise is located in the resistance R_1 (Fig. 6), then voltage fluctuation spectral density for it can be written as:

$$S_{U\,\mathrm{g-r\,out}} = AU^2 \frac{\tau}{1 + (2\pi f\tau)^2} \cdot \left(\frac{R_2}{R_1 + R_2}\right)^2; \quad (3)$$

where quantity A defines the intensity of the noise. Here we take into account that $R_3 \ll R_1$ and $R_{\mathrm{Load}} \gg R_{\mathrm{mn}}$. The relaxation time τ has been evaluated from the experimental g-r noise spectra at room

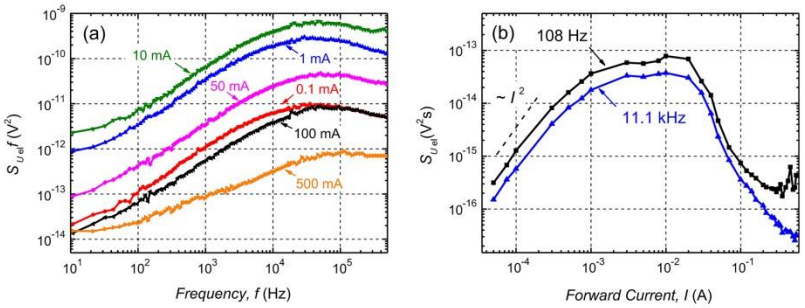


Fig. 5. (a) Normalized electrical noise spectra $S_{U\,el}\,f$ of the LD at different forward current values; (b) the voltage fluctuation spectral density ($S_{U\,el}$) dependencies on the forward current at 108 Hz and 11.1 kHz frequencies at room temperature.

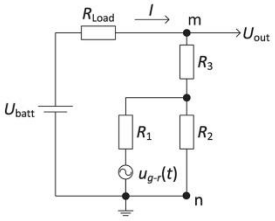


Fig. 6. The equivalent electrical circuit of the LD with the voltage g-r noise source $u_{g\text{-}r}(t)$. Thermal and $1/f$ noise sources are not shown because their level are many lower than the level of $u_{g\text{-}r}(t)$. There $R_{Load} \gg R_{mn}$.

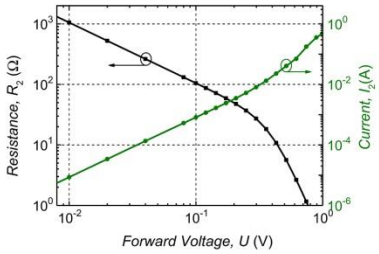


Fig. 7. Differential resistance R_2 and its current I_2 dependencies on the forward bias.

temperature (Fig. 5(a)): $\tau \approx 3.7$ μs. Comparison of the experimental results and computed one by (3) is presented in Fig. 8. Here, in a linear *I-U* range the level of g-r noise increases as U^2. The decrease in the g-r voltage noise spectral density above $U \approx 0.3$ V is explained by the shunting effect of the differential LD resistance R_2 due to steep decrease at higher voltages as it is observed from Fig. 7. Resistances R_2 and R_3 generate very weak $1/f^{\alpha}$-type electrical noise components, their levels are much smaller than the *g-r* noise level and they are visible only in the low-frequency region (<20 Hz). Thus, a good agreement between experimental and calculated dependencies of the LD g-r noise on the forward voltage (Fig. 8) confirms the idea that the resistance R_1 is the g-r noise source due to current leakage channel existing in the LD. The origin of this channel will be discussed in successive sections.

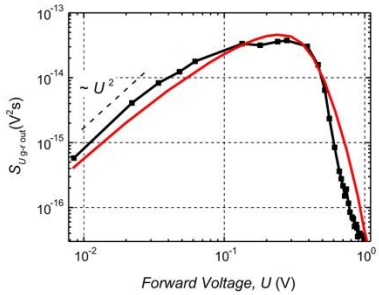


Fig. 8. Dependencies of voltage spectral densities $S_{U\,g\text{-}r\,out}$ of the equivalent circuit in Fig. 6 on the forward voltage at 11.1 kHz: black square symbols represent the experimental data and red curve – calculation results by (3).

3.4. The evaluation of relaxation time dependence on the temperature

In order to find the characteristic time and activation energy ΔE of the observed g-r processes, the electrical noise spectra have been measured in the temperature range from 230 K to 295 K. Typical normalized g-r noise spectra are proposed in Fig. 9(a). In this temperature interval the relaxation time $\tau = 1/(2\pi f_0)$ dependence on temperature can be described as [7]:

$$\tau = \tau_0 \exp(\Delta E/kT). \tag{4}$$

The activation energies of the all observed g-r processes in the forward current interval from 0.1 mA to 100 mA and temperature range from 230 K to 295 K are close to 0.37 eV (Fig. 9(b)). Regarding that the resistance R_1 is practically constant and at the small biases (<0.1 V) has a low value compared to the value of the own LD resistance R_2, the most presumable origin of the resistance R_1 can be considered as the resistance of the surface leakage current channel between the n^+ GaSb and the p^+ GaSb contacts. This channel is formed due to high density of the surface point g-r centers with the activation energy $\Delta E \approx 0.37$ eV.

3.5. Electrical noise characteristics at the reverse bias

In order to verify the role of the resistance R_1 and the origin of the g-r noise, the same research procedure and analysis has been

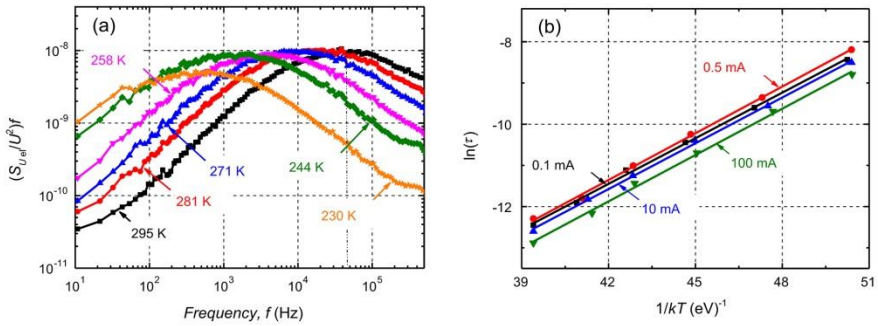


Fig. 9. (a) Normalized g-r noise spectra $(S_{U\,el}/U^2)f$ of the investigated LD at different temperatures at forward current I = 10 mA; (b) dependencies of the relaxation time on the temperature at different forward currents from 0.1 mA to 100 mA. Activation energy at all currents is $\Delta E \approx 0.37$ eV.

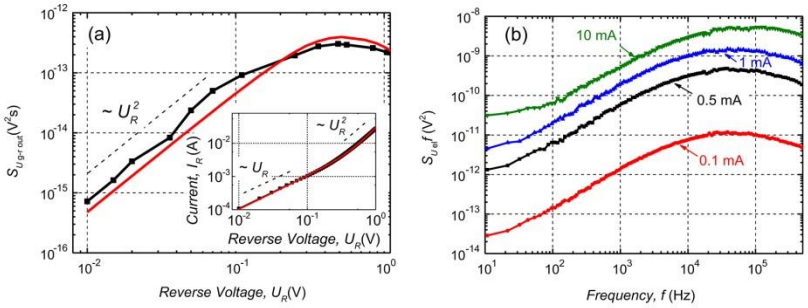


Fig. 10. (a) Dependencies of the voltage spectral density $S_{U\,g\text{-}r\,out}$ on the reverse voltage at 11.1 kHz. The inset shows *I-U* characteristic of the reverse biased LD. Here in (a) the black square symbols represent experimental values and the red curve – the calculation results by using (3) and (2). (b) Normalized electrical noise spectra $S_{U\,el}f$ of the LD at different reverse current values.

performed at the reverse bias as it has been described for LDs in the forward direction.

The experimental and calculated by (3) dependencies of the voltage spectral density $S_{U\ g\text{-}r\ out}$ on the reverse voltage at 11.1 kHz are depicted in Fig. 10(a). The ohmic part (resistance R_1, which is also about 75 Ω) of the reverse *I-U* characteristic (the inset in Fig. 10(a)) is characterized by analogical g-r noise characteristics: spectra are Lorentzian-type (Fig. 10(b)), the relaxation time τ in the investigated current interval does not depend on the reverse current, it coincides with the τ determined at the forward biases and the activation energy of the g-r process is the same ($\Delta E \approx$ 0.37 eV). Thus, the noise measurement results for both bias directions and the independence of the resistance R_1 value from the applied voltage polarity validates that the surface recombination due to formed surface leakage current channel is the main source of the observed g-r fluctuations. Formation of this channel strongly depends on technological variations during the LDs manufacturing as GaSb-based semiconductor lasers reported in [17,18] are characterized by different noise spectra (1/*f*-type electrical fluctuations) and the origin of these noise sources are also different.

4. Conclusions

Analysis of the origin of the low-frequency noise in 1.94 μm GaSb-based laser diodes has been performed.

Investigated LDs are characterized by the strong generation-recombination noise with Lorentzian-type spectra in the current range below the threshold at the forward and reverse biases with the same characteristic relaxation times, and the same activation energy (≈0.37 eV).

Analysis of the equivalent electrical noise circuit of the LD reveals that the ohmic part of the *I-U* characteristic (<0.1 V) is related to the resistance of the surface current leakage channel between the n^+GaSb and p^+GaSb contacts as the value of this resistance is independent on the applied voltage polarity.

Calculations of the voltage spectral density of the electrical g-r noise, which are in consistence with the experimental results, have shown that the origin of the observed g-r fluctuations can be explained by the surface recombination due to defects and imperfections at the LDs surface.

Conflict of interest

None.

Acknowledgements

The authors would like to thank Kristijonas Vizbaras and Augustinas Vizbaras (Brolis Semiconductors UAB, Vilnius, Lithua-

nia) for providing samples, their specifications and valuable consultations.

References

[1] M.T. Kelemen, J. Gilly, M. Rattunde, et al. Mid-infrared high-power diode lasers and modules, in: Proc. of SPIE, 2010, 7583:75830O.
[2] H.K. Choi, S.J. Eglash, High-power GaInAsSb-AlGaAsSb multiple quantum-well diode lasers emitting at 1.9 μm, IEEE Photon. Technol. Lett. 6 (1) (1994) 7–9.
[3] A. Vizbaras, E. Dvinelis, M. Greibus, et al. High-performance Single-spatial mode GaSb type-I laser diodes around 2.1 μm, in: Proc. of SPIE, 2014, 8993:899319.
[4] K. Vizbaras, M.C. Amann, Room-temperature 3.73 μm GaSb-based type-I quantum-well lasers with quinternary barriers, Semicond. Sci. Technol. 27 (032001) (2012) 1–4.
[5] K. Kashani-Shirazi, K. Vizbaras, A. Bachmann, Low-threshold strained quantum-well GaSb-based lasers emitting in the 2.5- to 2.7-μm wavelength range, IEEE Photon. Technol. Lett. 21(16) (2009) 1106–1108.
[6] G. Rainò, A. Salhi, V. Tasco, et al., Subpicosecond timescale carrier dynamics in GaInAsSb/AlGaAsSb double quantum wells emitting at 2.3 μm, Appl. Phys. Lett. 92 (2008) 101931.
[7] M.E. Levinshtein, S.L. Rumyantsev, Noise spectroscopy of local levels in semiconductors, Semicond. Sci. Technol. 9 (6) (1994) 1183–1189.
[8] B.K. Jones, Electrical noise as a reliability indicator in electronic devices and components, IEEE Proc. Circ. Dev. Syst. 149 (2002) 13–22.
[9] V. Palenskis, K. Maknys, Nature of low-frequency noise in homogenous semiconductors, Sci. Rep. 5 (18305) (2015) 1–7.
[10] R. Hakimi, M.C. Amann, Reduction of 1/f carrier noise in InGaAsP/InP heterostructures by sulphur passivation of facets, Semicond. Sci. Technol. 12 (1997) 778–780.
[11] S.L. Jang, K.Y. Chang, J.K. Hsu, Evidence of optical generation-recombination noise, Solid-State Electron. 38 (8) (1995) 1449–1453.
[12] X.Y. Chen, A. Pedersen, O.G. Hellesù, et al., Electrical noise of laser diodes measured over a wide range of bias currents, Microelectron. Reliab. 40 (2000) 1925–1928.
[13] R.Z. Fang, A.D. van Rheenen, A. van der Ziel, 1/*f* noise in double heterojunction AlGaAs/GaAs laser diodes on GaAs and on Si substrates, J. Appl. Phys. 68 (1990) 4087–4090.
[14] S.L. Jang, J.Y. Wu, Low-frequency current and intensity noise in AlGaAs laser diodes, Solid-State Electron. 36 (2) (1993) 189–196.
[15] Y. Dai, J. Shi, X. Zhang, A study of optical noise measurement as a reliability estimation for laser diodes, Microelectron. Reliab. 35 (4) (1995) 731–734.
[16] V. Palenskis, J. Matukas, S. Pralgauskaitė, et al., Experimental investigations of the effect of the mode-hopping on the noise properties of InGaAsP Fabry-Pérot multiple-quantum-well laser diodes, IEEE Trans. Electron Dev. 50 (2003) 336–371.
[17] Z. Chobola, M. Luňák, J. Vaněk, et al., Low-frequency noise measurements used for quality assessment of GaSb based lasers diodes prepared by molecular beam epitaxy, J. Electr. Eng. 66 (4) (2015) 226–230.
[18] J. Glemža, S. Pralgauskaitė, V. Palenskis, et al., Low-frequency noise investigation of 2–3 μm GaSb-based laser diodes, Solid-state Electron. 133 (2017) 70–77.
[19] A. Van der Ziel, Space-charge-limited solid-state diodes, in: R.K. Willardson, A. C. Beer (Eds.), Semiconductors and Semimetals: Lasers, Junctions, Transport, vol. 14, Academic Press, Inc., New York, 1979, pp. 195–248 (Chapter 3).
[20] V. Palenskis, J. Matukas, J. Vyšniauskas, et al., Analysis of noise characteristics of GaAs tunnel diodes, Fluct. Noise Lett. 12 (3) (2013) 1350014.

P3

J. Glemža, V. Palenskis, A. Geižutis, B. Čechavičius, R. Butkutė, S. Pralgauskaitė, J. Matukas,

Low-frequency noise investigation of 1.09 μm GaAsBi laser diodes,

Materials **12**, 673 (2019).
doi: 10.3390/ma12040673.

Visos teisės priklauso autoriams (2019). Tai atviros prieigos straipsnis, platinamas pagal Creative Commons Attribution licenciją (CC BY 4.0), kuri leidžia neribotą platinimą tinkamai cituojant originalų šaltinį ir nurodant licenciją.

Copyright © 2019 by the authors. This is an open access article distributed under the Creative Commons Attribution License (CC BY 4.0), which permits unrestricted reproduction, provided the appropriate credit and link to the license.

materials

MDPI

Article

Low-Frequency Noise Investigation of 1.09 μm GaAsBi Laser Diodes

Justinas Glemža [1,*], Vilius Palenskis [1], Andrejus Geižutis [2], Bronislovas Čechavičius [2], Renata Butkutė [2], Sandra Pralgauskaitė [1] and Jonas Matukas [1]

1 Institute of Applied Electrodynamics and Telecommunications, Vilnius University, Saulėtekio av. 3, LT-10257 Vilnius, Lithuania; vilius.palenskis@ff.vu.lt (V.P.); sandra.pralgauskaite@ff.vu.lt (S.P.); jonas.matukas@ff.vu.lt (J.M.)

2 Department of Optoelectronics, Center for Physical Sciences and Technology, Saulėtekio av. 3, LT-10257 Vilnius, Lithuania; andrejus.geizutis@ftmc.lt (A.G.); bronislovas.cechavicius@ftmc.lt (B.Č.); renata.butkute@ftmc.lt (R.B.)

* Correspondence: justinas.glemza@ff.vu.lt; Tel.: +370-5-223-4585

Received: 28 December 2018; Accepted: 20 February 2019; Published: 24 February 2019



Abstract: GaAsBi is a suitable and very attractive material system to be used as an active layer in laser diodes (LDs). To understand the performance and the reliability of such devices and also for further laser diode improvements, the origin of noise sources should be clarified. A detailed study of near-infrared 1.09 μm wavelength GaAsBi type-I laser diodes using the low-frequency noise spectroscopy in a temperature range of (180–300) K is presented. Different types of voltage fluctuation spectral density dependencies on the forward current far below the lasing threshold have been observed. According to this, investigated samples have been classified into two groups and two equivalent noise circuits with the corresponding voltage noise sources are presented. Calculations on the voltage spectral density of the electrical noise and current-voltage characteristic approximations have been performed and the results are consistent with the experimental data. The analysis showed that one group of LDs is characterized by $1/f^{\alpha}$-type electrical fluctuations with one steep electrical bump in the electrical noise dependence on forward current, and the origin of these fluctuations is the surface leakage channel. The LDs of the other group have two bumps in the electrical noise dependence on current where the first bump is determined by overall LD defectiveness and the second bump by Bi-related defects in the active area of LD with characteristic Lorentzian-type fluctuations having the activation energy of (0.16–0.18) eV.

Keywords: current-voltage characteristics; defects; electrical noise; fluctuations; GaAsBi laser diode; leakage channel

1. Introduction

Bismuth containing GaAs ($GaAs_{1-x}Bi_x$) is a novel and very promising material system for optoelectronic devices, especially in fiber optic communication laser diodes (LDs) operating in the (1.3–1.5) μm wavelength region due to numerous advantages [1,2]. Firstly, the incorporation of a small amount of Bi atoms into GaAs leads to a strong band gap energy reduction by (84–91) meV/%Bi [3], as well as temperature coefficient of the band gap being less sensitive to temperature [3,4]. Moreover, for relatively high Bi composition ($x > 10\%$), the spin-orbit splitting energy (Δ_{so}) becomes larger than the band gap, which lets us expect the suppression of Auger recombination and inter-valence band absorption processes [1,3]. This factor is the most important for bismide alloy application as active layers in telecommunication laser diodes [1]. Considering future applications, GaAsBi material is a potential candidate to be used in bio-inspired stretchable optoelectronics systems, e.g., for medicine

purposes, military or industry devices [5–7]. Despite the brittle and non-stretchable nature of GaAsBi, flexible electronic devices using the other brittle inorganic semiconductors such as GaAs or Si have already been successfully demonstrated [5].

However, the fast and wide application of GaAsBi alloys and the emission wavelength extension is slowed down by technological difficulties related to the growth of this material system. The growth temperature has to be lowered to $\leq$400 °C (the optimum growth temperature of GaAs is ~ 590 °C [8]) in order to prevent Bi surface segregation [1–4]. Due to this, it is difficult to produce laser structures with more than 4.4% of Bi by metal-organic vapor phase epitaxy (MOVPE). To incorporate more than 10% of Bi, molecular-beam epitaxy (MBE) is usually used, where lower growth temperature can be applied [1].

Surface segregation is not the only issue making the growth quality of this material worse, e.g., low As flux leads to the surface roughness, while excess of Bi forms droplets on the surface [2,4,9]. There are several methods allowing us to suppress these effects. It has been demonstrated that the two-substrate-temperature MBE technique, where GaAsBi quantum wells (QWs) are grown at lower temperature and GaAs layers at higher, significantly reduces the Bi segregation [2]. Also, a hybrid approach has been presented, where the active region is grown by MBE and the rest of the LD structure by MOVPE with the all following MOVPE advantages [1,10].

Despite all the mentioned improvements in GaAsBi growth methods, crystal quality still depends on a variety of factors and processes such as non-radiative recombination, non-uniform distribution of charge carriers, and carrier localization have a huge impact on electrical and optical characteristics of the alloy and overall semiconductor laser [1,4,8]. Thus, it is important to understand physical processes occurring not only during the growth of a laser diode but also during the device operation that affect LD's performance and reliability.

Due to the sensitivity to various defects, imperfections and structural non-idealities, low-frequency noise characteristics of optoelectronic devices are very informative. While $1/f$-type electrical fluctuations give information on the general quality of a material or a device, the generation-recombination (g-r) noise helps to detect and identify local energy levels in a semiconductor [11–13]. In [14–16] it has been demonstrated that the low-frequency noise spectroscopy is a suitable, very effective and non-destructive characterization method for LDs as the measurements are performed at a near equilibrium state. What is more, the investigation of samples is possible at bias currents far below the threshold current of laser generation [16,17]. Nevertheless, the obtained noise characteristics contain information about physical processes that more or less influence semiconductor laser operation at lasing and overall device reliability. The benefit of such a testing method is very important especially for multimode Fabry–Perot LDs—the sample is not only protected from damage of its internal structure caused by high flowing current through the specimen, but also the noise component, generated due to the mode hopping effect, is not recorded as the LD operates in the subthreshold region. Usually the level of noise amplitude during mode-hopping increases drastically and overheads the fluctuations from other noise sources [15,18], aggravating analysis. The noise behavior in a GaAsBi material system is not sufficiently studied as we have not found any GaAsBi LDs research based on low-frequency noise spectroscopy.

In this paper, we report a comprehensive investigation of 1.09 μm type-I GaAsBi laser diodes through the low-frequency noise characteristics at forward bias. The aim of this work is to determine the noise sources, to identify their possible origin and to propose equivalent circuits of the investigated devices based on LDs current-voltage and electrical noise characteristics.

2. Fabrication of Laser Diodes and Noise Measuring Technique

2.1. Investigated Laser Diodes Structure, Growth and Optical Characteristics

Multiple GaAsBi/GaAs quantum well-based laser diodes were grown using molecular beam epitaxy (MBE) reactor SVT-A equipped by standard metallic Ga, Al and Bi cells, and unique design

source for arsenic containing two independently controlled thermal zones for the bulk evaporator and cracking head for generating pure As_2 flux. The laser structure was grown on an *n*-type GaAs substrate (doped by Si; carrier density about 2×10^{18} cm^{-3}) oriented in the (100) crystalline plane.

The 1.4 μm-thick AlGaAs cladding layers containing 30% of Al and doped by Si and Be served as waveguides as well *n*- and *p*-contact layers in the laser structure, respectively. The AlGaAs layer was deposited on a 600 °C temperature substrate. The active area of a laser diode consisted of five 8 nm-thick GaAsBi wells (with 8% of Bi) surrounded by GaAs barriers. During the growth of a quantum well structure, the temperature was reduced to 360 °C. The bismide quantum wells were grown supplying arsenic and gallium fluxes with the beam equivalent pressure (BEP) ratio close to 1.09. The Bi to As BEP ratio was set to about 0.4 during the growth of QWs. To compensate residual *n*-type conductivity of pristine GaAs, the GaAs barriers were doped by Be. The growth temperature of barriers was 450 °C. The width of the outer and inner barriers was 25 nm and 7 nm, respectively. The observed reflection high-energy electron diffraction (RHEED) images during the growth of GaAsBi QW—(2 × 1) and GaAs barriers—(2 × 4) demonstrated stoichiometric BEP ratios of group V and III materials.

Finally, the temperature was increased to 600 °C, and 250 nm of highly Be-doped GaAs were grown on the top of the structures to improve the metal-semiconductor contact.

The 20 μm wide and (2–3) mm long Fabry–Perot cavities were formed by the cutting and leaving the facets as-cleaved. A 200 nm-thick Au-Ge contact was deposited on the bottom of thinned (to ~200 μm) substrate, and Au/Cr metal bilayer with thickness of about 250 nm was deposited through an open photoresist (PR) layer on the top of the epitaxial structure. The laser diodes were annealed inside a rapid thermal annealing (RTA) oven at 400 °C for 180 s to improve the metal-semiconductor contact. The sketch of the LD structure with 5 GaAsBi QWs is presented in Figure 1.

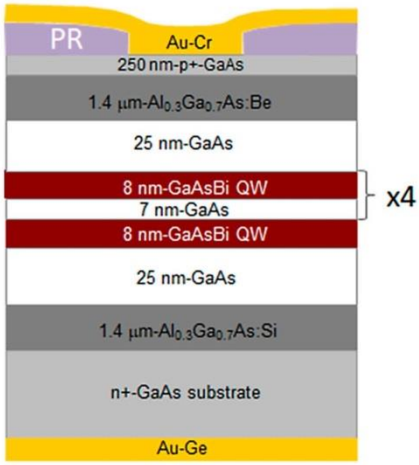


Figure 1. A schematic laser diode structure with 5 GaAsBi quantum wells (QWs).

An optical spectrum analyzer and optical power meters were used for the facet emission and pure spontaneous emission measurements of the as-cleaved LDs. Figure 2 demonstrates electroluminescence (EL) spectrum of the laser diode. The maximum EL peak was reached at 1.13 eV (~1.10 μm) when the temperature was 80 K. The radiation of spontaneous emission was collected from the opening on the top *p*-side stripe contact. The typical photoluminescence (PL) spectrum measured at room temperature (RT) with central peak at ~1.09 μm corresponding to ~8% of Bi in the well region is shown in the inset of Figure 2.

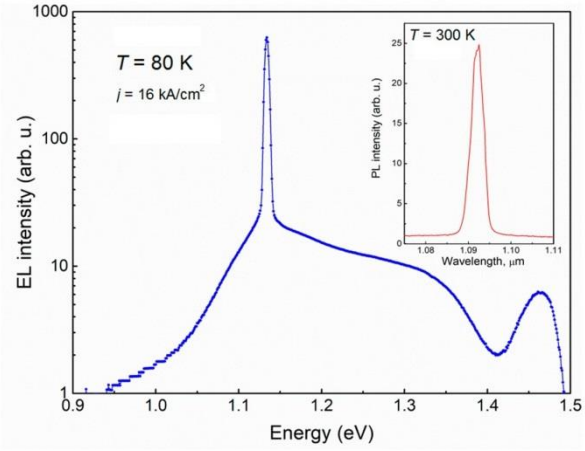


Figure 2. Electroluminescence spectrum measured for the laser diode at the temperature of 80 K. The room temperature (RT) dependence of photoluminescence (PL) intensity on wavelength is presented in the inset.

2.2. Details on Noise Measurement Technique

The low-frequency 10 Hz–200 kHz electrical noise (laser diode terminal voltage fluctuations) have been measured under constant forward bias current operation at RT using a thermoelectric cooler for stabilization of sample temperature and liquid nitrogen cooling for measurements in a (180–300) K temperature interval. The current–voltage (*I*–*U*) and noise characteristics have been measured in a current range far below threshold (up to 100 mA) where the temperature stabilization was valid in order to suppress the self-heating effect and to avoid damage of the quantum well region. Due to this reason, the lasing in these samples is achieved by a pulsed current operation. The noise measurement circuit has a low-noise amplifier, a filter system, an analogue-to-digital converter and a personal computer (Figure 3). The current generator mode is guaranteed for the LDs by choosing appropriate bias voltage and the load resistance $R_{\mathrm{LD\,load}}$, that is at least ten times higher than differential resistance of sample under investigation in a whole current range. A specially designed low-noise amplifier (LNA in Figure 3) with a noise equivalent resistance of 13 Ω (at 1 kHz) has been used to amplify the fluctuations. After amplification stage, this analogue signal was converted to a digital one by an analogue-to-digital converter (PCI-6115, National Instruments, Austin, Texas, United States). The spectral density of voltage fluctuations is estimated by the Cooley–Tukey fast Fourier transform-based spectrum analyzer program. The absolute spectral density value of measured noise voltage fluctuation is calculated by comparing it with the thermal noise of reference resistance, R_{ref}:

$$S_U = \frac{\overline{\Delta u_{\mathrm{LD}}^2} - \overline{\Delta u_{\mathrm{syst}}^2}}{\overline{\Delta u_{\mathrm{ref}}^2} - \overline{\Delta u_{\mathrm{syst}}^2}} 4kT_0R_{\mathrm{ref}}; \tag{1}$$

where $\overline{\Delta u_{\mathrm{LD}}^2}$, $\overline{\Delta u_{\mathrm{syst}}^2}$ and $\overline{\Delta u_{\mathrm{ref}}^2}$ are, respectively, the variances of the laser diode, the measuring system, and the reference resistor thermal noises in a narrow frequency band Δf; T_0 is the absolute temperature of the reference resistor. The noise measurements have been performed in a laboratory screened by iron and copper sheets—the Faraday cage. For *I*–*U* characteristic's evaluation, a precision source/measure unit Keysight B2901 has been used.

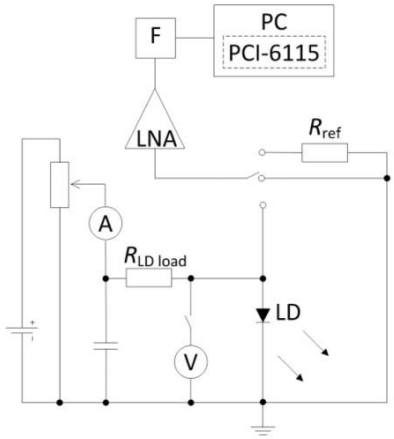


Figure 3. The noise measurement system: LD is the laser diode under investigation, $R_{LD\ load}$ is a load resistor, R_{ref} is a reference resistor, LNA is a low-noise amplifier, F is a filter system, PC is a personal computer with PCI-6115 analogue-to-digital converter and fast Fourier transform (FFT)-based spectrum analyzer program.

3. Results and Discussion

3.1. Electrical Noise Characteristics of GaAsBi Laser Diodes

Investigated devices can be classified into two groups—A and B—considering two different characteristic dependencies of the voltage fluctuation spectral density on the forward current. These experimental dependencies of samples are depicted in Figure 4. Thus, the group A LDs had two bumps (maxima) observed in the investigated current region, while group B had only one. The noise level of group B lasers was apparently higher (up to three orders of magnitude). The level of noise slightly varied (up to one order of magnitude) between LDs in the same group, but the number of observed bumps was constant.

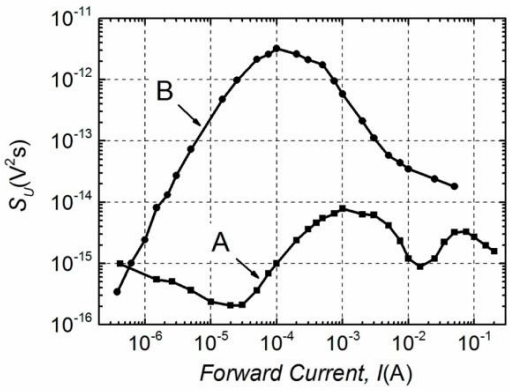


Figure 4. The experimental voltage fluctuation spectral density (S_U) dependencies on the forward current at 1 kHz frequency characteristic for group A and B LDs at room temperature.

Furthermore, differences in electrical noise spectra are observed between these two groups. Low-frequency electrical fluctuations of the group B LDs are distinguished by $1/f^{\alpha}$-type spectra in the entire investigated current region, where index α ranges from 0.9 to 1.4 (Figure 5a). In semiconductor

devices, the $1/f^{\alpha}$-type fluctuations originate from the superposition of Lorentzian-type spectra due to different charge carrier generation-recombination or capture-emission processes having wide distribution of relaxation times [19–21]. The electrical noise spectra of group A LDs, as it can be seen from Figure 5b, are also $1/f^{\alpha}$-type in a forward current range up to the second bump. This second maximum starts in the current interval from ~15 mA to ~25 mA for different samples of group A (Figure 4). The appearance of the second bump is related to the change of noise spectra—a clear Lorentzian-type component is observed, which is characteristic for generation-recombination noise (Figure 6). There equation $2\pi f_0\tau = 1$ holds for the maximum of the normalized g-r noise voltage spectral density with τ being the average relaxation time and f_0—the characteristic frequency at the maximum of the spectrum. The origin of these g-r fluctuations will be discussed in the next Sections. As it could be expected, differences between electrical noise characteristics of the group A and B LDs are also reflected in their current–voltage characteristics (Figure 7).

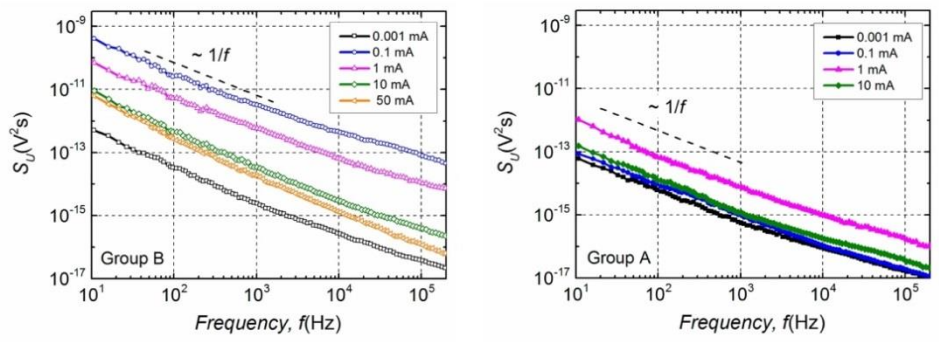


Figure 5. Electrical noise spectra S_U of the group B LD (**a**) at different current values in the whole investigated forward current range and of the group A LD (**b**) at different forward current values up to the second bump appearance (presented in Figure 4).

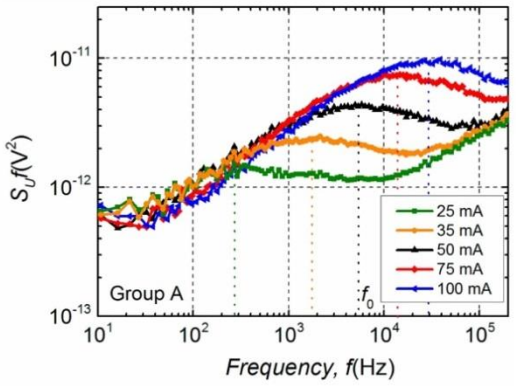


Figure 6. Normalized electrical noise spectra $S_U f$ of the group A LD in the current range of the second bump (I > 15 mA in Figure 4).

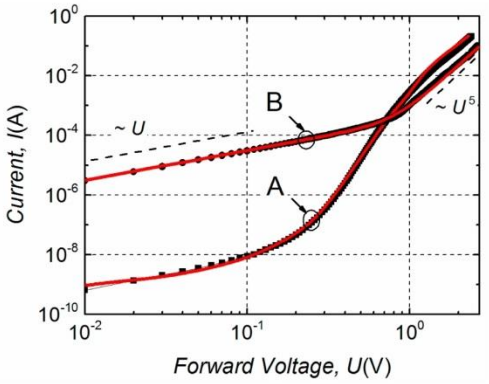


Figure 7. Typical *I–U* characteristics of the group A and B LDs in the current range far below the threshold; the black symbols represent experimental results and the red solid curves—an approximation by Equation (3) for the group A and by Equation (2) for the group B.

3.2. Current–Voltage Characteristics of the Group A and B LDs

It is well known, that for the optoelectronic devices, such as light-emitting diodes (LEDs) or LDs, there is a strong relation between the electrical noise and current–voltage characteristics [17,22], e.g., leakage channel existence is usually followed by an increased low-frequency electrical fluctuations' level [23].

Typical *I–U* characteristics of the investigated group A and B LDs are presented in Figure 7, where black curves with squares and dots represent the experimental data. A strong difference between these *I–U* curves is observed; the group B LD curve is far from an exponential dependence typical to an ideal diode and for the sake of convenience it can be written as a polynomial:

$$I = aU + bU^n; \tag{2}$$

where a and b are coefficients, and n is higher than 1 at forward voltages above 0.9 V. Meanwhile the *I–U* characteristic of the LD from group A can be expressed as usual:

$$I = I_0 \exp[q(U - IR_s)/(\eta kT)] + a_1 U; \tag{3}$$

where I_0 is the saturation current of a diode, q—an elementary charge, R_s—a series resistance, η—a non-ideality factor of the diode and the a_1U term describes the additional current at low bias U (in Equation (3) $\exp[q(U - IR_s)/(\eta kT)] >> I_0$). To approximate these experimental dependencies (red curves in Figure 7) the index $n = 5$ in Equation (2) has been used and the non-ideality factor η in Equation (3) has been determined from the best fit with the experimental curve ($\eta \approx 2.5$ in a current range from 10^{-6} A to 10^{-4} A; the other quantities in Equation (3) are $R_s \approx 3\ \Omega$ and $I_0 = 9.5 \times 10^{-10}$ A).

3.3. Noise Equivalent Circuits of the LDs and Their Analysis

Based on the results presented in Figures 4 and 7, the equivalent electrical circuits of group A and B LDs are proposed in Figure 8. In these equivalent electrical circuits, the R_1 describes parallel leakage resistance, however, it depends on applied bias differently for group A and B LDs. The diode symbol in Figure 8a represents an ideal *p–n* junction of the group A LDs with its own differential resistance $R_{diff} = (dU_{p-n}/dI)$. The corresponding differential resistance of group B LDs is denoted by R_2 (Figure 8b) according to the non-exponential *I–U* characteristic approximation (Equation (2)). The R_s in Figure 8 represents the series resistance of contacts and highly doped n^+ and p^+ layers.

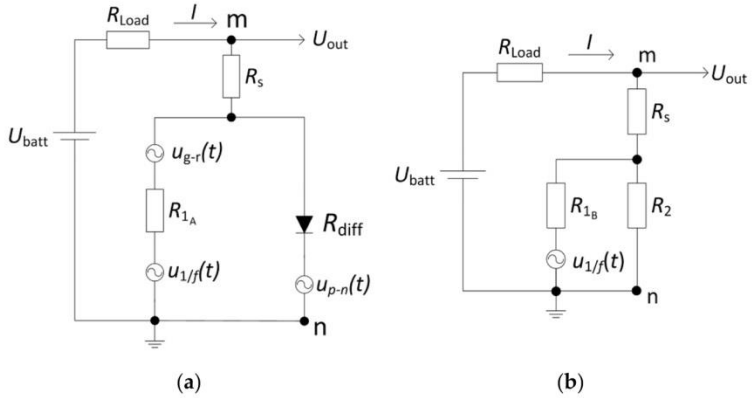


Figure 8. Equivalent electrical circuits of group A (**a**) and group B (**b**) LDs with the voltage noise sources ($R_{Load} >> R_{mn}$).

Calculated dependencies of the discussed leakage and differential resistances on forward voltage are presented in Figure 9. Such graphical representation of these dependencies is very useful to explain the electrical noise properties. For the group B LDs, the linear part of the *I–U* characteristic determines the resistance R_{1B} (~3200 Ω). Then, by differentiating Equation (2) and eliminating the ohmic part, the resistance R_2 can be expressed as $R_2 = 1/(0.0034 \times U^4)$. In the case of group A LDs, the dependence of the resistance R_{1A} on forward voltage has been evaluated regarding to the best coincidence between experimental data and approximated results of both *I–U* and electrical noise characteristics. R_{1A} decreases with increasing applied forward voltage more steeply in the bias range of the first electrical noise bump than in the second one (at $U > 0.9$ V) as it is shown in Figure 9.

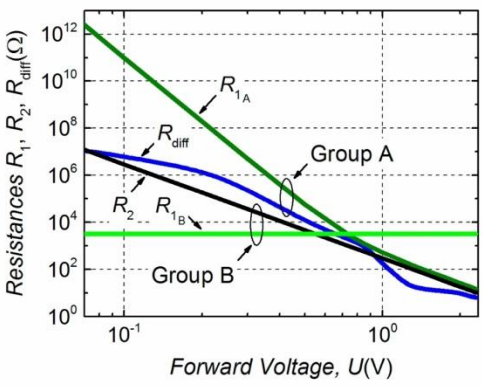


Figure 9. Calculated dependencies of R_1, R_2 and R_{diff} (presented in Figure 8) resistances on forward voltage.

For the $1/f$-type electrical fluctuations the current noise spectral density, S_I, for a *p–n* junction is proportional to the forward current [24]. As the flowing through the diode forward current increases, the differential resistance R_{diff} of an LD decreases and the voltage fluctuation spectral density is $S_U = S_I \cdot R_{diff}^2$. The corresponding voltage noise source in the equivalent electrical circuit is denoted as $u_{p-n}(t)$ (Figure 8a). However, the influence of fluctuations originating from this noise source is visible only in group A LD (Figure 4) where the relation:

$$S_{U\ p-n} = \frac{C}{f} \cdot \frac{1}{I^{\gamma}}; \tag{4}$$

is up to $I = 1 \times 10^{-5}$ A and the index γ is close to 1.

For the group A LDs the proportionality $S_U \sim I^{-\gamma}$ is no longer valid when $I > 1 \cdot 10^{-5}$ A (Figure 4). As a result, there should be additional voltage noise sources located parallel to the *p*–*n* junction (Figure 8a). It was mentioned earlier that for the group A samples the type of electrical noise spectra changes in the forward current interval from ~15 mA to ~25 mA, where the Lorentzian-type fluctuations prevail $1/f$-type. Thus, for $I > 1 \times 10^{-5}$ A the electrical noise spectral density $S_{U\ \mathrm{out}}$ can be expressed as a sum of two spectral densities of independent noise sources, $u_{1/f}$ (t) and $u_{\mathrm{g\text{-}r}}$ (t):

$$S_{U\ \mathrm{out\ A}} = S_{U\ 1/f\ \mathrm{out}} + S_{U\ \mathrm{g-r\ out}}; \tag{5}$$

where the $1/f$-type fluctuations are calculated as:

$$S_{U\ 1/f\ \mathrm{out}} = \frac{DU^2}{f} \cdot \left(\frac{R_{\mathrm{diff}}}{R_{1_A} + R_{\mathrm{diff}}}\right)^2; \tag{6}$$

and for the generation-recombination noise, i.e., the Lorentzian-type spectra fluctuations:

$$S_{U\ \mathrm{g-r\ out}} = 4EU^2 \frac{\tau}{1 + (2\pi f\tau)^2} \cdot \left(\frac{R_{\mathrm{diff}}}{R_{1_A} + R_{\mathrm{diff}}}\right)^2. \tag{7}$$

For group B samples, only the $1/f$-type electrical fluctuations have been observed in a whole investigated current region and their spectral density can be described as:

$$S_{U\ \mathrm{out\ B}} = \frac{FU^2}{f} \cdot \left(\frac{R_2}{R_{1_B} + R_2}\right)^2. \tag{8}$$

Here, in Equations (4), (6)–(8) C, D, E and F are coefficients. The comparison between experimental voltage fluctuation spectral densities and those calculated by Equations (4)–(8) are presented in Figure 10. The noise source $u_{p-n}(t)$ is not presented in Figure 8b because in the investigated current range the level of electrical fluctuations, arising from the *p*–*n* junction, is much lower than the level of fluctuations from the $u_{1/f}$ (t) noise source.

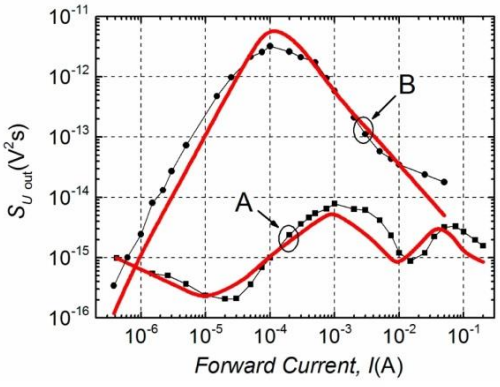


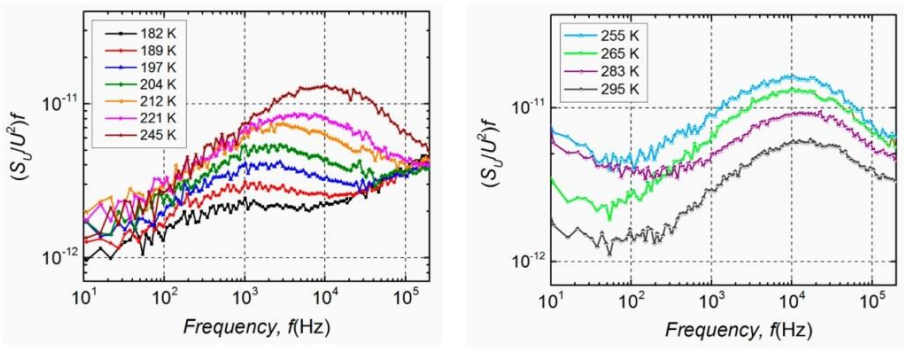
Figure 10. Comparison of the experimental voltage fluctuation spectral density dependencies on forward current at 1 kHz frequency (black curves with symbols) and the calculated data (red curves) for LDs of groups A and B at RT.

3.4. The Origin of Electrical Fluctuations in GaAsBi LDs

The resistance R_1 acts as a shunting resistance with respect to R_{diff} (or R_2). For example, in a case of group B, the voltage fluctuation spectral density increases as I^2 in a forward current interval up to ~0.1 mA (corresponding voltage ~0.5 V) (Figure 10), where $I \sim U$ (Figure 7). At the bias values $U > 0.5$ V, the level of electrical fluctuation rapidly decreases as now R_2 shunts R_{1B} (Figure 9). A similar electrical noise dependence on forward current with an evident one strong bump has been also observed in the GaSb-based laser diodes in a subthreshold region [17]. For GaAsBi group B LDs the leakage channel resistance R_{1B} is independent of the applied voltage (Figure 9) and the leakage current, corresponding to the ohmic part of the *I*–*U* characteristic, is larger up to four orders of magnitude compared to the samples from group A (Figure 7). This suggests that a surface leakage channel exists, which is responsible for the fluctuations observed in group B GaAsBi LDs. This channel is formed by the high density active g-r centers located on the LD surface that have widely distributed relaxation times leading to the $1/f$-type electrical fluctuations spectra. The formation of capture centers on the surface is very sensitive to the quality of cleavage process of the LD when a periodic crystal potential breaks off at a semiconductor surface leading to the origin of surface states [25]. An appropriate surface passivation would decrease surface state density and, consequentially, could reduce the low-frequency noise and increase the threshold of a catastrophic optical damage [25–27].

The origin of the leakage resistance R_1 in the group A LDs is different than in group B; the level of electrical fluctuations created by this resistance noise source is significantly lower (Figure 10) and R_{1A} depends on the applied voltage, i.e. it is not constant as R_{1B} (Figure 9). The voltage fluctuation spectral density of the first noise bump of the group A samples is increasing as $S_U \sim I$ up to $I \approx 1$ mA (Figure 10). The second weaker maximum in the group A LDs' electrical noise characteristic is related to the g-r noise appearance. The Lorentzian-type spectra emersion suggests that there is a strong active g-r center turning on at $U > 0.9$ V. For detection and identification of these local levels for the group A LDs and to relate them to the origin of the resistance R_{1A}, the g-r noise spectroscopy has been applied.

Normalized g-r noise spectra of group A LD at different temperatures are presented in Figure 11. When the temperatures are below 250 K (Figure 11a) the relaxation time $\tau = 1/(2\pi f_0)$ is dependent on temperature and is described as: $\tau = \tau_0 \exp(E_a/kT)$ [17], where E_a is the activation energy of an observed g-r process. The maximum $(S_U/U^2)f$ value appears when the Fermi level coincides with the trap energy level [13,28]. At temperatures $T > 250$ K the relaxation time is almost independent of temperature showing that the Fermi level is bound to the accumulation of defect levels in a particular place of the bandgap of the LD active region (Figure 11b).



(**a**) (**b**)

Figure 11. Normalized g-r noise spectra $(S_U/U^2)f$ of the investigated group A LD at different temperatures at forward current $I = 30$ mA: in the temperature range from 182 K to 245 K (**a**) and from 255 K to the room temperature 295 K (**b**).

The activation energies of the corresponding relaxation processes of different group A LDs' have been found in the range from 0.16 eV to 0.18 eV (Figure 12). Similar activation energies have been observed in MBE grown *n*-type $GaAs_{1-x}Bi_x$ layers on GaAs substrate by deep level transient spectroscopy (DLTS) [9]. In [9], it has been identified that the defects involving Bi atoms in their structure are responsible for detected trap levels. It is known that Bi incorporation into GaAs at low temperature enhances Bi surface migration, Bi cluster formation [3,4,8] and at the same time Bi-related defects are present [9]. According to the evaluated activation energy, the influence of strong g-r center created by defects involving Bi is increasing at $U > 0.9$ V leading to the Lorentzian-type fluctuations in electrical noise spectra. So, the second noise bump of the group A LD (Figure 10) is related to the LD active multi-quantum well (MQW) region (where GaAsBi QWs are embedded and its interfaces). While the first bump in the group A LD voltage fluctuation spectral density with characteristic $1/f^{\alpha}$-type electrical fluctuations is determined by sample defects and various charge carriers capture or release centers in the active region as well as in peripheral areas of the LD.

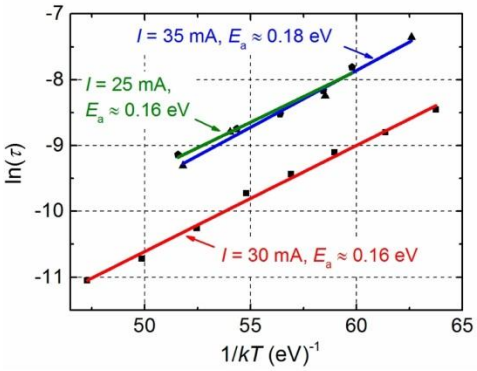


Figure 12. Dependencies of the relaxation time on the inverse temperature of different group A samples. The evaluated activation energies E_a and experimental conditions are presented near the curves (square symbols denote ln (τ) values obtained from LD electrical noise spectra presented in Figure 11a).

4. Conclusions

Low-frequency noise characteristics of 1.09 μm GaAsBi laser diodes have been investigated in the current range far below lasing threshold. Considering different voltage fluctuation spectral density dependencies on the forward current, the investigated samples have been classified into two groups; A and B.

Laser diodes of the group A are distinguished by two bumps in the electrical noise dependence on current. The first one is characterized by $1/f^{\alpha}$-type electrical fluctuations, the second one by Lorentzian type spectra with the activation energy (0.16–0.18) eV. The analysis of the current–voltage characteristics and the equivalent noise circuits has shown, that the origin of the first electrical noise bump is determined by the overall LDs (the active and the peripheral areas) defectiveness, while the second one by the large density g-r centers due to Bi-related defect states in the active MQW LDs layer and its interfaces.

The group B LDs are distinguished by one steep electrical noise bump in the dependence on forward current with $1/f^{\alpha}$-type electrical fluctuations in the whole investigated current range. In this case, equivalent circuit analysis has shown that the leakage resistance is independent of applied bias and the corresponding ohmic part of *I*–*U* characteristic is much higher compared to the group A LDs. The origin of these fluctuations is the leakage channel formed at a surface of LDs due to high density surface defects and charge carrier capture centers.

Author Contributions: Conceptualization, R.B., and J.M.; Formal Analysis, J.G., and V.P.; Growth by MBE, A.G., B.Č., and R.B.; Investigation, J.G., A.G., and B.Č.; Methodology, V.P., R.B., S.P., and J.M.; Supervision, R.B., and J.M.; Visualization, J.G., A.G., B.Č., and S.P.; Writing—Original Draft Preparation, J.G., and V.P.; Writing—Review and Editing, R.B., S.P., and J.M.

Funding: The APC was funded by Vilnius University.

Conflicts of Interest: The authors declare no conflict of interest.

References

1. Marko, I.P.; Jin, S.R.; Hild, K.; Batool, Z.; Bushell, Z.L.; Ludewig, P.; Stolz, W.; Volz, K.; Butkutė, R.; Pačebutas, V.; et al. Properties of hybrid MOVPE/MBE grown GaAsBi/GaAs based near-infrared emitting quantum well lasers. *Semicond. Sci. Technol.* **2015**, *30*, 1–10. [CrossRef]
2. Patil, P.K.; Luna, E.; Matsuda, T.; Yamada, K.; Kamiya, K.; Ishikawa, F.; Shimomura, S. GaAsBi/GaAs multi-quantum well LED grown by molecular beam epitaxy using a two-substrate-temperature technique. *Nanotechnology* **2017**, *28*, 105702. [CrossRef] [PubMed]
3. Pan, W.; Zhang, L.; Zhu, L.; Li, Y.; Chen, X.; Wu, X.; Zhang, F.; Shao, J.; Wang, S. Optical properties and band bending of InGaAs/GaAsBi/InGaAs type-II quantum well grown by gas source molecular beam epitaxy. *J. Appl. Phys.* **2016**, *120*, 105702. [CrossRef]
4. Mohmad, A.R.; Bastiman, F.; Hunter, C.J.; Richards, R.D.; Sweeney, S.J.; Ng, J.S.; David, J.P.R.; Majlis, B.Y. Localization effects and band gap of GaAsBi alloys. *Phys. Status Solidi B* **2014**, *251*, 1276–1281. [CrossRef]
5. Li, Z.; Wang, Y.; Xiao, J. Mechanics of curvilinear electronics and optoelectronics. *Curr. Opin. Solid State Mater. Sci.* **2015**, *19*, 171–189. [CrossRef]
6. Li, Z.; Xiao, J. Mechanics and optics of stretchable elastomeric microlens array for artificial compound eye camera. *J. Appl. Phys.* **2015**, *117*, 014904. [CrossRef]
7. Li, Z.; Wang, Y.; Xiao, J. Mechanics of bioinspired imaging systems. *Theor. Appl. Mech. Lett.* **2016**, *6*, 11–20. [CrossRef]
8. Mohmad, A.R.; Majlis, B.Y.; Bastiman, F.; Hunter, C.J.; Richards, R.D.; Ng, J.S.; David, J.P.R. Photoluminescence from localized states in GaAsBi epilayers. In Proceedings of the International Conference on Semiconductor Electronics (ICSE2014), Kuala Lumpur, Malaysia, 27–29 August 2014; pp. 354–357.
9. Gelczuk, Ł.; Kopaczek, J.; Rockett, T.B.O.; Richards, R.D.; Kudrawiec, R. Deep-level defects in n-type GaAsBi alloys grown by molecular beam epitaxy at low temperature and their influence on optical properties. *Sci. Rep.* **2017**, *7*, 1–11. [CrossRef] [PubMed]
10. Butkutė, R.; Geižutis, A.; Pačebutas, V.; Čechavičius, B.; Bukauskas, V.; Kundrotas, R.; Ludewig, P.; Volz, K.; Krotkus, A. Multi-quantum well Ga (AsBi)/GaAs laser diodes with more than 6% of bismuth. *Electron. Lett.* **2014**, *50*, 1155–1157. [CrossRef]
11. Vandamme, L.K.J. Noise as a diagnostic tool for quality and reliability of electronic devices. *IEEE Trans. Electron Devices* **1994**, *41*, 2176–2187. [CrossRef]
12. Sawyer, S.; Rumyantsev, S.L.; Shur, M.S.; Pala, N.; Bilenko, Y.; Zhang, J.P.; Hu, X.; Lunev, A.; Deng, J.; Gaska, R. Current and optical noise of GaN/AlGaN light emitting diodes. *J. Appl. Phys.* **2006**, *100*, 034504. [CrossRef]
13. Van Rheenen, A.D.; Bosman, G.; Zijlstra, R.J.J. Low frequency noise measurements as a tool to analyze deep-level impurities in semiconductor devices. *Solid State Electron.* **1987**, *30*, 259–265. [CrossRef]
14. Pralgauskaitė, S.; Palenksis, V.; Matukas, J. Chapter 8: Low frequency noise characteristics of multimode and singlemode laser diodes. In *Semiconductor Laser Diode Technology and Applications*; Patil, D.S., Ed.; InTech: London, UK, 2012; ISBN 978-953-51-0549-7. pp. 133–160.
15. Glemža, J.; Pralgauskaitė, S.; Palenskis, V.; Matukas, J. Low frequency noise investigation of 2–3 μM GaSb-based laser diodes. *Solid State Electron.* **2017**, *133*, 70–77. [CrossRef]
16. Guan, J.; Guo, S.; Wang, J.; Tao, M.; Cao, J.; Gao, F. Analysis of origin of measured $1/f$ noise in high-power semiconductor laser diodes far below threshold current. *Microelectron. Reliab.* **2016**, *59*, 55–59. [CrossRef]
17. Glemža, J.; Palenskis, V.; Pralgauskaitė, S.; Vyšniauskas, J.; Matukas, J. Properties of the surface generation-recombination noise in 1.94 μM GaSb-based laser diodes. *Infrared Phys. Technol.* **2018**, *91*, 101–106. [CrossRef]

18. Pralgauskaitė, S.; Palenskis, V.; Matukas, J.; Šaulys, B.; Kornijčuk, V. Analysis of mode-hopping effect in Fabry-Pérot multiple-quantum well laser diodes via low frequency noise investigation. *Solid State Electron.* **2013**, *79*, 104–110. [CrossRef]
19. Palenskis, V.; Maknys, K. Nature of low-frequency noise in homogenous semiconductors. *Sci. Rep.* **2015**, *5*, 1–7.
20. Palenskis, V.; Vyšniauskas, J.; Glemža, J.; Matukas, J. Charge carrier mobility fluctuations due to capture-emission process. *Lith. J. Phys.* **2018**, *58*, 261–266. [CrossRef]
21. Palenskis, V. The charge carrier capture-emission process—The main source of the low-frequency noise in homogeneous semiconductors. *Lith. J. Phys.* **2016**, *56*, 200–206. [CrossRef]
22. Park, J.; Kang, T.; Woo, D.; Son, J.-K.; Lee, J.-H.; Park, B.-G.; Shin, H. Non-ideal characteristic analysis of GaN-based light-emitting diode using current-voltage (I–V) and low-frequency noise experiment. In Proceedings of the 18th IEEE International Symposium on the Physical and Failure Analysis of Integrated Circuits (IPFA), Incheon, Korea, 4–7 July 2011; pp. 408–411.
23. Pralgauskaitė, S.; Palenskis, V.; Matukas, J.; Glemža, J.; Muliuk, G.; Šaulys, B.; Trinkūnas, A. Reliability investigation of light-emitting diodes via low frequency noise characteristics. *Microelectron. Reliab.* **2015**, *55*, 52–61. [CrossRef]
24. Hooge, F.N.; Kleinpenning, T.G.M.; Vandamme, L.K.J. Experimental studies on $1/f$ noise. *Rep. Prog. Phys.* **1981**, *44*, 479–532. [CrossRef]
25. Hakimi, R.; Amann, M.C. Reduction of $1/f$ carrier noise in InGaAsP/InP heterostructures by sulphur passivation of facets. *Semicond. Sci. Technol.* **1997**, *12*, 778–780. [CrossRef]
26. Bessolov, V.N.; Lebedev, M.V.; Shernyakov, Y.M.; Tsarenkov, B.V. Sulfur passivation of InGaAs/AlGaAs SQW laser (977 nm) facets in alcohol-based solutions. *Mater. Sci. Eng. B* **1997**, *44*, 380–382. [CrossRef]
27. Lambert, R.W.; Ayling, T.; Hendry, A.F.; Carson, J.M.; Barrow, D.A.; McHendry, S.; Scott, C.J.; McKee, A.; Meredith, W. Facet-passivation processes for the improvement of Al-containing semiconductor laser diodes. *J. Lightware Technol.* **2006**, *24*, 956–961. [CrossRef]
28. Palenskis, V.; Minkevičius, L.; Matukas, J.; Jokubauskis, D.; Pralgauskaitė, S.; Seliuta, D.; Čechavičius, B.; Butkutė, R.; Valušis, G. InGaAs diodes for terahertz sensing—Effect of molecular beam epitaxy growth conditions. *Sensors* **2018**, *18*, 3760. [CrossRef] [PubMed]



© 2019 by the authors. Licensee MDPI, Basel, Switzerland. This article is an open access article distributed under the terms and conditions of the Creative Commons Attribution (CC BY) license (http://creativecommons.org/licenses/by/4.0/).

P4

J. Glemža, J. Matukas, S. Pralgauskaitė, V. Palenskis,

Low-frequency noise characteristics of high-power white LED during long-term aging experiment,

Lith. J. Phys. **58**, 194–203 (2018).
doi: 10.3952/physics.v58i2.3749.

Visos teisės priklauso Lietuvos mokslų akademijai, 2018

Perspausdinta su Lietuvos fizikos žurnalo redakcijos leidimu

Reprinted with permission of the Lithuanian Journal of Physics

Lithuanian Journal of Physics, Vol. **58**, No. 2, pp. 194–203 (2018)
© Lietuvos mokslų akademija, 2018

LOW-FREQUENCY NOISE CHARACTERISTICS OF HIGH-POWER WHITE LED DURING LONG-TERM AGING EXPERIMENT

J. Glemža, J. Matukas, S. Pralgauskaitė, and V. Palenskis

Institute of Applied Electrodynamics and Telecommunications, Vilnius University, Saulėtekio 3, 10257 Vilnius, Lithuania
Email: justinas.glemza@ff.vu.lt; jonas.matukas@ff.vu.lt; sandra.pralgauskaite@ff.vu.lt; vilius.palenskis@ff.vu.lt

Received 27 October 2017; revised 27 November 2017; accepted 21 June 2018

Low-frequency electrical and optical noise characteristics of a high power white InGaN LED and the cross-correlation coefficient between these fluctuations are investigated during the long-term ageing experiment (28000 h). The analysis of cross-correlation shows that the correlated part of the low-frequency electrical noise, which indicates physical processes in the active area of the LED, varies during the ageing experiment. Two main stages are distinguished considering the rapid changes of the noise characteristics. The initial stage (after the first 1100 h) is followed by the decrease in the noise power at low forward currents and the increase in the light output. The final stage (after 28000 h) is characterized by a strong growth of the low-frequency noise, the decrease of the light output and the increase of the correlated part of electrical and optical fluctuations. These changes mean a failure in the active layer of the LED. The optical output decomposition into two spectral parts, the radiation generated by the LED chip and the radiation generated by the phosphor layer, enables evaluation of the phosphor layer influence on the degradation process of device optical characteristics. Despite the fact that this layer contributes to the variation of the LED chromatic properties, the cross-correlation analysis has shown that the phosphor layer does not act as a possible noise source during the ageing experiment.

Keywords: ageing, cross-correlation coefficient, electrical noise, light-emitting diode, optical noise

PACS: 72.70.+m, 85.60.Jb

1. Introduction

Advantages such as excellent optical quality, high efficiency and eco-friendliness make the white light-emitting diodes (LED) a superior replacement for traditional light sources, and that is why they are widely used in a variety of applications, e.g. solid state lighting, signalling, automotive industry, etc. [1–3]. Phosphor-converted white LEDs are very attractive and suitable for massive production due to their low price and a quite high colour rendering index (~80) which is appropriate in most situations [1]. There a semiconductor, mostly GaN-based, chip generates blue light and phosphors, usually yttrium-aluminium-garnet (YAG), produce an efficient broad yellow emission.

Despite wide manufacturing and application of white LEDs, their reliability investigation is still of high importance [3, 4]. While most standards of the LED industry for lifetime assessment are based on lumen maintenance [5], investigation of electrical characteristics is not less important [3]. Various processes, like growth of non-radiative recombination, instabilities of dopants or impurities, increase of thermal resistance, etc., accelerate GaN-based optoelectronic device degradation and lower performance [2]. Therefore, there is a demand for a sensitive diagnostic tool for both optical and electrical LED characterization. As modern LEDs have a complex structure, evaluating which part of the device is degrading is of high importance as well.

Low-frequency noise spectroscopy is a suitable candidate for such diagnostics. It is well known that excess noise in a semiconductor device is caused by defects, structural non-idealities and fabrication imperfections. The essential feature of low-frequency noise spectroscopy is that measurements are performed under normal bias conditions near the equilibrium state and are non-destructive [6, 7]. Due to this reason, the low-frequency noise characteristics of GaN-based LEDs are of high interest to scientific community [8–12]. However, there are practically no published investigations on the low-frequency noise characteristics of white LEDs during a long ageing experiment at room temperature and manufacturer permissible forward current. This is in contrast to highly accelerated testing techniques [2, 13] where usually both high temperature and forward current are degradation accelerating factors. What is more, the analysis of the cross-correlation method helps to determine which part of the cross-correlation coefficient between electrical and optical fluctuations is generated by the low-frequency fluctuations with $1/f$, $1/f^{\alpha}$ or Lorentzian type spectra and to identify the location of possible noise sources in the structure of LED: active or peripheral layers [10, 14]. As a white LED has an additional structural component – the phosphor layer, it also has a role in the device degradation process and could act as a possible optical noise source. Thus, it is necessary to separate the optical spectrum of the white LED into the radiation generated by the LED chip and by the phosphor layer in order to evaluate which structural element of the white LED leads to optical and electrical fluctuations.

The aim of this work was to clear up the sources of the high power white LED degradation, their appearance and influence on the low-frequency noise characteristics during the long-term ageing.

2. Experimental details

The paper presents the investigation results of a modern design high power (1 W) phosphor-converted 'cool' white multi-quantum well (MQW) InGaN LED.

Low-frequency 10 Hz–20 kHz voltage noise spectral density (optical noise is the emitted light power fluctuations and is detected by a photodiode; electrical noise is the light emitting diode voltage fluctuations) and the cross-correlation coefficient between optical and electrical fluctuations have been measured under CW operation at room temperature (293 K). Figure 1 shows the measurement circuit for a simultaneous investigation of two noise signals: optical and electrical. Each noise measurement channel has a low-noise amplifier, a filter system and an analog-to-digital converter NI PCI-6115. The current generator mode is guaranteed for the LED under test by choosing the appropriate bias voltage and the load resistance. Noise characteristic measurements were carried out in a special screened laboratory room (Faraday cage) in order to avoid interferences from the extrinsic electromagnetic field.

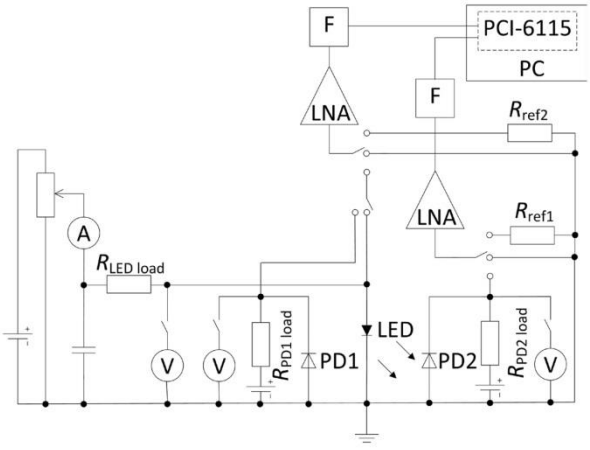


Fig. 1. The two-channel noise measurement system: LED, the light emitting diode under test; PD1 and PD2, BSR and RSR photodetectors, respectively; $R_{LED\ load}$, $R_{PD1\ load}$ and $R_{PD2\ load}$, load resistances; R_{ref1} and R_{ref2}, reference resistors; LNA, a low-noise amplifier; F, a filter system; PC, a personal computer; PCI-61115, an analog-to-digital converter.

The spectral density of voltage fluctuations is estimated by using the Fast Fourier Transform. The absolute value of the measured noise voltage spectral density is calculated by comparing it with the thermal noise of the reference resistance, R_{ref}:

$$S_U = \frac{\langle u_{LD}^2(t)\rangle - \langle u_{syst}^2(t)\rangle}{\langle u_{ref}^2(t)\rangle - \langle u_{syst}^2(t)\rangle} 4kT_0R_{ref}. \quad (1)$$

Here $\langle u_{LD}^2(t)\rangle$, $\langle u_{syst}^2(t)\rangle$ and $\langle u_{ref}^2(t)\rangle$ are, respectively, the variances of the noise signals of the LED, the measuring system, and the thermal noise of the reference resistor in the narrow frequency band Δf; T_0 is the absolute temperature of the reference resistor.

A simultaneous operation of two identical noise measurement channels enables one to measure the cross-correlation coefficient between optical and electrical fluctuations. The simultaneous cross-correlation coefficient was measured not only in the overall investigated frequency region (10 Hz–20 kHz) but also in every one-octave frequency range by using digital filters and was computed by the following expression:

$$k = \frac{\langle u_{el}(t)\cdot u_{op}(t)\rangle}{(\sigma_{el}^2\cdot\sigma_{op}^2)^{1/2}}. \quad (2)$$

Here brackets $\langle\cdots\rangle$ mean averaging both on time and on the number of realizations, $\sigma_{el}^2 = \langle u_{el}^2(t)\rangle$ and $\sigma_{op}^2 = \langle u_{op}^2(t)\rangle$ are the variances of electrical and optical fluctuations in the investigated frequency range, respectively.

Optical characteristics of the investigated LED were measured with a Si photodiodes matrix *Hamamatsu* S9702 which consists of three parts sensitive to different regions of the visible light spectrum: the blue spectral range (BSR) with the peak sensitivity wavelength $\lambda_{p\,B}$ = 460 nm, the green range (GSR) with $\lambda_{p\,G}$ = 540 nm and the red one (RSR) with $\lambda_{p\,R}$ = 620 nm. The BSR diode is sensitive to the light coming out from the active layer of the LED chip while GSR and RSR diodes are sensitive to the luminescence from the phosphor layer. In this work the results measured with BSR and RSR diodes are presented, as spectral response ranges of these photodiodes do not overlap and physical processes occurring in different parts of the white LED structure (i. e. the active area and the phosphor layer) can be properly separated.

The ageing experiment was performed at room temperature at the maximum manufacturer-allowed forward current (350 mA). The current–voltage (I–V), the light output power (which is proportional to the photovoltage U_{photo} on the load resistance of a photodetector), noise characteristics and optical spectra measurements were periodically performed upon interrupting the ageing procedure.

3. Results and discussion

3.1. Noise characteristics of unaged LED

The measurement results have shown that electrical fluctuations of the investigated LED are characterized by $1/f^{\alpha}$-type noise, where α is close to 1 (Fig. 2(a)). In the majority of semiconductor devices $1/f^{\alpha}$-type fluctuations originate from a superposition of many charge carrier generation-recombination (g-r) processes in the capture centres with widely distributed relaxation times [15]. These centres are formed during device fabrication and also during ageing due to the device degradation. The noise voltage spectral density of electrical fluctuations, $S_{U\,el}$, decreases as the forward current increases up to 10 mA. After that, the electrical noise level increases (the inset in Fig. 2 (a)). This can be explained as follows. For the *pn* junction the flowing current, I, is proportional to the total free charge carrier number in the sample, N: $I \sim N$. Therefore, the current fluctuation spectral density, S_I, is proportional to the current. The differential resistance of the diode $R_d \sim 1/I$, thus the voltage spectral density is inversely proportional to the current: $S_U \sim S_I R_d^2 \sim 1/I$. When $I \approx 10$ mA, R_d reaches the serial resistance value R_s, which is practically constant, and $S_U \sim I^2$.

Optical noise spectra are characterized by a weak $1/f^{\alpha}$-type component that dominates up to 100 Hz and the 'white' noise (Fig. 2(b)). This 'white' noise can be attributed to the shot noise as its level depends on the light output power of the LED and is caused by the random photon emission process. The decrease of the normalized optical noise spectral density with the forward current increase is determined by the light output power increase (the inset in Fig. 2(b)).

The cross-correlation measurement and the analysis broaden the information obtained from noise

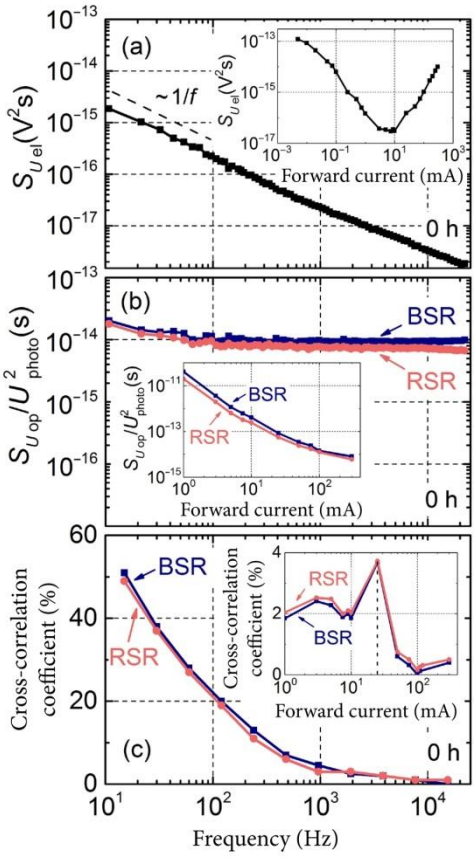


Fig. 2. Electrical (a) and optical (b) noise spectra at 100 mA forward current and (c) the cross-correlation coefficient between electrical and optical fluctuations at 25 mA forward current before ageing (0 h). Insets of (a) and (b) show the dependences of the voltage spectral density of electrical (S_{Uel}) and normalized optical (S_{Uop}/U^2_{photo}) noise on the forward current at 22 Hz, while the inset of (c) shows the cross-correlation coefficient dependence on the forward current in the overall frequency range 10 Hz–20 kHz. There the normalized optical noise and the cross-correlation coefficient are presented for both spectral ranges of the photodiode (BSR and RSR).

characteristics. As seen from Fig. 2(c), the cross-correlation coefficient between electrical and optical noise signals is largest at low frequencies where $1/f^{\alpha}$-type fluctuations dominate in both electrical and optical noise spectra. This positive cross-correlation coefficient indicates that the observed $1/f^{\alpha}$-type electrical and optical fluctuations are caused by defects in the active region (QWs area) of the LED: defects modulate randomly the free charge carrier number in the QWs region and, as a consequence, lead to the photon number (optical) fluctuations in the same phase as electrical ones. Electrical and optical fluctuations are not completely correlated at low frequencies because fluctuations at contacts or electrical noise from the passive layers of the LED do not influence the emitted light fluctuations, i.e. the voltage noise spectral density of electrical noise can be written as a sum of correlated and uncorrelated (to the optical fluctuations) parts [14].

However, the 'white' noise in the optical fluctuations does not correlate with the $1/f^{\alpha}$-type electrical noise and due to this the cross-correlation coefficient in all investigated frequency range of the unaged LED is rather small – the maximum value is ~4% at 25 mA forward current as shown in the inset of Fig. 2(c).

3.2. Noise characteristics during the ageing experiment

This section represents the changes of noise characteristics (intensity, spectrum, cross-correlation coefficient) and their link to current–voltage (I–V) and light output characteristics.

Long-term (in total 28000 h) ageing was performed and two main stages could be distinguished where a significant change in electrical and optical noise intensity occurs: the initial stage just after the first 1100 h ageing and the final stage after 28000 h. After 28000 h of operation the light output of the investigated LED decreases to 65% of the initial value at the currents above 1 mA (measured in BSR, Fig. 3). Usually, the decrease of the initial lumen output by 30% is the threshold when the human eye notices a light output reduction and this time, required to reach 70% of the initial lumen output, is called a lifetime of the LED (Alliance for Solid State Illumination System and Technology, TM-21 [1]). Therefore, we consider that the LED went out of order after 28000 h of ageing.

The investigated sample demonstrates a good linearity of the light output vs current characteristics before and after the ageing experiment

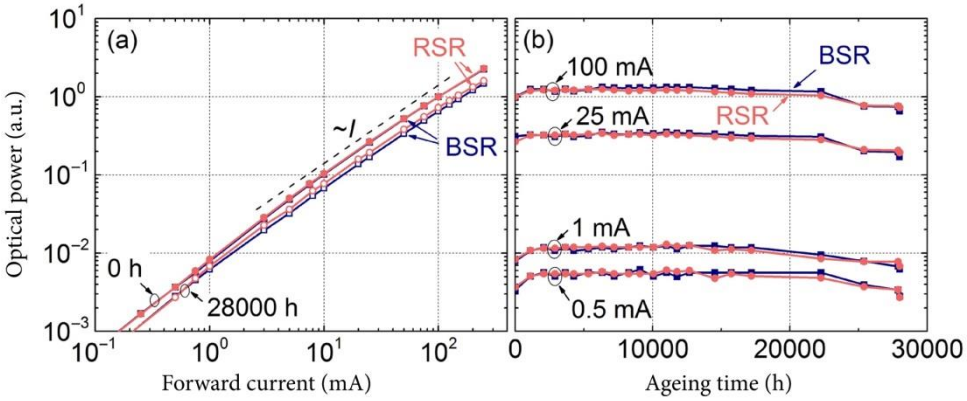


Fig. 3. The light output power dependences on the forward current at different ageing time (a): 0 h (solid symbols), 28000 h (open symbols); and on the ageing time at different forward current values (b) for both spectral ranges of the photodiode: BSR and RSR.

(Fig. 3(a)). At the early stage (1100 h) of ageing the LED output power increases by approximately 20% compared to the initial value (Fig. 3(b)). This suggests that small changes of the potential barrier occur in the active layer of the device that determine the increase of the charge carriers flow to the quantum wells and, as a consequence, a more intensive charge carrier recombination in the QWs region produces a more intensive light emission [16].

In order to understand changes of electrical fluctuations during ageing it is necessary to analyse the *I–V* characteristics of the device. These characteristics of the LED (Fig. 4) can be modelled as for a typical diode, which consists of the *p-n* junction differential resistance R_d, contact resistance R_s and parallel leakage resistance R_p. As demonstrated in the inset of Fig. 4, the evident leakage current is dominant up to 0.01 mA and the deviation from the exponential law at forward current values higher than 20 mA is due to the series resistance of the LED. Knowing current values where these different carrier transport mechanisms dominate makes the interpretation of electrical noise characteristics easier.

The variation of electrical noise intensity during the ageing is represented in Fig. 5(a). During the ageing electrical noise spectra remained

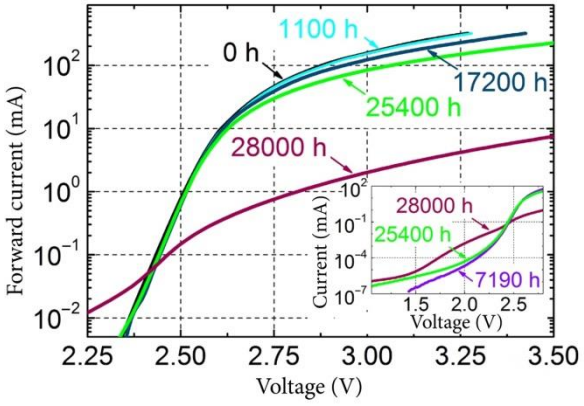


Fig. 4. *I–V* characteristics of the investigated LED at different ageing times. The inset represents *I–V* characteristics at the small current region (leakage currents).

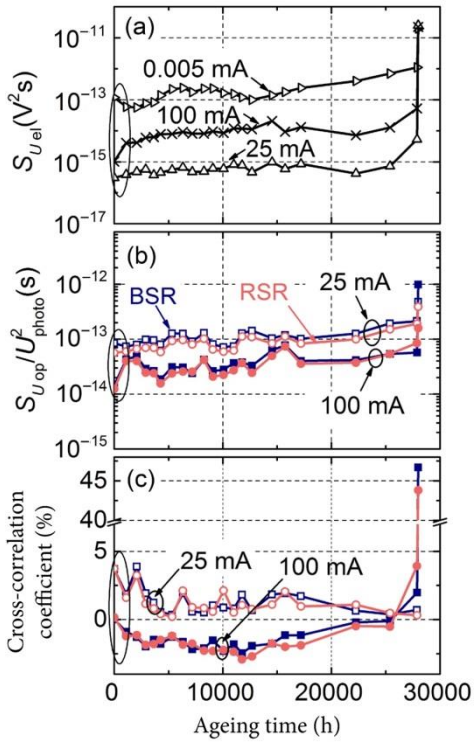


Fig. 5. Dependences of the electrical (a) and normalized optical noise (b) on the ageing time at different forward current values at 22 Hz and the dependence on the ageing time of the cross-correlation coefficient between electrical and optical fluctuations in the overall frequency range 10 Hz–20 kHz at different forward current values (c). Circles denote the initial stage of ageing (1100 h).

$1/f^{\alpha}$-type over all the investigated frequency range. At the initial stage of ageing, the voltage spectral density of electrical noise decreases when current flowing through the specimen is small (0.005 mA). However, at 25 and 100 mA, the electrical noise increases by one order of magnitude compared to the unaged sample noise level. This increase of the electrical noise level in the higher current region can be attributed to the electromigration-induced void formation in contact metallization [3]. In the low current region the noise level decreases more presumptively due to defect reordering or annealing [17] which determines fluctuations in the parallel leakage resistance value. These material migration and reordering processes also influence changes in the potential barrier and, as a consequence, determine light output power increase after 1100 h.

In order to calculate the cross-correlation coefficient, the optical noise (Fig. 5(b)) during ageing has been measured. The character of the voltage spectral density of optical fluctuations remains the same during all experiment – $1/f^{\alpha}$-type at low frequencies which is prevailed by the shot noise at higher ones. The cross-correlation coefficient between electrical and optical fluctuations becomes negative in all investigated frequency range at I = 100 mA after 1100 h (Fig. 5(c)). This slightly negative cross-correlation at higher currents indicates forward current redistribution between the active and neighbour regions [16].

Between the initial and the final stages of ageing the series resistance of the investigated LED increases gradually and the leakage current also increases slightly, as seen from I–V (Fig. 4). Such behaviour is quite common for GaN-based optoelectronic devices during ageing tests [3, 9]. While these changes are small (a number of additional non-radiative recombination centres is not high enough), they practically do not affect the light output characteristic. However, the increase of the electrical noise level is more noticeable in the region where the leakage current dominates (0.005 mA), while at higher forward current values only a small variation of noise intensity is observed (Fig. 5(a)). Also, small variations in the optical noise level and the cross-correlation coefficient dependences on the ageing time are observed between these stages (Fig. 5(b, c)).

The final ageing stage, which is accompanied by a strong growth of the spectral density of electrical noise (more than two orders) in all forward current range (Fig. 5(a)), should be distinguished. This is in coincidence with I–V changes (Fig. 4) indicating the presence of parasitic leakage paths and also with a considerable light output power decrease (Fig. 3(b)) revealing the formation of a high number of non-radiative recombination centres. The increased optical noise level and especially the increased positive cross-correlation coefficient between the electrical and optical fluctuations (Fig. 5(b, c)) indicate high defectiveness of the LED active area. However, it is useful to separate the electrical low-frequency noise

components into correlated and uncorrelated parts which can prove this idea.

As mentioned in the Introduction, the cross-correlation method enables estimating which part of the electrical low-frequency noise is related to the optical fluctuations (this is represented by the quantity d_j that shows which part of the spectral component $S_{el\,j}(f)$ of the electrical noise is correlated to the emitted light fluctuations) and gives useful information on the noise origins in the device. In Fig. 6 the result of the calculation of quantity d_j during the ageing is presented. The cross-correlation method has been fully described earlier in [10, 14]. Here, the index $j = 1$ describes the variance of $1/f$ fluctuations and $j = 2$ is the variance of $1/f^{\alpha}$ fluctuations (the shot noise and the noise of the measuring system are uncorrelated).

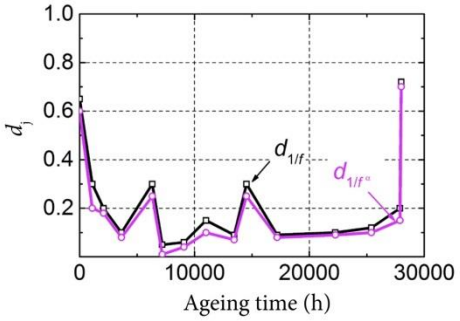


Fig. 6. Dependences of quantities d_j on the ageing time at $I = 25$ mA.

Before ageing at $I = 25$ mA (where a maximum of the cross-correlation dependence on forward current is present (inset in Fig. 2(c)) quantities d_j for the $1/f$ and $1/f^{1.3}$ noise components have similar values: $d_{1/f} = 0.65$ and $d_{1/f^{\alpha}} = 0.6$. These results mean that more than a half of the electrical low-frequency fluctuations are related to the low-frequency optical fluctuations. After the initial ageing stage, the correlated part of electrical fluctuations decreases and this is in coincidence with the abovementioned idea of material migration and contact degradation: the electrical noise level increases due to noise sources in the passive layers of the LED. And at the final ageing stage there is a sudden increase in quantities d_j exceeding their values before ageing: $d_{1/f} = 0.72$ and $d_{1/f^{\alpha}} = 0.7$. This verifies a sudden growth of the noise source in the active area of the LED.

The most plausible reason of such abrupt changes of noise and I–V characteristics after 28000 h of ageing is an increased self-heating of the device which has led to rapid defect formation, migration and clustering mostly in the active area of the LED. As reported in [2, 3], it can be related to a partial detachment of the layer containing the semiconductor chip from the package base, the so-called delamination, when a small air gap occurs between the LED chip and the package base. This strongly accelerates degradation of the device.

3.3. Changes of optical characteristics influenced by the phosphor layer

Changes in the performance of the phosphor layer have an impact on the alteration of optical characteristics (e.g. decrease in optical power) and the correlated colour temperature (CCT) shift. Also, as the optical noise is modulational, the LED current fluctuations modulate the emitted 'blue' photon flow, then this 'blue' photon flow modulates the 'yellow' emittance of the phosphor layer, and the determination whether this additional layer acts as a noise source is possible.

Figure 7 represents the optical spectra of the investigated LED during the ageing experiment, which is typical of the white LED: it is composed of

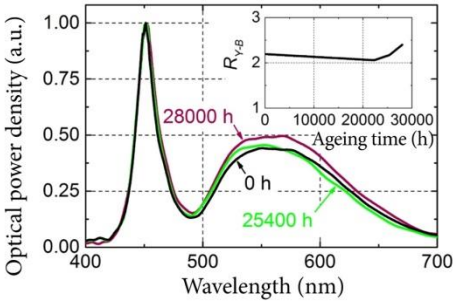


Fig. 7. Optical spectra measured at 100 mA forward current after different ageing time. All spectra are normalized to the peak of the 'blue' radiation. The inset shows the variation of the $R_{Y\text{-}B}$ ratio during the ageing experiment.

the blue part of the spectrum up to 480 nm produced by the LED chip and the remaining yellow part due to the partial conversion of the chip radiation by the phosphor layer.

There is no significant wavelength change in the blue part of the spectrum (the central wavelength λ = 452 nm) during ageing. The ratio $R_{Y\text{-}B}$ between intensities of the yellow and the blue parts of the optical spectrum is calculated as follows:

$$R_{Y-B} = \frac{\int_{480}^{780} P(\lambda)\mathrm{d}\lambda}{\int_{380}^{480} P(\lambda)\mathrm{d}\lambda}. \quad (3)$$

Here $P(\lambda)$ is the optical power density (W/nm). This ratio varies during the ageing experiment. It slightly decreases up to 22260 h and then starts to increase indicating colour changes of the emitted light. In some applications, e.g. in museum lighting or medicine, chromatic stability is very important. The colour shift of light is represented in the CIE 1931 colour space (Fig. 8) where x, y and z are chromaticity coordinates and $z = 1 - x - y$, so it can be depicted in the Cartesian plane. Applying the third order polynomial equation [18], the correlated colour temperature (CCT) has been computed using the CIE 1931 coordinates x, y. Generally, the main factors that influence chromatic properties of the LED are blue LED chip degradation, change in phosphor layer efficiency and darkening of the phosphor-encapsulating material [2]. The change of CCT from the initial (0 h) 6225 K to 6306 K after 22600 h of ageing can be related to the decrease of the phosphor layer efficiency as the blue light output power of the chip is practically stable (excluding the initial light output increase just after 1100 h) (Fig. 2(b)). As stated in [19], the increase in the phosphor conversion efficiency is possible only during the early ageing stage. At the same time, browning of the phosphor-encapsulating material also takes place. While all these factors contribute to the LED light output degradation, their rate of kinetics differs [5]. During ageing, these rates vary, so this affects chromatic properties of the device differently. The yellowing of optical spectra of the investigated sample after 22260 h is also confirmed by the light output measurement (Fig. 2(b)): the optical power measured with RSR oversteps the light power measured with the BSR photodiode despite the fact that the general light output decreases. The calculated CCT after the 28000 h ageing experiment is 6040 K. So, the variation of chromatic properties of the investigated LED is determined by a volatile ratio between the blue and yellow components of optical spectra.

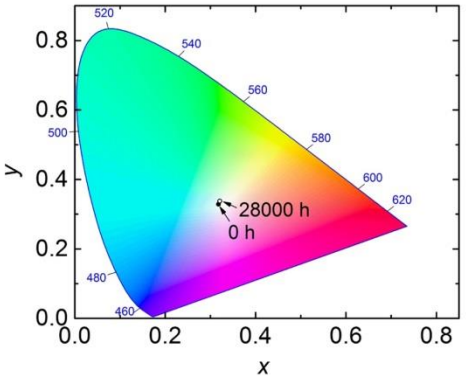


Fig. 8. Variation of the CIE 1931 chromatic coordinates measured before (CCT 6225 K) and after the 28000 h ageing experiment (CCT 6040 K) at 100 mA forward current.

From the noise point of view, there is a quite good agreement between the cross-correlation coefficient dependences on the frequency when the optical noise is measured with the BSR photodiode, and when it is measured with the RSR photodiode, during all the ageing experiment (Fig. 5(c)). The phosphor layer only reemits part of the LED chip radiation and the changes in the efficiency of this layer affect just the level of the optical fluctuations measured with RSR. These phosphor layer efficiency fluctuations are very small, so they do not cause a significant mismatch between BSR and RSR cross-correlation coefficient values. Thus, it can be stated that the phosphor layer practically does not act as an additional noise source in the investigated ageing time interval. The main source of the optical noise is the active area of the LED.

4. Conclusions

The investigation of noise characteristics and other supplementary electrical and optical characteristics

(*I*–*V*, light output power, optical spectra) of a high-power InGaN white phosphor-converted LED has been performed during the long-term (28000 h) ageing experiment.

At the initial stage of ageing (1100 h), the increase of light output and the decrease of electrical noise at the small forward current region are related to annealing or reordering of some defects leading to potential barrier changes. The growth of the electrical noise level at larger currents is mostly caused by contact degradation which is supported by *I*–*V* and negative cross-correlation characteristics indicating forward current redistribution between the active (QW region) and the neighbour areas.

Between the initial and the final stages of ageing, small variations occur in the optical and electrical noise intensity, and the correlated electrical noise part decreases.

The final stage of ageing is characterized by a high electrical and optical noise growth and a strong positive cross-correlation between them, indicating a high defectiveness of the active area of the LED.

The obtained calculation results using the cross-correlation method prove this idea. At this stage in the active area current leakage paths are formed by defects that act as non-radiative recombination centres and thus considerably lower light output power. The most presumable reason of this damage of the active area is the increased device self-heating.

A clear coincidence of two cross-correlation coefficient measurements, between electrical and LED blue light intensity fluctuations and between electrical and phosphor radiation intensity fluctuations, shows that the phosphor layer does not act as a noise source at given ageing conditions and time. However, this layer contributes to the variation of chromatic properties of the LED. Due to different kinetic rates of the degradation of separate LED parts (chip, the phosphor layer and the encapsulating material) two different CCT shifts are observed during the ageing experiment.

References

[1] M. Yazdan Mehr, W.D. van Driel, and G.Q. Zhang, Accelerated life time testing and optical degradation of remote phosphor plates, Microelectron. Reliab. **54**, 1544–1548 (2014).

[2] M. Meneghini, L.R. Trevisanelloa, F. de Zuania, N. Trivellin, G. Meneghesso, and E. Zanoni, Extensive analysis of the degradation of Phosphor-Converted LEDs, Proc. SPIE **7422**, 74220H-1 (2009).

[3] A. Jayawardena and N. Narendran, Analysis of electrical parameters of InGaN-based LED packages with aging, Microelectron. Reliab. **66**, 22–31 (2016).

[4] J. Fan, K.-C. Yung, and M. Pecht, Lifetime estimation of high-power white LED using degradation-data-driven method, IEEE Trans. Device Mater. Reliab. **12**(2), 470–477 (2012).

[5] M. Yazdan Mehr, W.D. van Driel, and G.Q. Zhang, Reliability and lifetime prediction of remote phosphor plates in solid-state lighting applications using accelerated degradation testing, J. Electron. Mater. **45**(1), 444–452 (2016).

[6] B.K. Jones, Electrical noise as a reliability indicator in electronic devices and components, IEE Proc. Circ. Dev. Syst. **149**, 13–22 (2002).

[7] L.K.J. Vandamme, Noise as diagnostic tool for quality and reliability of electronic devices, IEEE Trans. Electron Dev. **41**, 2176–2187 (1994).

[8] S. Bychikhin, D. Poganya, L.K.J. Vandamme, G. Meneghesso, and E. Zanoni, Low-frequency noise sources in as-prepared and aged GaN-based light-emitting diodes, J. Appl. Phys. **97**, 123714 (2005).

[9] S. Sawyer, S.L. Rumyantsev, and M.S. Shur, Degradation of AlGaN-based ultraviolet light emitting diodes, Solid State Electron. **52**, 968–972 (2008).

[10] V. Palenskis, J. Matukas, S. Pralgauskaitė, and B. Saulys, A detail analysis of electrical and optical fluctuations of green light-emitting diodes by correlation method, Fluct. Noise Lett. **9**(2), 179–192 (2010).

[11] K.K. Leung, W.K. Fong, and C. Surya, Low-frequency noise in GaN diodes, in: *Proceedings of the 21st International Conference on Noise and Fluctuations* (IEEE, 2011) pp. 291–296.

[12] I.-H. Lee, A. Y. Polyakov, S.-M. Hwang, N.M. Shmidt, E.I. Shabunina, N.A. Tal'nishnih,

N.B. Smirnov, I.V. Shchemerov, R.A. Zinovyev, S.A. Tarelkin, and S.J. Pearton, Degradation-induced low frequency noise and deep traps in GaN/InGaN near-UV LEDs, Appl. Phys. Lett. **111**, 062103 (2017).

[13] L. Liu, J. Yang, and G. Wang, The investigation of LED's reliability through highly accelerated stress testing methods, in: *Proceedings of the 14th International Conference on Electronic Materials and Packaging (EMAP)* (IEEE, 2012) pp. 1–3.

[14] V. Palenskis, J. Matukas, and B. Šaulys, A detailed analysis of electrical and optical fluctuations of light-emitting diodes by correlation method, Lith. J. Phys. **49**, 453–460 (2009).

[15] V. Palenskis and K. Maknys, Nature of low-frequency noise in homogenous semiconductors, Sci. Rep. **5**, 18305 (2015).

[16] V. Palenskis, J. Matukas, and S. Pralgauskaitė, Light-emitting diode quality investigation via low-frequency noise characteristics, Solid State Electron. **54**(8), 781–786 (2010).

[17] J. Hu, L. Yang, L. Kim, and M.W. Shin, The ageing mechanism of high-power InGaN/GaN light-emitting diodes under electrical stresses, Semicond. Sci. Technol. **22**, 1249–1252 (2007).

[18] C.S. McCamy, Correlated color temperature as an explicit function of chromaticity coordinates, Color Res. Appl. **17**(2), 142–144 (1992).

[19] Z. Qin, J. Feng, C. Zhaohui, X. Ling, W. Simin, and L. Sheng, Effect of temperature and moisture on the luminescence properties of silicone filled with YAG phosphor, J. Semicond. **32**(1), 012002 (2011).

DIDELĖS GALIOS BALTOS ŠVIESOS DIODO ŽEMADAŽNIO TRIUKŠMO CHARAKTERISTIKOS ILGALAIKIO SENDINIMO EKSPERIMENTO METU

J. Glemža, J. Matukas, S. Pralgauskaitė, V. Palenskis

Vilniaus universiteto Taikomosios elektrodinamikos ir telekomunikacijų institutas, Vilnius, Lietuva

Santrauka

Ilgalaikio sendinimo eksperimento metu (28000 val.) tirtos didelės galios InGaN pagrindu pagaminto baltos šviesos diodo žemadažnio elektrinio ir optinio triukšmo charakteristikos bei jų tarpusavio koreliacijos koeficientas. Koreliacinė analizė rodo, kad koreliuoto žemadažnio elektrinio triukšmo dalis, kuri atspindi fizikinius procesus, vykstančius šviesos diodo aktyviojoje srityje, sendinimo eksperimento metu kinta. Atsižvelgiant į staigius triukšmų charakteristikų pokyčius išskiriami du pagrindiniai etapai. Pradinis etapas (po pirmųjų 1100 val.) yra susijęs su elektrinio triukšmo mažėjimu tekant bandiniu mažoms srovėms ir spinduliuotės galios padidėjimu, o galutinis etapas (po 28000 val.) charakterizuojamas staigiu žemadažnio triukšmo augimu, spinduliuotės galios sumažėjimu ir elektrinio triukšmo koreliuotosios dalies su optiniu triukšmu didėjimu. Tai rodo aktyviosios srities gedimą. Optinio spektro skaidymas į puslaidininkio šviesos diodo lusto spinduliuotę ir perspinduliuotą fosforo sluoksnio leidžia įvertinti fosforo sluoksnio įtaką prietaiso optinių charakteristikų blogėjimui. Nepaisant to, kad šis sluoksnis itin prisideda prie šviesos diodo chromatinių savybių kitimo, tarpusavio koreliacijos koeficiento analizė rodo, kad fosforo sluoksnis sendinimo eksperimento metu nėra triukšmo šaltinis.

P5

J. Glemža, S. Pralgauskaitė, V. Palenskis, J. Matukas,

Low-frequency noise of near UV LEDs,

Lith. J. Phys. **59**, 146–155 (2019).
doi: 10.3952/physics.v59i3.4081.

Visos teisės priklauso Lietuvos mokslų akademijai, 2019

Perspausdinta su Lietuvos fizikos žurnalo redakcijos leidimu

Reprinted with permission of the Lithuanian Journal of Physics

Lithuanian Journal of Physics, Vol. **59**, No. 3, pp. 146–155 (2019)
© Lietuvos mokslų akademija, 2019

LOW-FREQUENCY NOISE OF NEAR UV LEDs

J. Glemža, S. Pralgauskaitė, V. Palenskis, and J. Matukas

Institute of Applied Electrodynamics and Telecommunications, Vilnius University, Saulėtekio 3, 10257 Vilnius, Lithuania
Email: justinas.glemza@ff.vu.lt; sandra.pralgauskaite@ff.vu.lt; vilius.palenskis@ff.vu.lt; jonas.matukas@ff.vu.lt

Received 17 May 2019; revised 27 June 2019; accepted 30 September 2019

Low-frequency noise characteristics of high power near ultraviolet light-emitting diodes (LEDs) with peak radiative wavelengths in a range of 380–410 nm are investigated in a temperature interval of 110–293 K. The defect-assisted tunnelling current component has been observed in some 380 nm peak wavelength samples with corresponding Lorentzian-type electrical noise spectra. Other samples (with a peak wavelength of 390–410 nm) have mainly $1/f^{\alpha}$-type electrical fluctuations. Cross-correlation coefficient analysis between electrical and optical fluctuations has been performed in order to evaluate whether the observed defect levels, responsible for additional generation–recombination (g–r) noise components in LEDs noise spectra, are related to the active layer or to the peripheral area of the device. Activation energies of these g–r centres have been also evaluated using g–r noise spectroscopy.

Keywords: cross-correlation coefficient, fluctuation, light-emitting diode, noise, tunnelling

PACS: 72.70.+m, 85.60.Jb

1. Introduction

Due to numerous advantages, such as a small size and increased efficiency, ultraviolet (UV) light-emitting diodes (LEDs) have gained a lot of demand for applications in UV lighting, as light sources for microscopes and for chemical excitation in medicine and biotechnology, for sterilization and disinfection, for banknote identification, counterfeit detection, etc. [1–3]. For the fabrication of near UV (300–400 nm) light-emitting diodes [1], the InGaN material system is of a high importance. It is well known that non-uniformities in the indium concentration in InGaN/GaN quantum wells (QWs) create localized states which are responsible for the effective radiative recombination [4, 5]. However, near UV LEDs contain less indium, and this results in a lower radiative efficiency and, at the same time, in an increased impact of threading dislocations on the overall performance of the UV emitter [3, 6].

Low-frequency excess noise is very sensitive for defectiveness and fabrication imperfections of semiconductor devices. Usually, the level of electrical $1/f$-type fluctuations (flicker noise) of LEDs is much higher than the level of shot noise or thermal noise in the low-frequency region (up to 10 MHz for modern devices) [7]. In some cases, when generation–recombination (g–r) noise with the Lorentzian-type spectrum is observed, it helps one to identify the energy levels of localized centres. $1/f$-type fluctuations not only characterize the quality of the semiconductor crystal, but also the dependence of noise spectral density on the current reveals information about the current flowing through the sample paths. For InGaN material system based devices, which suffer from a high density of defects, this investigation is crucial [8–11]. What is more, for the characterization of optoelectronic devices, e. g. LEDs or laser diodes (LDs), it is important to identify the location of noise sources in the structure. This would allow one to discover the relation between the low-frequency noise characteristics and the indium amount in QWs that determines the emission wavelength in near UV LEDs. However, the presence of additional noise sources in the LED peripheral area usually aggravates this analysis. In

our previous works [11, 12] it has been demonstrated that the cross-correlation analysis between electrical and optical fluctuations together with the evaluation of other electrical, e. g. current–voltage (*I*–*U*), characteristics is a powerful tool for the characterization of green and white LEDs. The ability to determine the location of noise sources in LDs or LEDs when measurements are performed under the normal bias condition near the equilibrium state makes the low-frequency noise and cross-correlation analysis method highly attractive.

Despite the fact that near UV LEDs with a sufficiently high external quantum efficiency have been already demonstrated [1], their low-frequency noise has not been studied enough [13]. The impact of fluctuation origins and defects that are present in the structure on the LED conduction mechanism and overall performance still needs to be researched in a more detailed way. The aim of this work is not only to investigate the low-frequency noise characteristics of the near UV LEDs, but also to identify the location of the sources of Lorentzian-type fluctuations in the near UV LEDs of different emission wavelength using cross-correlation analysis between the electrical and optical fluctuations.

2. Experimental details and investigated devices

Low-frequency noise characteristics such as electrical noise – the terminal voltage fluctuations of LED (10 Hz–100 kHz), optical noise – fluctuations of the emitted light power detected by a UV-blue *pin* photodiode (10 Hz–20 kHz), and the cross-correlation between electrical and optical fluctuations (10 Hz–20 kHz) were measured under constant current operation at the forward bias at room temperature (RT). When generation–recombination noise spectroscopy was performed, cooling by liquid nitrogen was used and measurements were performed in a temperature interval of 110–293 K. For the measurement of current–voltage characteristics a precision source/measure unit *Keysight* B2901 was used. Emitted light spectra were registered by an optical spectrum analyzer *Advantest* Q8341. A detailed noise measurement scheme can be found in our previous work [11].

The investigated high power (~1 W) InGaN-based near UV LEDs are summarized in Table 1.

The light output power characteristics and optical spectra of the investigated LEDs are presented in Fig. 1. The measurements show that the LEDs with the highest amount of In in QWs and, therefore, the largest wavelength (group D) have the most symmetrical optical spectrum (Fig. 1(a)), while the samples with the lowest amount of In and the shortest wavelength (group A) have the lowest light output power (Fig. 1(b)).

Table 1. Families of the investigated LEDs grouped by peak radiative wavelength.

Peak wavelength	~380 nm	~390 nm	~400 nm	~410 nm
Group name	A	B	C	D

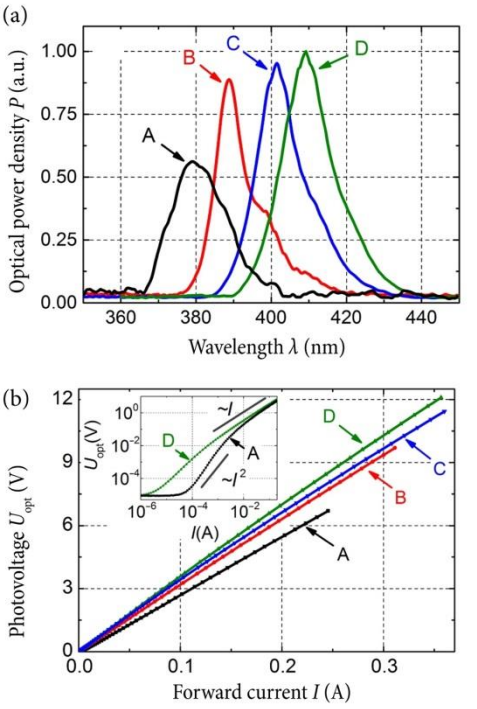


Fig. 1. Typical optical spectra of the investigated LEDs measured at 250 mA forward current (a); the emitted light output power (which is proportional to the photovoltage U_{opt} of the load resistance of a photodetector) vs the current characteristics for different LEDs (b). The inset represents the latter characteristics of group A and D LEDs in a log–log scale.

3. Results and discussion

3.1. Analysis of the tunnelling current component

For the analysis of the electrical characteristics of InGaN-based LEDs, the determination of the conduction mechanism is very important [6, 14–18] and it also broadens the interpretation of low-frequency fluctuations.

As presented in Fig. 2, the *I*–*U* characteristic of particular LEDs from the group A (AI curve) differs from that of the remaining samples from this group (AII curve) and from other diodes of groups B–D. For the evaluation of the LED conduction process, the method described in [14] and [16] was used. The *I*–*U* relation for the tunnelling through defects is expressed as

$$I \sim P \cdot E^2 \exp(-1/E), \quad (1)$$

where I is the forward current, P has a meaning of the tunnelling probability between defects, which is temperature independent, and E is the electric field [14]. Thus, for only tunnelling current component existence, the $\log(I/U^2)$ dependence on $1/U$ should be linear and the characteristic energy $E_T = nkT$ in the *I*–*U* relation $I = I_0 \exp(qU/E_T)$ should be temperature independent. Here I_0 is the saturation current of the diode, q is the elementary charge, n is the non-ideality coefficient, and k is the Boltzmann constant. The energy E_T reflects the transparency of the energy barrier for the tunnelling process [14, 17].

The described procedure has been applied to the characteristics of the LEDs under investigation. The *I*–*U* curves of the AI sample at different temperatures are presented in Fig. 3, and the linear $\log(I/U^2)$ vs $1/U$ dependences are also depicted in Fig. 4(a). The characteristic energy E_T of the particular LEDs

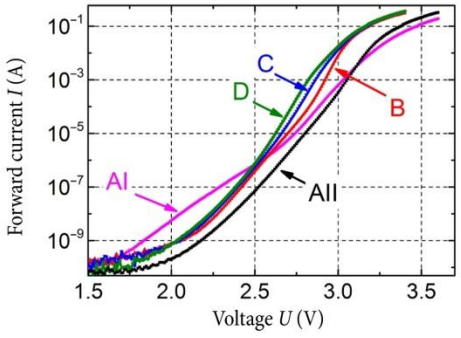


Fig. 2. *I*–*U* characteristics of different wavelength LEDs at RT.

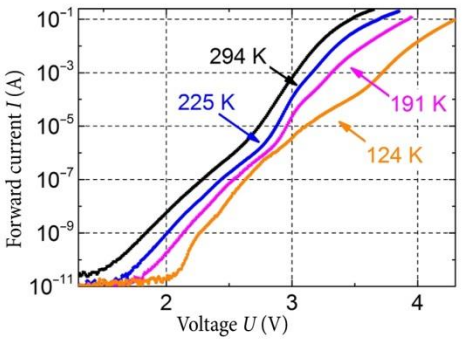


Fig. 3. *I*–*U* characteristics of AI LED in a temperature range of 124–294 K.

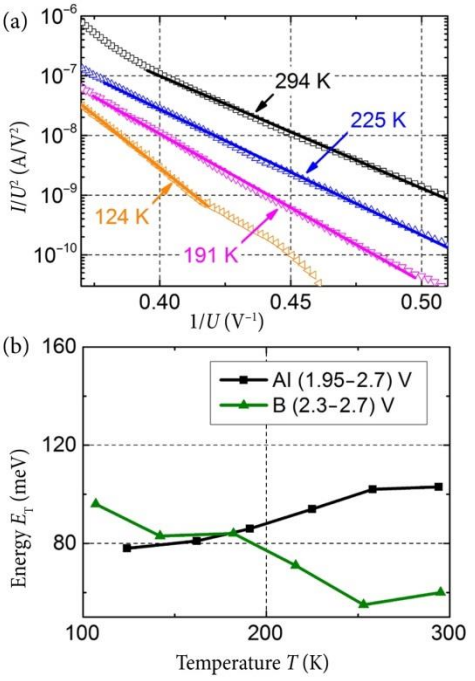


Fig. 4. (a) I/U^2 vs $1/U$ curves of AI LED in a low bias regime in a temperature range of 124–294 K (solid lines represent the linear approximation). (b) Comparison of the characteristic energy E_T dependences on the temperature of AI LED and LED from the group B in 1.95–2.7 V and 2.3–2.73 V, respectively, forward bias intervals.

from the group A has been found to be higher than that of the samples from other investigated groups, e. g. ~100 meV (for AI) in comparison to ~60 meV (for B) at RT in a low bias regime (up to ~2.7 V). Other samples of the A family, group C and D LEDs have similar E_T dependences on temperature as the group B sample presented in Fig. 4(b). The variation of the characteristic energy E_T with temperature for the AI LED is weaker compared to, for example, that of the group B sample. High E_T indicates the high non-ideality factor of I–U relation ($n \approx 4$ at RT) of the diode, also suggesting that some LEDs of the group A have a dominant tunnelling current component at a low bias [14]. At higher bias the conduction is mixed of diffusion, recombination and tunnelling processes. No clear tunnelling current component has been observed in the samples of families B–D at a low bias.

The obtained results suggest that the quality of some samples from the group A is lower, i.e. they have a higher density of defects mainly such as threading dislocations and defects in the vicinity of them. This would allow one to explain the tunnelling process through the deep trap levels [17]. However, further analysis is needed to conclude this, thus, low-frequency noise investigation has been performed. Here in the group A the samples with the observed tunnelling component are denoted as AI, and LEDs without it as AII.

3.2. Noise characteristics

The electrical noise spectra of the investigated LEDs are presented in Figs. 5 and 6. Lorentzian-type fluctuations (with a small $1/f^{\alpha}$ noise component up to ~1 kHz) in the whole investigated forward current region were observed only in the AI LEDs noise spectra (Fig. 5(a)). Such type noise spectrum usually indicates the presence of a discrete generation–recombination (g–r) centre in the device. The trapping level with shorter than ~1.6 μs effective relaxation time ($1/\tau = 1/\tau_c + 1/\tau_e$, where τ_c and τ_e are the average charge carrier capture and emission times from the defect level, respectively [19]) is responsible for the observed Lorentzian-type noise spectra. Regarding the fact that g–r noise is also observed at a low bias for AI LEDs, it can be stated that the observed trapping level acts as an intermediate state for the tunnelling

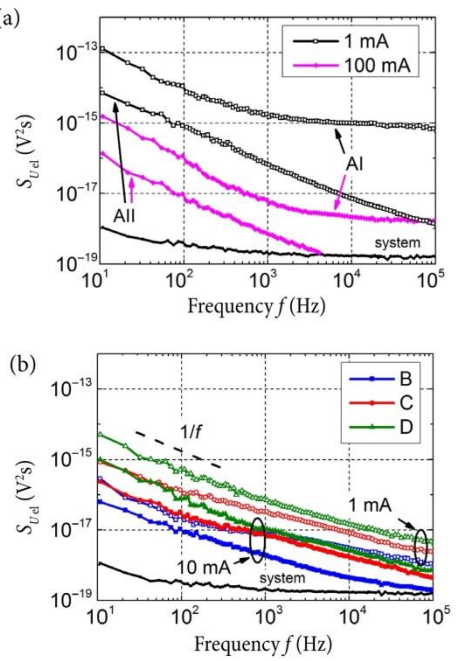


Fig. 5. Electrical noise spectra of the group A LEDs (a) and the LEDs of groups B–D (b) at different forward current values at RT. 'System' represents the measurement system noise floor.

charge carriers [6]. Thus, the tunnelling process in these AI samples can be considered as defect-assisted. Figure 1(b), where the emitted light power characteristics for the samples of groups A and D are compared in log scales, confirms the idea of a high defectiveness of AI LEDs. The radiated optical power is proportional to the forward current as $U_{opt} \sim I^r$ [16], where the parameter $r > 2$ for AI LEDs in a wide current interval up to ~20 mA and $1 < r < 2$ for the D samples in a narrower interval (up to ~ 1 mA). In the case of AI LED a higher value of the parameter r shows that the density of defects is higher in these devices compared to, for example, that of the group D LED (Fig. 1(b)). These defects act as non-radiative recombination centres and effectively lower the radiative efficiency of the device [6, 16].

The noise spectra of the AII and group B–D samples are characterized by $1/f^{\alpha}$-type electrical fluctuations (Fig. 5) up to the forward current value where the series resistance-limited current arises.

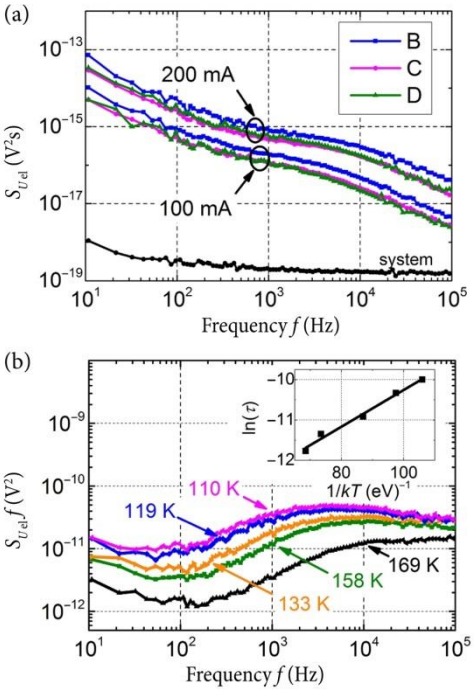


Fig. 6. Electrical noise spectra of the group B–D samples at RT in the series resistance-limited current regime (a); normalized electrical noise spectra ($S_{U\,el}f$) of the group B LED in a temperature range of 110–169 K at 100 mA forward current (b). The inset in (b) represents the relaxation time dependence on the inverse temperature (square symbols denote experimental values).

As known, in semiconductor devices $1/f^{\alpha}$-type fluctuations originate as a result of the superposition of Lorentzian-type spectra due to different capture and emission processes of charge carriers in defects with a very wide distribution of relaxation times [20, 21]. The series resistance-limited current tends to dominate at about 100 mA for the AII LEDs and for the samples of groups B–D at 5–50 mA. While it is hard to determine these values from the *I–U* characteristics accurately (Fig. 2), the dependences of electrical noise spectral density on the forward current clearly indicate that (Fig. 7). The series resistance R_s is mainly caused by resistances of contacts and highly doped n^+ and p layers. Thus, when the differential resistance of the LED reaches the serial resistance ($R_{diff} \approx R_s$), the electrical noise starts to increase (Fig. 7). In the forward current range, where the voltage fluctuation spectral density decreases, the differential resistance of the diode $R_{diff} \sim 1/I$, and for $1/f^{\alpha}$-type electrical fluctuations the current noise spectral density for the *pn* junction is proportional to the forward current: $S_I \sim I$ [22]. This leads to the relation $S_U \sim S_I \cdot R^2_{diff} \sim 1/I$. Such observed 'V'-shape dependences of voltage fluctuation spectral densities on the forward current are similar as for a phosphor-converted white LED with a 'blue' InGaN chip [11]. There only AI samples are distinguished by apparently higher noise level in a low current regime (up to ~1 mA, Fig. 7(a)) due to a high defectiveness as discussed earlier.

For the samples of groups B–D the voltage fluctuation spectral density increase that starts in a current interval of 5–50 mA is followed by the Lorentzian-type noise spectra appearance (Fig. 6(a)). An

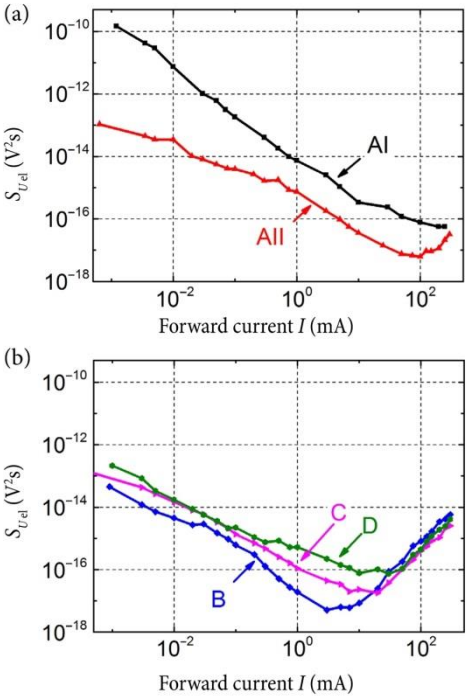


Fig. 7. Dependences of the voltage fluctuation spectral density ($S_{U\,el}$) on the forward current of the group A LEDs (a) and the LEDs of groups B–D (b) at 108 Hz frequency.

example of the normalized electrical noise spectra ($S_{U\,el}f$) of the group B LED at different temperatures is presented in Fig. 6(b). There noise peaks fulfil the condition $2\pi f_0\tau = 1$, where f_0 is the characteristic frequency of the spectrum maximum and τ is the effective relaxation time ($\tau \approx 8$ μs at RT). In a temperature interval of 170–293 K the noise maximum $S_{U\,el}f$ position is practically independent of the temperature. This means that the Fermi level is bound to the accumulation of defect levels. It is assumed that these g–r centres or interface states responsible for the mentioned fluctuations are located in the passive area of LED in highly doped n^+ or p layers as the flowing current through the specimen is restricted by series resistance. In the interval of lower temperatures, the relaxation time dependence on temperature has been observed and the activation energy E_a of the responsible g–r process has been evaluated by the equation $\tau = \tau_0\exp(E_a/kT)$ (the inset in Fig. 6(b)). The activation energy is determined to be in a range of 0.03–0.045 eV for different B–D samples. The appearance of the g–r noise component in the experiment for AII LEDs has been practically unnoticeable as R_{diff} reaches R_s at higher currents $I > 100$ mA (Fig. 7(a)).

Another g–r centre with ~0.19 eV activation energy has been identified in some samples of the group B in the 0.5–10 mA current region. The normalized electrical noise spectra of such LED at different temperatures are presented in Fig. 8. In the case of the group B sample the effective relaxation time

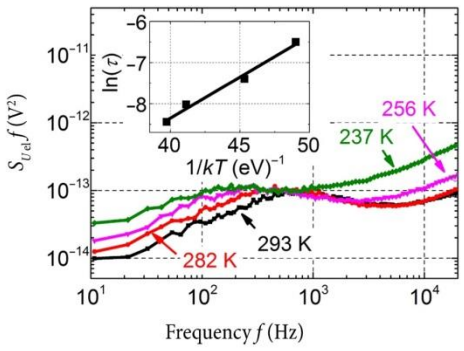


Fig. 8. Normalized electrical noise spectra ($S_{U\,el}f$) of the group B LED in a temperature range of 237–293 K at 1 mA forward current. The inset represents the relaxation time dependence on the inverse temperature (square symbols denote experimental values).

($\tau \approx 0.2$ ms at RT) is longer and the electrical noise level is also lower than in the case of AI LEDs, so it is expected that a different defect level is responsible for the observed Lorentzian-type fluctuations. For the verification of the discussed location of g–r noise sources, cross-correlation analysis between electrical and optical fluctuations has been performed and it is presented in the next subsection.

3.3. Cross-correlation coefficient between electrical and optical fluctuations

The cross-correlation measurement between electrical and optical noise helps one to identify whether the low-frequency fluctuations originate from the active layer of LED or the peripheral ones [12]. The simultaneous cross-correlation coefficient is calculated as follows:

$$k = \frac{\left\langle u_{el}(t)\cdot u_{op}(t)\right\rangle}{(\sigma_{el}^2\cdot\sigma_{op}^2)^{1/2}}. \qquad (2)$$

Here brackets $\langle\ldots\rangle$ mean averaging both over time and over number of realizations, $\sigma^2_{el} = \langle u^2_{el}(t)\rangle$ and $\sigma^2_{op} = \langle u^2_{op}(t)\rangle$ are the variances of electrical and optical, respectively, fluctuations in the frequency range from 10 Hz to 20 kHz. Note: for electrical and optical noise signals $[\langle u_{el}(t)\rangle]^2 = 0$ and $[\langle u_{op}(t)\rangle]^2 = 0$.

The optical noise spectra of the investigated samples are presented in Fig. 9(a). As seen, the group A LEDs are distinguished by stronger optical $1/f^\alpha$-type fluctuations (up to ~ 5 kHz) than the samples from the groups B–D. The normalized optical noise $S_{U\text{opt}}/U^2_{opt}$ of the family A LEDs is significantly higher than the noise of the remaining samples at frequencies where $1/f^\alpha$-type optical fluctuations dominate (Fig. 9(b)). Here in Fig. 9(b) $S_{U\text{opt}}/U^2_{opt}$ decreases as the forward current increases due to the light power increase. At higher frequencies (above ~5 kHz) the optical noise is 'white' – the spectrum is determined by the photocurrent induced shot noise (Fig. 9(a)).

Figure 10 shows that the highest cross-correlation coefficient between electrical and optical fluctuations is for group AI LEDs (up to 70%). This indicates a high defectiveness of the active area of LED, which leads to suppose that the earlier observed trap level in the group AI LEDs is also related to the structure of QWs and barrier layers.

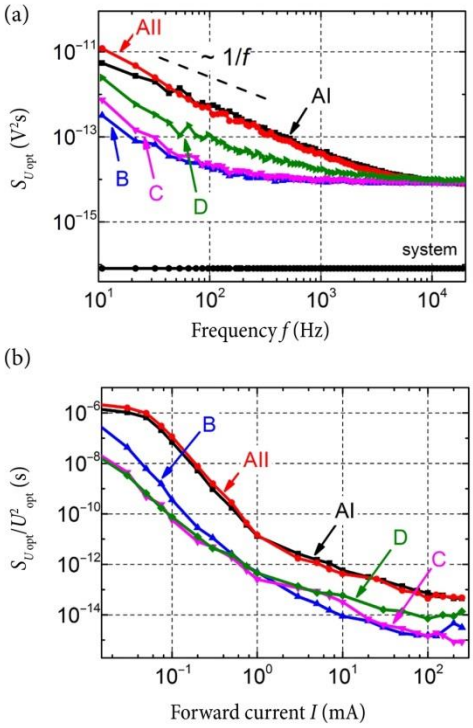


Fig. 9. Optical noise spectra ($S_{U_{opt}}$) of the investigated LEDs at 100 mA forward current (a); dependences of the voltage spectral density of the normalized optical noise (S_{Uopt}/U^2_{opt}) on the forward current for the investigated samples at 108 Hz frequency (b).

For the families of other samples the cross-correlation coefficient is lower and its maximum value varies in the forward current interval from 2 to 10 mA (Fig. 10(b)). At low current values optical $1/f^{\alpha}$-type or g–r noise components are too small to correlate effectively with the electrical noise. At higher current values the shot noise level increases drastically in the optical noise spectra and the electrical noise from the peripheral or contact areas of LED also starts to dominate. This explains different forward current values corresponding to the cross-correlation coefficient maxima. For the samples of groups B–D at $I > 50$ mA the coefficient becomes even slightly negative (down to –8%, Fig. 10(b)). The negative cross-correlation indicates the forward current redistribution between the active and passive layers of LED [23] due to defects located in the vicinity of the active QW region. Practically, no positive cross-correlation in the series resistance-limited current regime verifies that the detected noise sources responsible for the Lorentzian-type fluctuations are in the peripheral area of LED.

A comparison between the LEDs of group B with or without a g–r component in the noise spectra shows that devices with Lorentzian-type fluctuations in a current interval of 0.5–10 mA have a higher cross-correlation coefficient (Fig. 10(b)). There are no dramatic changes in the electrical noise level between these samples in this current regime. However, a stronger correlation between

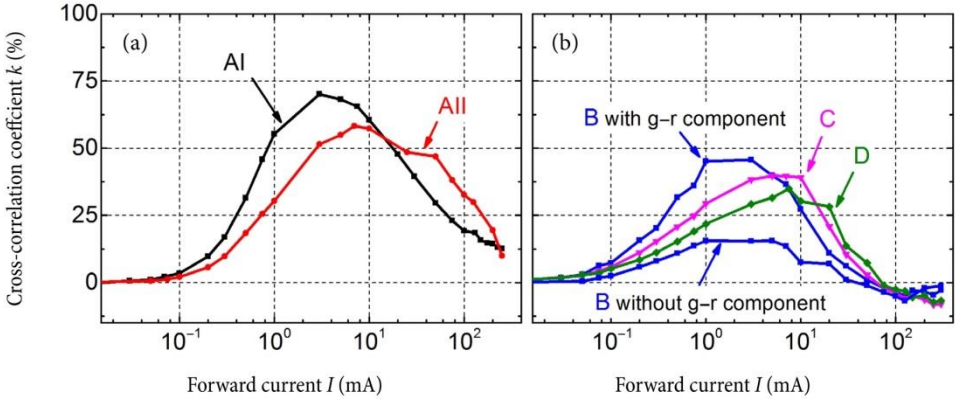


Fig. 10. Dependences of the cross-correlation coefficient between electrical and optical fluctuations on the forward current in the frequency range from 10 Hz to 20 kHz for the group A LEDs (a) and the LEDs of groups B–D (b).

the electrical and optical fluctuations in the B samples with the detected g–r noise component suggests that the part of electrical noise arising in the active layer of LED in this case is higher than in the case of specimens without a g–r noise component. There the total electrical noise can be expressed as $S_{\text{el total}} = S_{\text{el corr}} + S_{\text{el uncorr}}$, where $S_{\text{el corr}}$ represents the part of electrical fluctuations related to the active layer of the LED and $S_{\text{el uncorr}}$ is the part of electrical fluctuations arising from the peripheral area of the LED [12]. Thus, the observed Lorentzian-type fluctuations are determined by the presence of an additional defect level in the active InGaN QW region of some group B LEDs.

4. Conclusions

Investigation of the low-frequency noise characteristics of high power near UV LEDs has been performed. The tunnelling current component has been detected in some 380 nm peak wavelength LEDs at low bias. Such samples are distinguished by the Lorentzian-type electrical noise spectra in the whole investigated current range and a strong cross-correlation between electrical and optical fluctuations exists. This identifies the location of the trapping level in the active area of this group LEDs and contributes to the tunnelling process through defects.

LEDs of other groups with a peak wavelength of 390, 400 and 410 nm are characterized by the $1/f^{\alpha}$-type electrical fluctuations with Lorentzian-type noise components appearing only at the series resistance-limited currents. Defect levels with the activation energy in a range of 0.03–0.045 eV have been identified responsible for these g–r fluctuations. No positive cross-correlation between electrical and optical fluctuations in this current regime means that the Lorentzian-type fluctuation source is in the peripheral area of the LED, e.g. in highly doped layers.

Some of 390 nm peak wavelength LEDs are distinguished by an additional Lorentzian-type noise component in a current range of 0.5–10 mA with 0.19 eV activation energy. Such samples have a higher cross-correlation between electrical and optical fluctuations than samples with only $1/f^{\alpha}$-type noise spectra. This suggests that the location of the detected g–r noise centre is related to the InGaN QW structure.

References

[1] Y. Muramoto, M. Kimura, and S. Nouda, Development and future of ultraviolet light-emitting diodes: UV-LED will replace the UV lamp, Semicond. Sci. Technol. **29**, 1–8 (2014).

[2] D. Morita, M. Sano, M. Yamamoto, T. Murayama, S. Nagahama, and T. Mukai, High output power 365 nm ultraviolet light emitting diode of GaN-free structure, Jpn. J. Appl. Phys. **41**, L1434–L1436 (2002).

[3] J.T. Oh, Y.T. Moon, D.S. Kang, C.K. Park, J.W. Han, M.H. Jung, Y.J. Sung, H.H. Jeong, J.O. Song, and T.Y. Seong, High efficiency ultraviolet GaN-based vertical light emitting diodes on 6-inch sapphire substrate using *ex-situ* sputtered AlN nucleation layer, Opt. Express **26**, 5111–5117 (2018).

[4] K.C. Shen, W.Y. Lin, H.Y. Lin, K.Y. Chen, and D.S. Wuu, Self-textured oxide structure for improved performance of 365 nm ultraviolet vertical-type light-emitting diodes, Opt. Express **22**, 17600–17606 (2014).

[5] P. Ruterana, S. Kret, A. Vivet, M. Grzegorz, and P. Dłużewski, Composition fluctuation in InGaN quantum wells made from molecular beam or metalorganic vapor phase epitaxial layers, J. Appl. Phys. **91**, 8979–8985 (2002).

[6] X.A. Cao, K. Topol, F. Shahedipour-Sandvik, J. Teetsov, P.M. Sandvik, S.F. LeBoeuf, A. Ebong, J. Kretchmer, E.B. Stokes, S. Arthur, A.E. Kaloyeros, and D. Walker, Influence of defects on electrical and optical characteristics of GaN/InGaN-based light-emitting diodes, Proc. SPIE **4776**, 105–113 (2002).

[7] L.K.J. Vandamme, Noise as diagnostic tool for quality and reliability of electronic devices, IEEE Trans. Electron Dev. **41**, 2176–2187 (1994).

[8] S. Bychikhin, D. Pogany, L.K.J. Vandamme, G. Meneghesso, and E. Zanoni, Low-frequency noise sources in as-prepared and aged GaN-based light-emitting diodes, J. Appl. Phys. **97**, 123714 (2005).

[9] S.L. Rumyantsev, C. Wetzel, and M.S. Shur, Wavelength-resolved low-frequency noise of GaInN/GaN green light emitting diodes, J. Appl. Phys. **100**, 084506 (2006).

[10] A.E. Chernyakov, M.E. Levinshtein, N.A. Talnishnikh, E.I. Shabunina, and N.M. Shmidt, Low-frequency noise in diagnostics of power blue InGaN/GaN LEDs, J. Cryst. Growth **401**, 302–304 (2014).

[11] J. Glemža, J. Matukas, S. Pralgauskaitė, and V. Palenskis, Low-frequency noise characteristics of high-power white LED during long-term aging experiment, Lith. J. Phys. **58**, 194–203 (2018).

[12] V. Palenskis, J. Matukas, S. Pralgauskaitė, and B. Šaulys, A detail analysis of electrical and optical fluctuations of green light-emitting diodes by correlation method, Fluctuation Noise Lett. **9**, 179–192 (2010).

[13] I.H. Lee, A.Y. Polyakov, S.M. Hwang, N.M. Shmidt, E.I. Shabunina, N.A. Tal'nishnih, N.B. Smirnov, I.V. Shchemerov, R.A. Zinovyev, S.A. Tarelkin, and S.J. Pearton, Degradation-induced low frequency noise and deep traps in GaN/InGaN near-UV LEDs, Appl. Phys. Lett. **111**, 062103 (2017).

[14] J. Kim, Y. Tak, J. Kim, S. Chae, J.Y. Kim, and Y. Park, Analysis of forward tunneling current in InGaN/GaN multiple quantum well light-emitting diodes grown on Si (111) substrate, J. Appl. Phys. **114**, 013101-1–4 (2013).

[15] P. Perlin, M. Osinski, P.G. Eliseev, V.A. Smagley, J. Mu, M. Banas, and P. Sartorid, Low-temperature study of current and electroluminescence in InGaN/AlGaN/GaN double-heterostructure blue light-emitting diodes, Appl. Phys. Lett. **69**, 1680–1682 (1996).

[16] X.A. Cao, E.B. Stokes, P.M. Sandvik, S.F. LeBoeuf, J. Kretchmer, and D. Walker, Diffusion and tunneling currents in GaN/InGaN multiple quantum well light-emitting diodes, IEEE Electron Device Lett. **23**, 535–537 (2002).

[17] M. Lee, H. Lee, K.M. Song, and J. Kim, Investigation of forward tunneling characteristics of InGaN/GaN blue light-emitting diodes on freestanding GaN detached from a Si substrate, Nanomaterials **8**, 543-1–7 (2018).

[18] V.K. Malyutenko and S.S. Bolgov, Effect of current crowding on the ideality factor in MQW InGaN/GaN LEDs on sapphire substrates, Proc. SPIE **7617**, 76171K (2010).

[19] M.J. Kirton and M.J. Uren, Noise in solid-state microstructures: A new perspective in individual defects, interface states and low-frequency (1/*f*) noise, Adv. Phys. **38**, 367–468 (1989).

[20] V. Palenskis and K. Maknys, Nature of low-frequency noise in homogenous semiconductors, Sci. Rep. **5**, 18305-1–7 (2015).

[21] V. Palenskis, The charge carrier capture-emission process – the main source of the low-frequency noise in homogeneous semiconductors, Lith. J. Phys. **56**, 200–206 (2016).

[22] F.N. Hooge, T.G.M. Kleinpenning, and L.K.J. Vandamme, Experimental studies on 1/*f* noise, Rep. Prog. Phys. **44**, 479–532 (1981).

[23] V. Palenskis, J. Matukas, and S. Pralgauskaitė, Light-emitting diode quality investigation via low-frequency noise characteristics, Solid State Electron. **54**, 781–786 (2010).

ARTIMOSIOS UV SRITIES ŠVIESOS DIODŲ ŽEMADAŽNIAI TRIUKŠMAI

J. Glemža, S. Pralgauskaitė, V. Palenskis, J. Matukas

Vilniaus universiteto Taikomosios elektrodinamikos ir telekomunikacijų institutas, Vilnius, Lietuva

Santrauka

Atlikti didelės galios artimosios ultravioletinės (UV) srities šviesos diodų su smailiniu bangos ilgiu 380–410 nm intervale žemadažnio triukšmo charakteristikų tyrimai 110–293 K temperatūroje. Kai kurie 380 nm smailinio bangos ilgio bandiniai turi vyraujančią tunelinės srovės komponentę, atsirandančią dėl defektų, esant pridėtai žemai įtampai, ir pasižymi generacinio-rekombinacinio triukšmo spektriniais tankiais visame tirtame srovių intervale. Likę bandiniai yra charakterizuojami $1/f^{\alpha}$-tipo fliuktuacijomis, tačiau, pasiekus nuoseklios varžos ribojamą laidumo sritį, triukšmų spektriniuose tankiuose išryškėja papildoma generacinio-rekombinacinio triukšmo komponentė. Dalis 390 nm smailinio bangos ilgio bandinių srovių 0,5–10 mA intervale taip pat pasižymi generacinio-rekombinacinio tipo fliuktuacijomis. Generacinio-rekombinacinio triukšmo spektroskopija rastos šių krūvininkų pagavimo lygmenų aktyvacijos energijos. Siekiant nustatyti triukšmo šaltinių vietą bandinyje ir įvertinti, ar minėti defektų lygmenys yra susiję su aktyviąja ar pasyviąja šviesos diodo sritimi, buvo atlikta abipusės koreliacijos koeficiento tarp elektrinių ir optinių fliuktuacijų analizė 10 Hz–20 kHz dažnių srityje. Tobulinant šviesos diodų gamybos technologiją, triukšmo šaltinių vietos nustatymas yra ypač svarbus.

UŽRAŠAMS

Vilniaus universiteto leidykla
Saulėtekio al. 9, III rūmai, LT-10222 Vilnius
El. p. info@leidykla.vu.lt,
www.leidykla.vu.lt
Tiražas 12 egz.